國 立 交 通 大 學

生物科技研究所

博士論文

溶藻弧菌胺醯組胺酸雙胜肽酶之晶體結構與突變分析

Crystal Structure and Mutational Analysis of Aminoacylhistidine Dipeptidase (PepD) from *Vibrio alginolyticus*

研究生：張晉源

Student: Chin-Yuan Chang

指導教授：吳東昆 博士

Advisor: Prof. Tung-Kung Wu Ph.D

中華民國一〇〇年七月

溶藻弧菌胺醯組胺酸雙胜肽酶之晶體結構與突變分析

Crystal Structure and Mutational Analysis of Aminoacylhistidine Dipeptidase (PepD) from *Vibrio alginolyticus*

研究生：張晉源　　Student: Chin-Yuan Chang

指導教授：吳東昆 博士　Advisor: Prof. Tung-Kung Wu Ph.D

國立交通大學
生物科技研究所
博士論文

A Dissertation

Submitted to Department of Biological Science and Technology

College of Biological Science and Technology

National Chiao Tung University

in partial Fulfillment of the Requirements

for the Degree of Doctor of Philosophy

in Biological Science and Technology

Hsinchu, Taiwan, Republic of China

July, 2011

中華民國一〇〇年七月

摘要

胺醯組氨酸雙胜肽酶(PepD，EC 3.4.13.3)為胜肽酶家族M20中的一員，具有寬廣受質專一性，包括可水解肌雙胜(carnosine)及相關之加長肌雙胜(homocarnosine)以及一些三胜肽。基本上PepD可催化水解Xaa-His雙胜肽而釋放出N端的胺基酸。在此論文中，主要研究溶藻弧菌PepD的蛋白質結構、生化特性和金屬催化機轉。利用蛋白質結晶學解出PepD的晶體結構，結果顯示PepD為同源單體所組成的一個二聚體，每個單體包含一個“蓋子區域”和一個雙鋅離子依存的“催化區域”。不同於其他M20家族的二聚體，PepD二聚體結構展現一個獨特的十字構形是經由蓋子區域接觸面間的交互作用力所形成。突變分析確定幾個重要的殘基對於蛋白質結構、受質的辨認、與酵素的活性扮演著關鍵的角色。另一方面，銅離子取代PepD活性中心的雙鋅離子，結果產生兒茶酚氧化活性。我們發現”雙銅−PepD”能氧化末端帶有極性的兒茶酚衍生物，而無法氧化兒茶酚或是帶有非極性支鏈的3,5−叔丁基鄰苯二酚(DTC)。蛋白質−配體入塢結果顯示，此類帶有極性末端的兒茶酚衍生物可與”雙銅−PepD”結合。綜合言之，此研究對胺醯組氨酸雙胜肽酶的酵素結構-功能-反應機制之關係提供更進一步的了解，同時加速開發抗體−酵素導向之前導藥物治療(ADEPT)。此外，我們證實了金屬取代是造成PepD水解酵素功能酵和氧化活性之間轉換的關鍵，因此對於酵素趨異演化開啟了一個嶄新的方向。

Abstract

Aminoacylhistidine dipeptidase (PepD, EC 3.4.13.3), a member of peptidase M20 family, exhibits a broad substrate specificity for unusual dipeptides carnosine (*β*-Ala-L-His) and homocarnosine (γ-aminobutyl-His) and a few tripeptides. Basically, PepD catalyzes the cleavage and release of N-terminal amino acid from Xaa-His dipeptide molecules. In this thesis, the PepD from *Vibrio alginolyticus* was physically and chemically characterized for protein 3D structure, biochemical property, and metal-catalyzed mechanism. The 3D structure was solved by X-ray crystallography, showing that PepD is a homodimer. Each monomeric subunit of the homodimer is composed of a lid domain and a catalytic domain, in which two zinc ions dwell in the active site. In distinction to other M20 family enzymes, the PepD's dimeric structure exhibits a unique criss-cross configuration that is likely formed through interface interaction of respective lid domains. By performing mutational analysis, crucial residues were identified for maintaining PepD architecture, substrate recognition and enzymatic activity. In addition, changing the active site zinc ions with copper ions, converts PepD to catechol oxidase. The CuCu-PepD is able to oxidize catechol derivatives with a polar tail, but not catechol or 3,5-di-*tert*-butylcatechol (DTC) that carries non-polar side chains. This result agrees with protein-ligand docking analysis. Collectively, this study advances our overall understanding for aminoacylhistidine dipeptidase in the structure-activity relationships and facilitates future development of antibody-directed enzyme prodrug therapy (ADEPT). Most importantly, the identification of PepD functionality conversion from peptidase to oxidase has paved a new avenue for divergent enzyme evolution.

誌謝 (Acknowledgement)

過去七年的研究生活，過的很充實，也覺得自己獲益良多。

而論文能順利完成，最要感謝的是我的指導教授－吳東昆博士，讓一個從對生物完全不懂的小毛頭，到現在對"酵素"這一塊一定的了解。不只是指導我實驗方向，也教導我人生應有的態度－積極！還有對研究的熱情與執著，不怕失敗的精神更是我仿效的榜樣。我相信在未來，秉著這樣的態度將受用無窮。在此獻上最深的敬意與謝意。同步輻射陳俊榮老師讓我有機會進入蛋白質結構的領域一探究竟，也讓 PepD 原形畢露，也謝謝您不斷給予學生支持與討論。口試委員李耀坤老師、李宗璘老師以及楊裕雄老師陪我度過修業期間的幾個重要考試，謝謝您們不吝提供寶貴意見以及對於疏漏處的指正，使得論文更臻完備。也非常感謝師母賴美伶小姐在生活上的關心與照顧，還有許多系務上的幫忙。

做研究總是問題就在下一秒、挫折就在每一天，幸運的是總能化險為夷，一步一步的朝著目標邁進。很感謝陪著我度過這段歲月的每一個人，給我打氣，給我支持，給我繼續向前的動力。

謝謝媛婷讓我這幾年成長很多，不厭其煩的跟我討論實驗，雖然每每都會意見不合而吵架，但還是很謝謝妳，希望未來的日子可以繼續跟妳一起成長。程翔學長教我正確的實驗邏輯與技巧，很感謝你從我碩一進實驗室到現在一直以來的支持與幫忙。感謝裕國學長一路以來的支持與鼓勵，教我許多實驗，做抗體，質譜分析等等，也帶我出去玩，很懷念住在一起像家人般的那段日子。晉豪是我的好室友與好學長，很謝謝你在儀器與生活上的幫忙。謝謝我的戰友文鴻，總是關心照顧我生活的總總，也很謝謝你在細胞培養技術上的指導與幫忙。小紅妳讓我在苦悶的研究中找到生活的樂趣。依鵑學姊平常的支持與打氣，還有討論實驗，每次跟你聊天都有很多收穫。PepD 第一棒大鳥，也是我的好室友好戰友，謝謝你奠定很好的實驗基礎，讓我後面做出一些很不錯的成果。還有 PepD 第二棒怡親學妹，謝謝妳在純化養晶上的幫忙。也謝謝良偉學弟在 PepD 上的貢獻。我唯一的徒弟奕汝，很開心可以教到一個那麼聰明可愛的"學弟"，很感謝你在我很忙的時候一直 Cover 我的實驗。文祥學弟，很開心能交到你這個好朋友，那段瘋狂的日子，我現在還記憶猶新。謝謝宏城學長平日的關心與照顧，小八學姊在我碩一懞懂無知的時候教導我實驗。還有跟我同屆的開心果宏明和令宗，謝謝你們在我低潮的時候陪我談心。而分屬其它計劃的 Allen、Mili、欣芳、世穎、怡臻、欣怡、孟兒、欣樺、婉婷以及富生，謝謝你們平日的幫忙與豐富我的生活。

中研院的弘寬學長，謝謝你那麼溺愛我這位學弟，這七年來不斷的支持鼓勵，

在實驗上也一直幫忙，有求必應，教我蟲蟲細胞表現，還有一些 data 的分析，真的很謝謝你，還有大年初二就叫我回去作實驗，這種積極的態度，小弟我謹記在心。同步輻射的殷程學長，謝謝你教導我從養晶到解結構的過程，每當我問一堆很沒 Sense 的問題，你都不厭其煩的跟我解惑。還有我的超級戰友加好兄弟庭蔚，很高興在同步還可以交到你這位好朋友，總是一直在鼓勵我，直到現在拿到學位，希望以後能繼續一起奮戰！

另外還要感謝我的好朋友們─秦兄彼此的互相打氣，小胖、老徐、毒蛇常常給予我加油、打氣，每次跟你們見完面，都會讓我更有勇氣面對下一個挑戰。

最後，特將本論文獻給我最親愛的家人─在天堂的阿公，我想跟您說，我拿到博士學位了！阿媽、爸爸、媽媽一路以來的栽培，讓我沒有後顧之憂，專心攻讀博士學位，從小頑皮到大讓你們頭痛的我，希望以後的我可以讓您們驕傲。哥哥和大嫂品容，謝謝你們縱容我的任性，分擔我的不愉快，還時常請我飲茶。妹妹則是家裡的一塊寶，謝謝你讓家裡增添許多色彩。這段日子很辛苦，但我過的很開心。感謝所有關心我，陪伴著我的人。謹記在心。

老吳說：『積極的面對每一件事』，願以此期勉自己的未來，能夠發揮所學，對社會進一份心力。加油!

晉源 謹誌於

交通大學生物科技研究所

中華民國一 OO 年八月八日

Table of Contents

Table of Figures

Table of Tables

List of Abbreviations

Ala	Alanine
Arg	Arginine
Asn	Asparagine
Asp	Aspartic acid
bp	Base Pair
BSA	Bovine serum albumin
CD	Circular dichroism
Cys	Cysteine
ddH_2O	Double Distilled Water
DMF	Dimethylformamide
dNTP	Deoxynucleoside triphosphate

EDTA	Ethylenediamine-tetraacetic acid
Gln	Glutamine
Glu	Glutamic acid
Gly	Glycine
H, His	Histidine
HPLC	High Performance Liquid Chromatography
Ile	Isolucine
IPTG	Isopropyl-1-thio-β-D-galactopyranoside
kb(s)	kilobase(s)
Lys	Lysine
LA	Lanosterol
LB	Luria-Bertani
Leu	Leucine
Met	Methionine
OPA	*o*-phthaldialdehyde
PCR	Polymerase Chain Reaction
PEG	Polyethylene glycol
Phe	Phenylalanine
Pro	Proline
RT	Room temperature
Ser	Serine
T, Trp	Tryptophan
TEMED	*N*,*N*,*N*',*N*'-tetramethylethylenediamine
Thr	Threonine
TLC	Thin Layer Chromatography
Tris base	Tris(hydroxymethyl)aminomethane
Tyr	Tyrosine
U, Ura	Uracil
Val	Valnine
WT	Wild-type
X-gal	5-bromo-4-chloro-3-indolyl-β-D-galactopyranoside

List of Genes or proteins

Acy1	Acylase 1
*Ap*AP	*Aeromonas proteolytica* aminopeptidase
βAS	β-alanine synthase
CAT	Catalytic domain
CN1	Carnosinase 1
CN2	Carnosinase 2
CPG_2	Carboxypeptidase G_2
CuCu-PepD	Copper-substituted Peptidase D
CuCu-*Sg*AP	Copper-substituted *Streptomyces griseus* aminopeptidase
LID	Lid domain
*Sg*AP	*Streptomyces griseus* aminopeptidase

CHAPTER 1

Introduction

1.1 Binuclear Metallohydrolases

Nearly all metabolic and signaling pathways involve at least one event of hydrolytic cleavage of peptides or phosphate ester bonds. Although both types of bonds are considered as thermodynamically sensitive to hydrolysis, significant kinetic barriers exist that help keep these reactions tightly regulated under normal conditions[1]. For example, several hydrolases contain a co-catalytic metallo-active site that mediates reactions by lowering to the transition energy state. The binuclear metallohydrolases catalyze a diverse set of reactions including degradation of DNA, RNA, phospholipid, phosphoester, and polypeptides (Fig. 1.1). These enzymes are involved in a wide array of physiologic processes, such as hormone level regulation, tissue repair, protein maturation and degradation, and cell-cycle control[1-4]; likewise, perturbing the activities of binuclear metallohydrolases has been implicated in the early onset and progression of disease, such as carcinogenesis. Binuclear metallohydrolases have also been shown to mediate degradation of agricultural neurotoxins, urea, β-lactam-containing antibiotics, and several phosphorus materials used in chemical weaponry[4]. The majority of binuclear metallohydrolases are Zn^{2+}-dependent proteins, but not exclusively, as the enzymes containing other divalent metal ions such as Mn^{2+}, Co^{2+}, Ni^{2+}, and Cu^{2+} also exist.

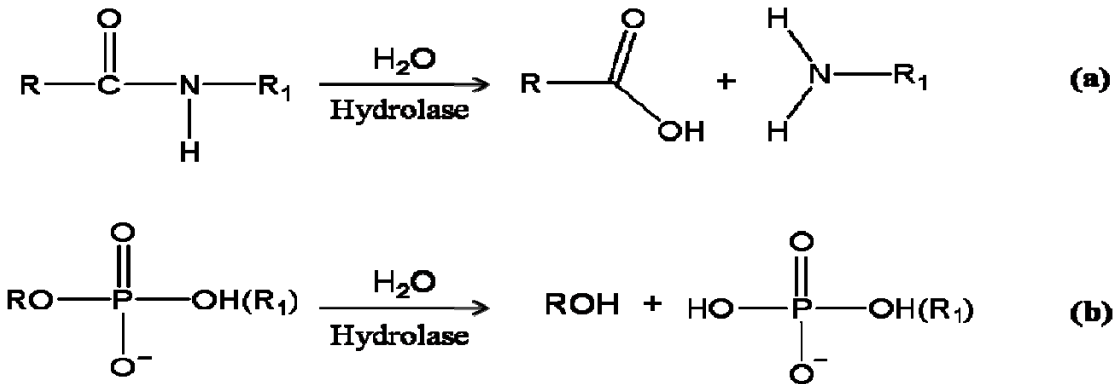

Figure 1.1. Binuclear metallohydrolases catalyze hydrolysis of peptide or phosphate ester bonds. Molecular illustrations for (a) peptidases that catalyze the hydrolysis of peptide bonds in polypeptides, and (b) phosphoesterases and nucleases that catalyze the hydrolysis of phosphoester bonds in phosphorylated amino acids and saccharides, nucleotides, DNA, and RNA.

1.2 Metallopeptidases

Peptidase that requires a metal ion as a cofactor for catalytic activity was designated as metallopeptidase. The classification of metallopeptidases is based on the given functional groups within their active sites. The MEROPS database (http://merops.sanger.ac.uk) grouped the entire set of metallopeptidases into 15 evolutionarily-related clans (based on commonalities among the structural fold) and more than 50 families[5, 6]. Depending on the number of metal ions required for catalysis, metallopeptidases can be divided into two broad types: in many metallopeptidases: one which requires only one metal ion (in the major metallopeptidase) and the other one that requires two metal ions in "co-catalysis" (a special sub-set in the family). All known co-catalytic metallopeptidase functions as exopeptidase, including aminopeptidase, carboxypeptidase, dipeptidase, and tripeptidase. In contract, metallopeptidase that contains only one catalytic metal ion can act as either exopeptidases or endopeptidases,

in spite of existing some exceptions exist.

In metallopeptidase, the metal ions that coordinates with amino acid residues often serves as Lewis acid. These residues in coordination are usually charged residue, such as His, Glu, Asp, or Lys. In addition, at least one other residue is essential for catalysis, which has been theorized to act as a nucleophile that activates the metal ions and binds substrates. Results from crystallographic studies of solved metallopeptidases suggested that about one-half belongs to three clans, MA, MB and MX/MBA, and that each of these family members contains the HEXXH pentapeptide for chelating zinc ions[5, 7].

Metallopeptidases play fundamental roles in certain biochemical events, such as protein maturation and degradation, tissue repair and cell-cycle control[8]. In these enzymes, the nucleophile (from water molecule) attacks an amide bond to become a tetrahedral intermediate (Fig. 1.2). The water molecule is activated by divalent metal cations, usually zinc but sometimes cobalt, manganese, nickel or copper[9].

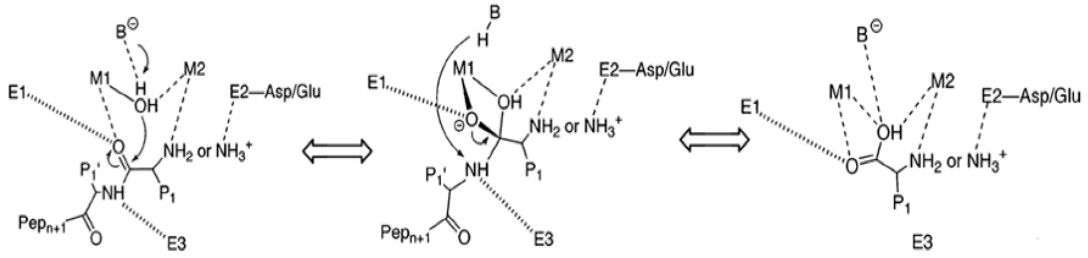

Figure 1.2. A generalized mechanistic scheme for metallopeptidases. First, the substrate binds to the metallopeptidase active site, with the carbonyl group of the scissile peptide bond interacting with M1 and a conserved enzyme residue, E1. The *N*-terminus either interacts with M2 or with one or more acidic enzyme residues in the vicinity (indicated in the middle reaction by E2). Additional enzymatic histidine or backbone carbonyl group interactions, at E3, facilitate substrate binding in the correct register. The scissile peptide bond is then attacked by a solvent molecule that has been activated by its interaction with the metal ions, and by an enzyme residue that functions as a general

base, B^-. Whether or not the subsequent tetrahedral intermediate is stabilized by interactions with both metal ions and E2 side chains depends upon the particular enzyme system. Breakdown of the intermediate is most likely promoted by the addition of a proton to the amine group that has departed from the former general base, B-H, as first suggested in studies of thermolysin[9].

1.3 Aminoacylhistidine dipeptidases in the peptidase M20 family

The 15 clans of metallopeptidases in the MEROPS database (http://merops.sanger.ac.uk)[10] are: MA, MC, MD, ME, MF, MG, MH, MU, MK, MM, MN, MO, MP, MQ, and M-. The clan MH contains a variety of co-catalytic zinc-dependent peptidases that bind two atoms of zinc per monomer. The zinc atoms are held by five amino acid ligands, and binding can be inhibited by the presence of a general metal chelator, such as ethylenediamine-tetraacetic acid (EDTA) or orthophenanthroline (1,10-phenanthroline)[6]. The peptidase clan MH is further divided into four families: M18, M20, M28, and M42. The M20 peptidases, in particular, were characterized by their property of binding a water molecule along with by two zinc ions which are held by five residues at the active site, in the order of His/Asp, Asp, Glu, Glu/Asp, and His. Additional Asp and Glu residues adjacent to metal-binding residues are also are thought to be important for catalysis[5]. The Asp residue between two catalytic residues binds both metal ions. Several kinds of M20 family enzymes exhibit a binuclear-binding domain, including the dipeptidases (PepD[11], PepT[12], PepV[13]), aminopeptidases (*Streptomyces griseus*, *Sg*AP)[14], carnosinases (CN1, CN2)[15], carboxypeptidases (CPG_2)[16], β-alanine synthases (βAS)[17], desuccinylases (DapE)[18] and deacetylases (ArgE)[19]. Variations exist in the individual sub-families that are revealed upon amino acid sequence alignment. Peptidase family M20 has been further divided

into four sub-families, based upon the distinct active site residues: M20A, M20B, M20C, and M20D.

Aminoacylhistidine dipeptidases (EC 3.4.13.3, published under the names Xaa-His dipeptidase, X-His dipeptidase, carnosinase, and PepD) belong to the M20C sub-family. These zinc-containing metallopeptidases catalyze the cleavage and release of an N-terminal amino acid, usually a neutral or hydrophobic residue, from Xaa-His dipeptides or polypeptides (Fig. 1.3)[5].

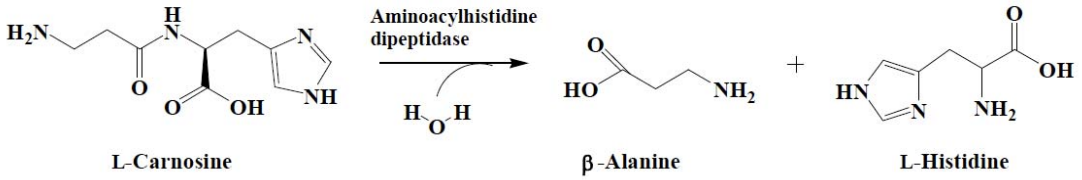

Figure 1.3. Aminoacylhistidine dipeptidase catalyzes hydrolysis of a dipeptide L-carnosine (β-Ala-L-His) into two amino acids.

The gene encoding aminoacylhistidine dipeptidase is evolutionarily conserved in the genomes of prokaryotes and eukaryotes. The first direct experimental evidence of aminoacylhistidine dipeptidase activity was obtained in 1974 when the carnosinase from the bacteria *Pseudomonas aeruginosa* was demonstrated to hydrolyze the dipeptide L-carnosine[20]. Over the next few years, more of these enzymes were discovered in several other bacterial species or higher order organisms; however, only the PepD from *Escherichia coli* has been fully characterized using genetic and biochemical approaches[21].

The *E. coli pepD* gene encodes a 52 kDa protein and is active as a homodimer, having a molecular mass of 100 kDa[22]. The pure enzyme exhibits a pH and temperature optimum of pH 9.0 and 37°C, respectively. *E. coli* PepD appears to function principally as an aminoacylhistidine dipeptidase with broad substrate specificity, which is activated

by Co^{2+} and Zn^{2+} and deactivated by metal chelators[21]. The previous report described how the expression of *pepD* negatively affects biofilm formation, a necessary process for infection to be established in a host system; in this case, a fish system was used to determine the molecular mechanisms by which bacterial infection may be significantly impacting fish mortality, and consequently marine economy[23]. The specific role of PepD in infection makes it a promising therapeutic target to control bacterial pathogenic infectious disease.

In more general terms, however, dipeptidases are involved in the final breakdown of protein degradation fragments produced by the targeted actions of other peptidases, or of dipeptides being processed for subsequent utilization of their amino acid components. Indeed, studies involving PepD-deficient mutants of *E. coli*[24] and *Salmonella typhimurium*[25], have indicated that PepD can hydrolyze dipeptides needed as an amino acid source. However, the full biological impact of PepD remains unclear.

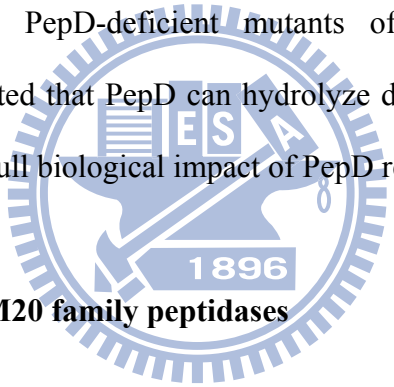

1.4 Crystal structures of M20 family peptidases

To date, several of the M20 family enzymes have been crystallized and reported in the literature. These enzymes have exhibited an overall two-domain organization, including a di-zinc binding catalytic domain and a structurally similar but smaller domain. Nearly all M20 enzymes exist as homodimers. The Peptidase V (PepV) from *Lactobacillus delbrueckii*, however, represents a notable exception as it appears to exist only as a monomer[26].

1.4-1 Carboxypeptidase G_2 (CPG_2) from *Pseudomonas* sp. strain RS-16

Enzymes of the carboxypeptidase G class catalyze the C-terminal glutamate moiety hydrolyzation from folic acid and its analogues such as methotrexate[27]. In 1997, Brick and colleagues reported the first crystal structure of an M20 metallopeptidase[28, 29]. To obtain the crystal structure of carboxypeptidase G_2 (CPG_2) from *Pseudomonas* sp. strain RS-16 at 2.5 Å resolution, the group used multiple isomorphous replacement (MIR) methods. CPG_2 was determined to be a typical homodimer of the peptidase M20 family, in which each subunit is a component of a larger catalytic domain containing two zinc ions in the active site. The smaller domain forms the dimer interface by means of hydrophobic interactions between helices, as well as through hydrogen bonding between two β strands from each subunit (Fig. 1.4).

The catalytic domain of CPG_2 comprises residues 23-213 and 326-415, which contain the N- and C-terminal of the polypeptide chain, respectively. The dimerization domain of CPG_2 consists of a single, 110 residues insertion in the catalytic domain sequence, comprising residues 214-325. In the metal ions binding site within the catalytic domain of CPG_2, two zinc ions (Zinc 1 and Zinc 2) are present, which are 3.3 Å away from each other. Zinc 1 is bound by Asp^{141}, Glu^{176} and His^{385}, while Zinc 2 is bound by the other carboxylate oxygen of Asp^{141}, Glu^{200} and His^{112}. Furthermore, a water molecule is bound by Glu^{175} underneath and in the middle of the two zinc ions; this molecule is activated by the zinc ions in order to facilitate the nucleophilic attack on the substrate, which in turn forms the tetrahedral intermediate (Fig. 1.5).

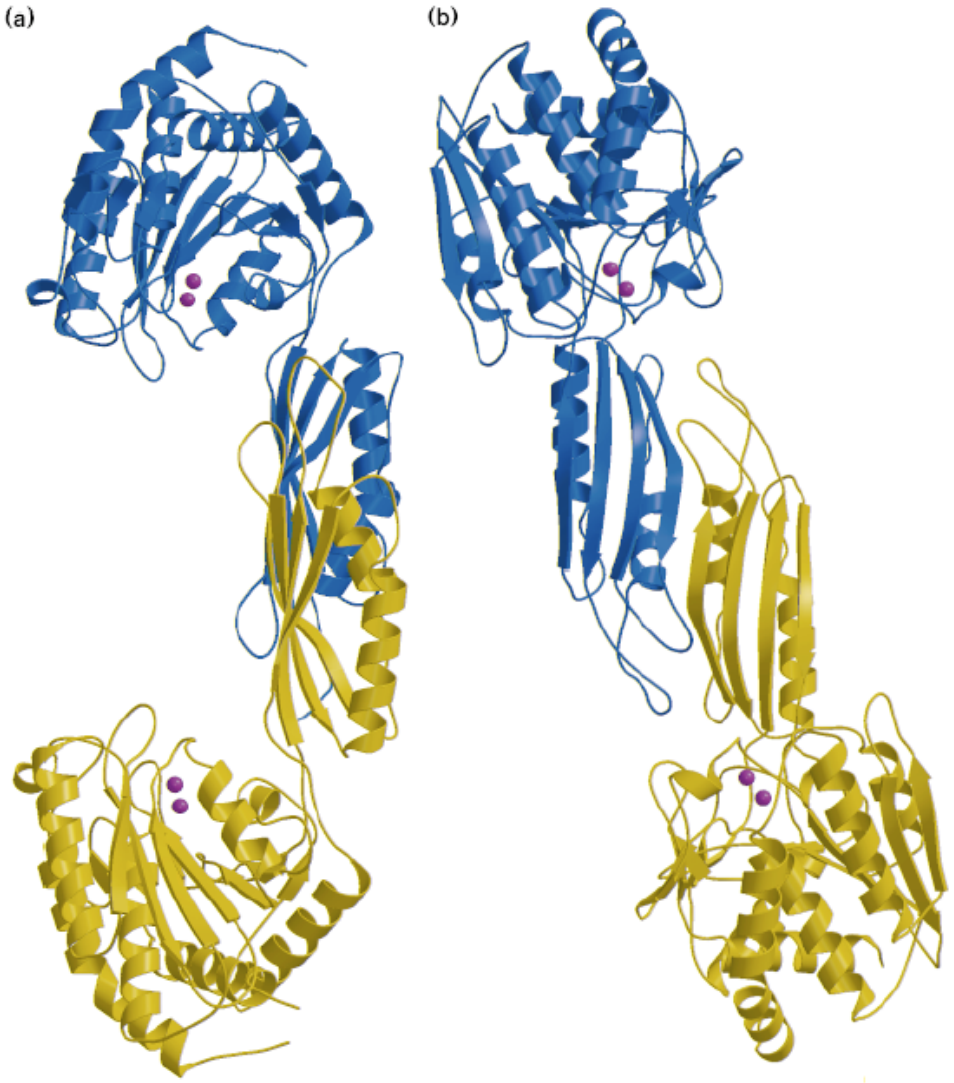

Figure 1.4. Ribbon diagrams of the CPG_2 dimers. Views from different orientations are presented in (a) and (b). The two subunits are coloured in *blue* and *yellow*, respectively. The *magenta spheres* represent bound zinc ions. In (b), the continuous β sheet is visible across the two subunits forming the dimer interface[29].

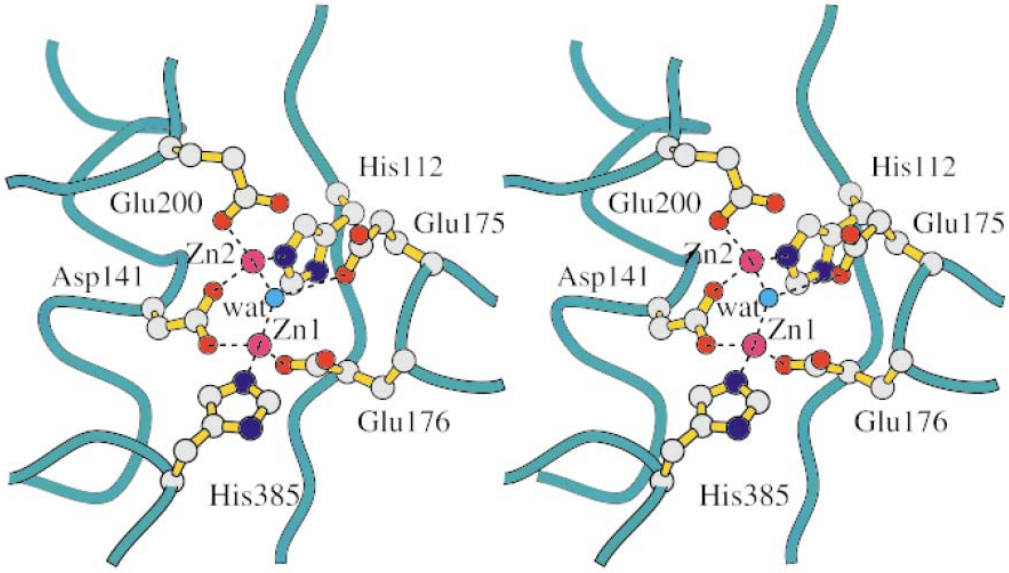

Figure 1.5. Stereo view of the metal ions binding site in CPG_2. Ball-and-stick representation of the two zinc ions and their binding residues are shown. Atoms are in standard colours. The bridging active-site water molecule (wat) is indicated as a *light blue sphere*. The Glu^{175} residue is presumed to promote the attack of the water molecule on the substrate[29].

1.4-2 Peptidase V (PepV) from *Lactobacillus delbrueckii*

The *L. delbruekii pepV* gene is 1413 nucleotides in length and consists of 470 amino acids that encode a protein with predicted molecular mass of 52 kDa. PepV functions as an aminoacylhistidine dipeptidase or carnosinase, cleaving Xaa-His dipeptide to generate a source of histidine. It has been characterized as a relatively non-specific dipeptidase, with demonstrated ability to cleave a variety of dipeptides. The broad dipeptide species is able to be hydrolyzed, especially those with an unusual β-alanyl residue in the N-terminus; in addition, the N-terminal amino acid has been shown to be targeted for removal from a few distinct tripeptides[30].

PepV is related not only to peptidases, but also to acetylornithine deacetylase

(ArgE, EC 3.5.1.16) and succinyldiaminopimelate desuccinylase (DapE, EC 3.5.1.18). Most recently, it has been described as a member of the aminoacylase-1 family[31], which can hydrolyze amide bonds in a zinc-dependent manner. Interestingly, when the dipeptidase *pepV* gene was deleted from *Lactobacilli* a significant decrease in growth rates was observed, but the final cell density remained unaffected.

PepV from *L. delbruekii* was the first discovered crystallized dinuclear dipeptidase with carnosine-hydrolyzing enzymatic activity in the M20 family[26]. To date, PepV remains the only monomeric among all of the M20 family aminopeptidases. Based on its crystal structure, PepV was recognized as a metallopeptidase haboring two zinc ions in a single monomer. Therefore, it was theorized and demonstrated that PepV could be inhibited by metal chelation agents, such as 1,10-phenanthroline or EDTA. The 3D structure of PepV protein reveals two distinct domains, designated as the catalytic domain and the lid domain (Fig. 1.6A). The catalytic domain encompasses residues from Met^{1} to Gly^{185} and from Ser^{388} to Glu^{468}, whereas the lid domain comprises the residues from Glu^{186} to Gly^{387}. In the catalytic domain, five residues – His^{87}, Asp^{119}, Glu^{154}, Asp^{177} and His^{439} – are critically responsible for chelating the two zinc ions (Fig. 1.6B). The mechanisms of substrate binding and hydrolysis are mediated by Glu^{153}, Asn^{217}, His^{269}, Arg^{350} and Glu^{415} (Fig. 1.7).

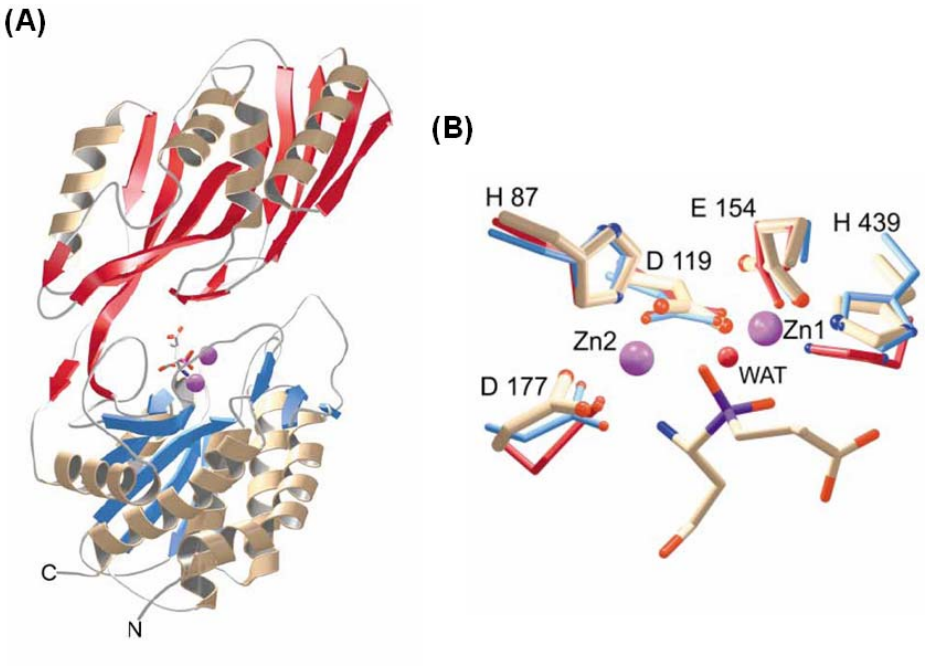

Figure 1.6. The crystal structure of *L. delbrueckii* PepV. Ribbon diagram (A) of the enzyme and local view (B) of the zinc ion binding cavity. In Fig. B, the inhibitor of PepV (beige) is superimposed upon the zinc binding residues of *Aeromonas proteolytica* *Ap*AP (*blue*) and CPG_2 (*red*). Residues are numbered according to PepV sequence. The catalytic water molecule of CPG_2 is depicted in *red* (WAT)[26].

The two zinc ions, as described by Jozic *et al*., are presumed to play two different roles in the hydrolysis of substrates, that which stabilizes the substrate-enzyme tetrahedral intermediate and that which activates the catalytic water molecule (Fig. 1.7). Zinc 1, which is associated with the imidazole group of His^{439} and the carboxylate oxygen of Glu^{154} and Asp^{119}, appears to primarily facilitate binding with His^{269} via an "oxyanion binding hole". Such binding results in polarization of the scissile carbonyl group and consequently promotes nucleophilic attack by the catalytic water molecule. Zinc 2 is coordinated by His^{87}, the carboxylate oxygen of Asp^{177}, and the bridging Asp^{119}. This ions appears to primarily function in the activation of the catalytic water molecule,

and acts as the strong Lewis acid promoting binding and hydrolysis.

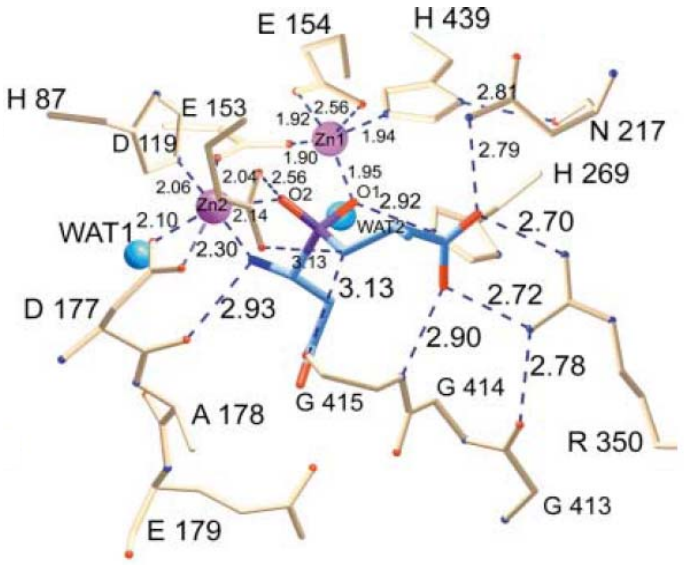

Figure 1.7. Schematic of the active site of PepV. The Asp-Ala phosphinate inhibitor mimics the dipeptide substrate, as shown in *blue*. The bridging catalytic water attacks the carbonyl carbon of the scissile peptide bond, forming the sp^3-orbital substrate-enzyme tetrahedral intermediate[26].

1.5 Application of M20 family peptidases in Antibody-Directed Enzyme Prodrug Therapy (ADEPT)

M20 family enzymes hold great potential for biotechnological applications and therapeutic significance[13, 26, 30-34] based upon their crucial roles in a wide variety of the most basic physiologic processes. For example, *Lactobacillus* sp. PepV[13] and *S. typhimurium* peptidase T (PepT)[32] function in amino acid utilization, whereas *E. coli* allantoate amidohydrolase and yeast *Saccharomyces kluyveri* β-alanine synthase (βAS)[33] are involved in the nucleotide catabolic pathways. In addition, other species-specific dipeptidases represent promising molecular tools to manipulate a desired physiologic state; these include the *E. coli* K12 PepD[21], human brain-specific carnosinase (CN1) and

nonspecific carnosinase (CN2)[15], and mouse CN2[35], that can regulate unusual dipeptides, such as L-carnosine (β-Ala-His) and L-homocarnosine (γ-amino-butyl-His), as well as a few other distinct tripeptides. Epidemiologic studies investigating the underlying molecular mechanisms of signal transduction-related diseases by evaluating sibships have indicated that deficiencies in serum carnosinase are significantly associated with tremor, myoclonic seizures, hypotonia, and profound psychomotor retardation[36-40]. The gastric ulcer- and cancer- causing *Helicobacter pylori* bacteria expresses a succinyldiaminopimelate desuccinylase that may be an effective target of antimicrobial agents[41] to clear infection. Likewise, *Pseudomonas* sp. strain RS-16 carboxypeptidase G_2 (CPG_2) has been proposed for use in antibody-directed enzyme prodrug therapy for the development of a rescue agent in cases of methotrexate overdoses[16, 29, 42-44].

The idea of using enzymes as amplifiers to convert relatively nontoxic prodrugs into active cytotoxic agents was first explored in the 1960s. This strategy, is known as ADEPT[45, 46], has been successfully applied to elimination of cancer cells[47, 48]. In principle (Fig. 1.8), an enzyme-monoclonal antibody (or fragment) conjugate, known as an antibody-enzyme conjugate (AEC), is administered systemically or locally at the tumor site. The molecule-specific antibody acts as a guidance system to target a specific antigen present the surface of the tumor cell (membrane) or in the extracellular fluid surrounding the tumors. Thus, the AEC is trapped in the region of the tumor, and in theory will not detrimentally affect normal tissues. The unbound AEC is expected, and has been demonstrated, to be cleared from the body through the standard urinary route.

Following administration of the AEC, the prodrug, an exogenous substrate for a particular endogenous enzyme, is administered systemically. In this manner, the prodrugs are only converted to active cytotoxic drugs when they reach the targeted tumor sites and diffuse through the tumor mass to enter cells. This approach is

advantageous in that it does not require a specific antigenic marker to be present on the tumor cells. Such site-selective prodrug activation has been demonstrated to result in reduced side effects to remote non-cancerous tissues.

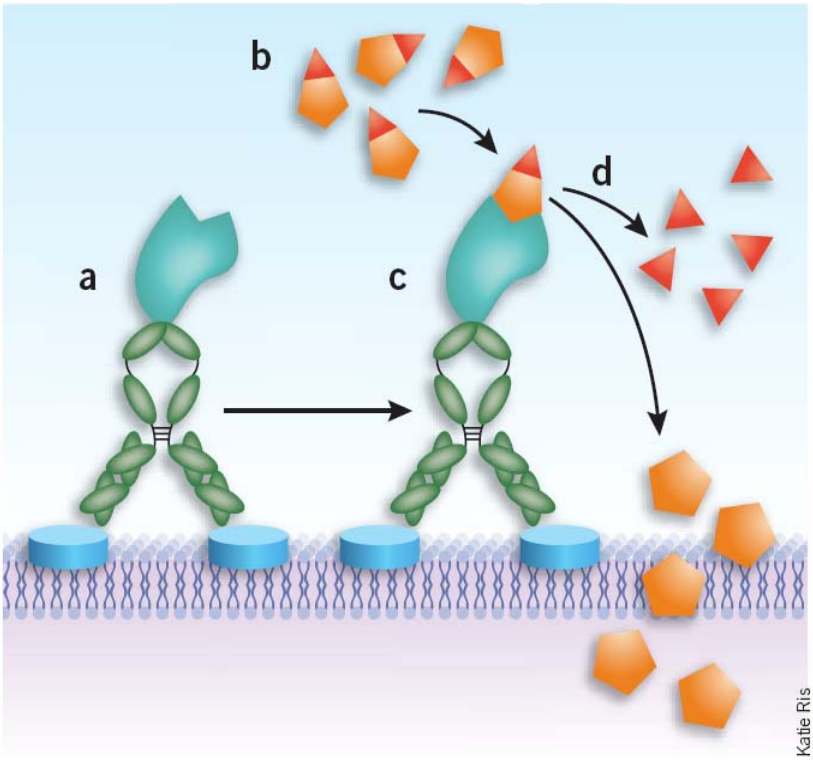

Figure 1.8. Schematic of Antibody-Directed Enzyme Prodrug Therapy (ADEPT)[42]. (a) First, the mAb-enzyme conjugate binds to its target tumor cell-surface antigen. (b-d) After unbound mAb-enzyme is actively or passively cleared from circulation, the cytotoxic agent is administered in an inactive (prodrug) form (b), which is selectively bound by the mAb-enzyme on the tumor cell surface (c), causing cleavage of the inactivating sequence from the prodrug and releasing multiple copies of active drug into the tumor microenvironment[48].

ADEPT has been used in animal tumor models of human choriocarcinoma and colonic and breast carcinoma[49-51]. Recently, Francis *et al*. reported the results of a phase I ADEPT trial, in which a murine $F(ab')_2$ anti-carcinoembryonic (anti-CEA) antigen

fragment linked to the bacterial enzyme carboxypeptidase G_2 (CPG_2) was used in conjunction with the bis-iodo phenol mustard prodrug in patients with advanced colorectal carcinoma or other CEA-expression tumors[52]. Although this trial did not result in tumor regressions, it did demonstrate that a potent prodrug could be administered with acceptable toxicities and that were primarily limited to myelosuppression.

In 1985, the Charing Cross group developed monoclonal antibodies (W14 and SB10) to human β chorionic gonadotrophin and anti-CEA antibody (A5B7)[45]. They designed their studies and reagents based on the fact that target antigens should be expressed on the membrane of tumor cells or secreted into the extracellular space of tumors. Oncogen products or overexpressed gene products that have an external domain on the cell membrane, such as some growth factor receptors, should also be considered as useful targets. The synthetic benzoic acid mustard prodrug (4-[bis-(2-chloroethyl)-amino] benzoyl-L-glutamic acid), the investigators chose to use is known to be targeted by CPG_2 for cleavage of its terminal glutamic acid residue to generate the active alkylating agent 4-[(2chloroethyl)[2(mesylozy)ethyl]-amino] benzoic acid (Fig. 1.9), and subsequently be actived in cancer cells.

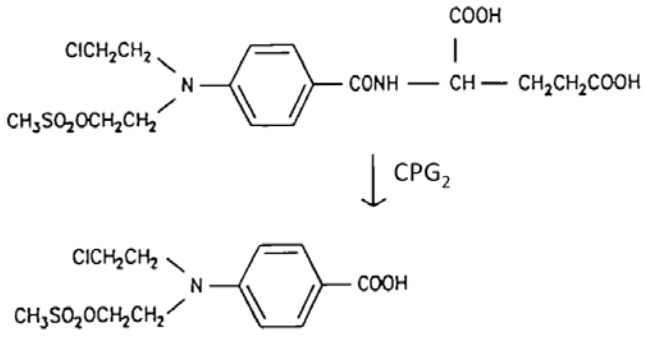

Figure 1.9. Benzoic acid mustard prodrug (4-[bis-(2-chloroethyl)-amino] benzoyl-L-glutamic acid) is cleaved by carboxypeptidase G_2.

1.6 Catechol oxidase / tyrosinase

Catechol oxidases (EC 1.10.3.1) and tyrosinase (EC 1.14.18.1) are structurally similar enzymes and both belong to the type-3 copper proteins[53]. These enzymes are widely distributed among plant, animal and fungal species, in which they facilitate production of melanin derivatives (Fig. 1.10)[54]. Two-electron transfer reactions are carried out during the oxidation step involving a broad range of *o*-diphenols and the corresponding *o*-quinones[55, 56]. Once activated, the quinones are auto-polymerized and are able to form the brown polyphenolic catechol melanins, which act to protect animal skin from sun damage and plants from penetration by pathogens or insects[57]. Furthermore, tyrosine is able to be oxidized by tyrosinase to produce L-3,4-dihydroxyphenylalanine (L-Dopa) in animals, and L-dopa is the upstream substance of several neurotransmitters, such as dopamine and epinephrine. Thus, catechol oxidase/tyrosinase is not only the key enzyme in synthesis of melanin derivatives, but also regulates the biosynthesis and metabolism of neurotransmitters[58, 59].

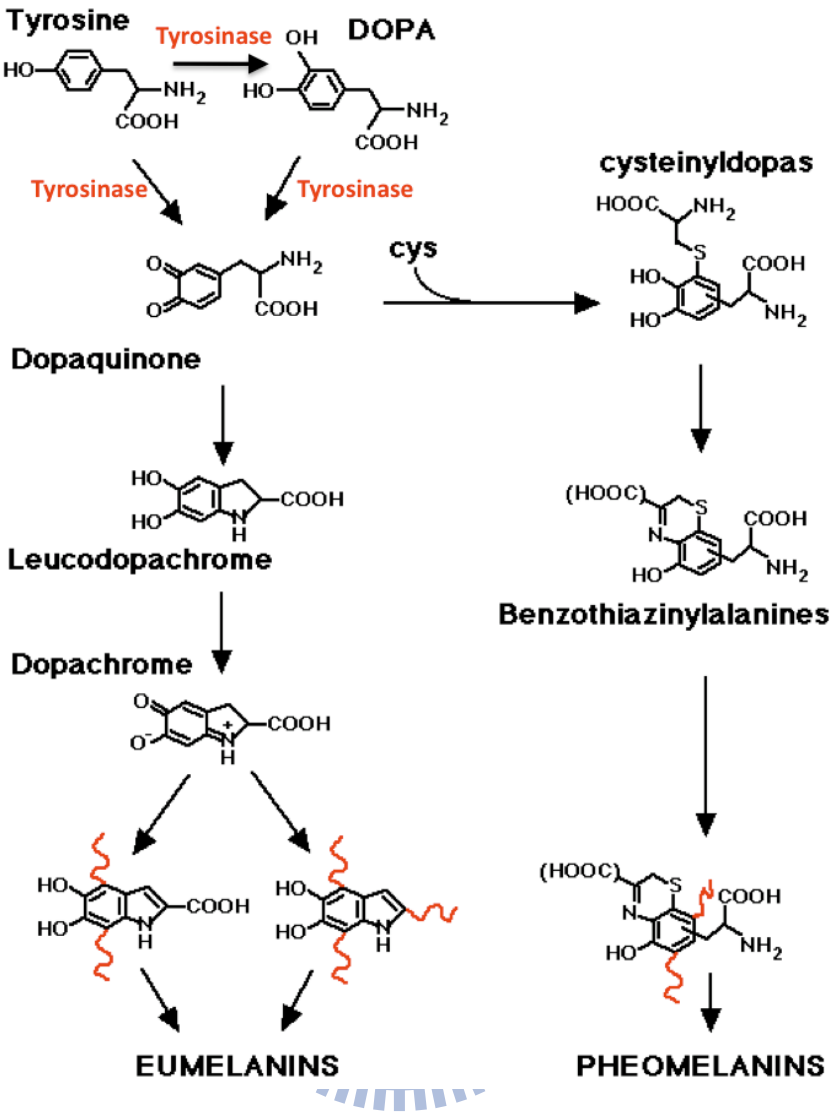

Figure 1.10. The tyrosine metabolism pathway. Tyrosinase catalyzes the *o*-hydroxylation of phenols, and further oxidation of the resultant catechol leads to processing of *o*-quinone.

1.7 Crystal structure of the catechol oxidase from sweet potato

In 1998, the first crystal structure of catechol oxidase from sweet potato was determined by Klabunde and colleagues.[60] The structure revealed a monomer of ~39,000 M_r that formed an ellipsoid shape with dimensions of 55 × 45 × 45 Å (Fig. 1.11A). In the di-Cu^{2+} binding cavity of this catechol oxidase, each copper was defined as being

coordinated by three histidine residues. Specifically, CuA is chelated by His^{88}, His^{109} and His^{118}, while CuB is chelated by His^{240}, His^{244} and His^{274} (Fig. 1.11B). Notably, there is a covalent cycteine-histidine bond that exists between the Cε atom of His^{109}, one of the copper ions, and the sulfur atom of Cys^{92} in metal ions center. The covalent cysteine-histidine bond has been suggested to maintain an enatic state that stabilizes the electronic structure of the metal to facilitate oxidation of the *o*-diphenol substrate and the following rapid electron transfer of the redox processes.

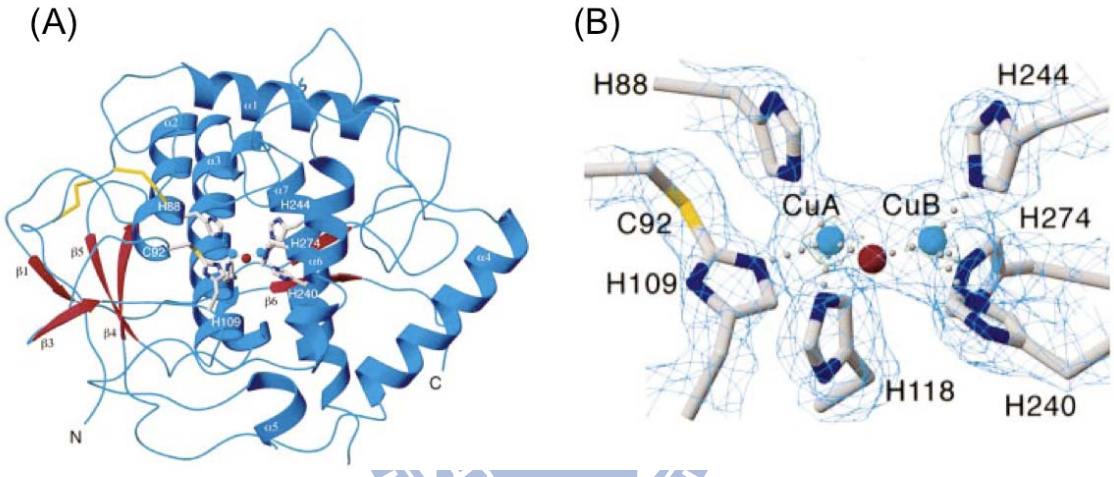

Figure 1.11. Crystal structure of catechol oxidase from sweet potato[60]. (A) Ribbon diagrams of overall structure. (B) Diagram of the electron density in the oxidized catalytic dinuclear copper site. The sulfur atom of Cys^{92} presented here does not ligate to the copper center, but represents that covalently bound to the Cε atom of His^{109}.

Based on the crystal structure of catechol oxidase in the resting dicupric Cu(II)-Cu(II) state, it appears that oxidation of the reduced dicuprous Cu(II)-Cu(II) form, as well as that in complex with the inhibitor – phenylthiourea (PTU), is carried out in the dicopper center by means of a four-electron reduction of the molecular oxygen to water (Fig. 1.12a). In the reduced enzyme state, the dioxygen molecule binds to the dicuprous metal center, replacing the water molecule bonded to CuA (Fig. 1.12b, and top of Fig.

1.12a). Next, the dicopper center opens via the rotation of the side chain of Phe^{261} to allow the catechol substrate (CAT) access to the active site. The crystal structure of the catechol oxidase-PTU complex (Fig. 1.12e, and bottom of Fig. 1.12a) suggested that simultaneous binding of CAT and dioxygen is feasible. Furthermore, it appears that the complex favors a mono-dentate binding model (Fig. 1.12c, and second from the top in Fig. 1.12a) in which the *ortho*-hydroxyl groups from CAT bind to CuB after deprotonation. The finding of the Glu^{236} hydrogen bound to a solvent molecule proximal to the dicopper center suggested a potential role for this residue in substrate deprotonation. In the proposed ternary catechol oxidase-O_2^2-CAT complex, protonation of the peroxide group and cleavage of O-O bond are carried out by two-electrons transfer from the substrate to the peroxide. Glu^{236} along with the second non-coordinating hydroxyl group of the substrate might donate a proton and promote the loss of water and the eventual production of *o*-quinone. Finally, protonation of the bridging group by solvent leads to the active site entering into a resting hydroxide-bridged dicupric state (Fig. 1.12d, and second from the bottom in Fig. 1.12a).

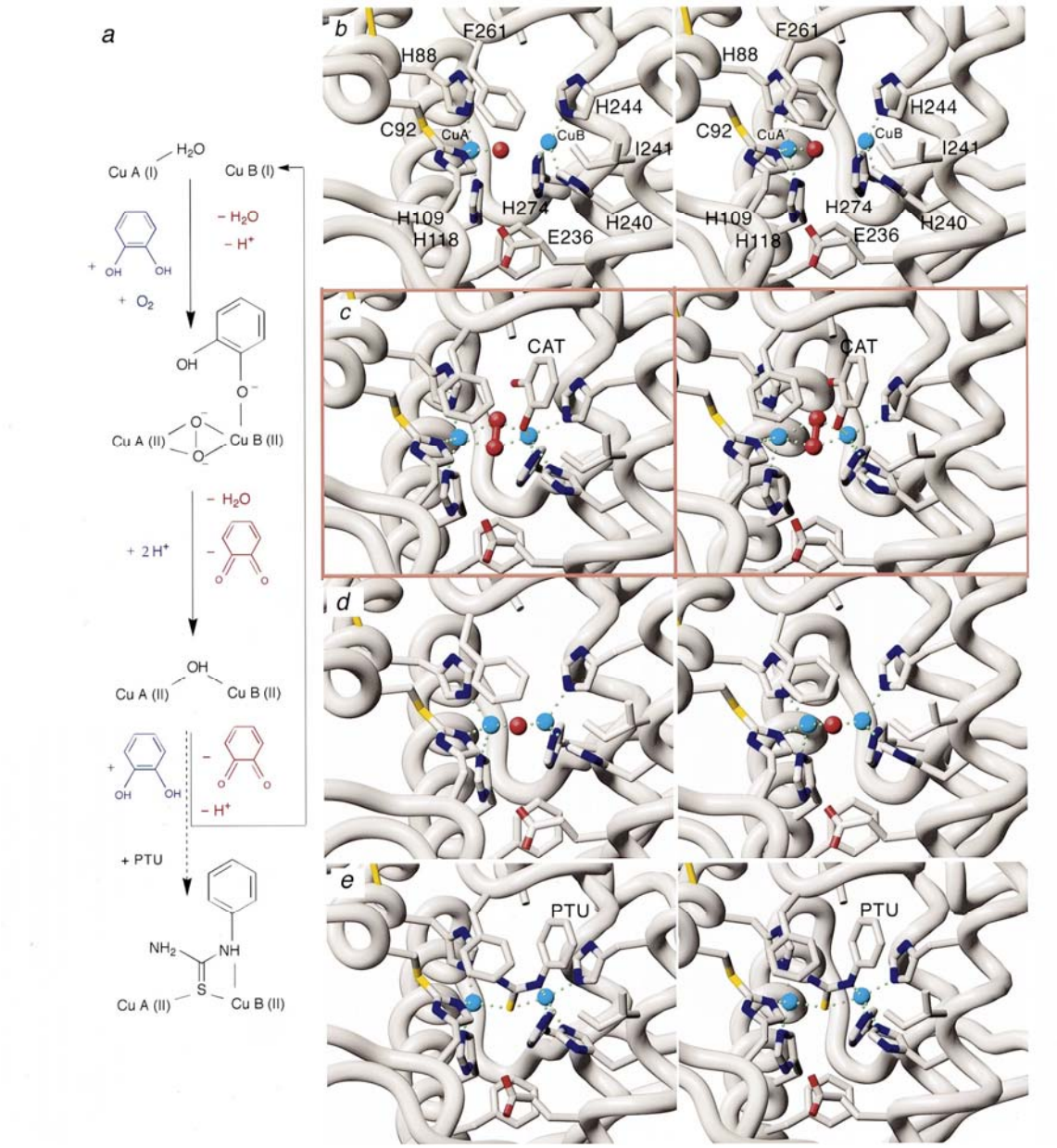

Figure 1.12. Proposed reaction pathway of catechol oxidase. (a) Schematic diagram of the reaction catalyzed by catechol oxidase. (b-d) The 3D structure is presented for each of the reaction steps, as derived from crystallographic analysis. Note that the ternary catechol oxidase-O_2^2-CAT complex shown in (c) is a model structure, guided by (**e)**, the binding mode observed for the inhibitor PTU[60].

1.8 Catechol oxidase activity of di-Cu^{2+}-substituted aminopeptidase from *Streptomyces griseus* (*Sg*AP)

It is generally believed that enzyme catalysis has evolved in order to carry out specific chemical changes in stable transition states of a given substrate that is required for normal physiologic processes. One such example is that of the peptide-bond hydrolysis mediated by metallopeptidases that occurs during the tetrahedral transition state[61]. However, enzymatic promiscuity is a common occurrence in nature, that being when more than one type of reaction is catalyzed by a single enzyme, and is believed to have resulted from distinct routes of evolution among members of a superfamily[62-65]. In recent years, the novel approaches to explore and discover the new metalloprotein systems were carried out to regulate their activities with the active-site metals that using apo metalloprotein molecules as natural ligands and observing the effects of binding. To date, however, only a few papers have reported results from altering catalytic specificity by simple metal substitution of metalloenzymes[66].

Recently, the dinuclear aminopeptidase from *Streptomyces griseus*, *Sg*AP, was found to exhibit a high efficiency of catalytic promiscuity toward phosphoester hydrolysis under different physiological conditions[67-69]. Moreover, the peptide hydrolysis activity of *Sg*AP[70, 71] was able to be converted to catechol oxidative activity by performing a di-Cu^{2+} substitution of the di-Zn^{2+} in the metal binding center[72, 73]. The resultant CuCu-*Sg*AP could effectively catalyze oxidation of catechol and catechol derivatives, such as 3,5-di-*tert*-butylcatechol (DTC), dopamine, and 4,5-dichlorocatechol (DCC). In fact, the oxidative efficiency of CuCu-*Sg*AP for DTC (k_{cat}/K_m = 3295 $M^{-1}s^{-1}$) was much better than that of a number of artificial synthetic metal complexes and was only ~10 times smaller than the natural catechol oxidase from *gypsywort* (k_{cat}/K_m = 32 $mM^{-1}s^{-1}$)[74]. When the metal ions binding sites of *Sg*AP and

catechol oxidase were structurally compared, it was determined that they both harbor a "*met*like" di-metal ions site with a bridging OH or H_2O between the two metal ions centers that likely plays a critical role in catalysis[75]. Although the active sites in these two enzymes are quite different (one being a mixed His/carboxylate environment (Fig. 1.5 and Fig. 1.6B), the other an all-His environment (Fig. 1.11B)), the catalytic promiscuity of *Sg*AP reflects that the active site does not need to be restricted to one structural pattern. This finding revealed a new direction of oxidation catalysis for rational design for ligands and proteins. To date, *Sg*AP and its metal-substituted derivatives remain the only protein system with obvious multiple and diverse catalytic activities, those being phosphodiesterase and catechol oxidase. Therefore, this enzyme and its metal-substituted derivatives are considered amenable to preparations as unique dinuclear systems that may provide further detailed understanding of the correlation between structure and mechanism of metal-centered hydrolytic and oxidation/oxygenation chemistry. In addition, this study may also serve as a "living fossil" system to untangle the mysteries of divergent enzyme evolution.

1.9 Thesis purpose

Aminoacylhistidine dipeptidase is widely distributed among prokaryotes and eukaryotes, and its biological significance and function have been evolutionarily conserved as well. PepD is well known to hydrolyze physiologically-important dipeptides into two amino acids, such as carnosine and homocarnosine, but the structure-reaction relationship of PepD has yet to be studied in detail. *V. alginolyticus* PepD shares only 20% amino acid sequence identity with the several other M20 family enzymes whose crystal structures have been reported[76]. In our previous studies, we had cloned and expressed the *V. alginolyticus pepD* gene and were able to carry out detailed

biochemical characterization, including defining the enzyme kinetics of the produced recombinant protein[76]. The subsequent studies that comprised this thesis aimed at investigating the structure-function relationship by using protein X-ray crystallography coupled with site-directed mutagenesis[77, 78]. Enzyme kinetic studies were also carried out to determine the reaction rate and underlying catalytic mechanism. Ultimately, our characterization of the active-site architecture of PepD enzyme will aid in future studies to identify residues that may be modified to yield alternative substrate recognition properties and improve the potential therapeutic value of this protein and its closely related family members.

On the other hand, previous studies have reported that substituting zinc ions for copper ions in the active site of aminopeptidases allowed for the enzyme function to be effectively converted from peptide hydrolase to catechol oxidase[72]. Therefore, the copper-substituted PepD (CuCu-PepD) was prepared to investigate whether conversion of enzyme function could be attained. Moreover, the robustness of the new activity was evaluated, as well as the new substrate selectivity, by using several catechol derivatives. The findings from this study are expected to provide further insights into the general enzyme activities of peptide hydrolysis and catechol oxidation, and advance our understanding of the correlation between specific metal ions and enzyme function. Finally, this study might also reveal a new direction for divergent enzyme evolution.

CHAPTER 2

Materials and Methods

2.1 Materials

2.1-1 Bacterial strains, molecular cloning/expression vectors, and resin

In this study, bacterial strains *Escherichia coli* XL1-Blue, BL21(DE3) and BL21(DE3) pLysS were purchased from Novagen. Plasmid vector pET-28a(+) and pCR®2.1-TOPO were purchased from Invitrogen and Novagen, respectively. Bacterial growth condition, agar plate preparation, recombinant DNA purification, DNA sequence determination, agarose gel electrophoresis and protein concentration determination were performed according to standard procedures or the commercial kit. Ni-NTA His-Band® Resin was purchased from Amersham Pharmacia Biotech.

2.1-2 Enzymes, chemicals, equipments, and reagents

(1) Enzymes: All restriction enzymes were purchased from New England BioLabs lnc. The pfu DNA polymerase was purchased from Stratagene. The T4 DNA ligase was purchased from Promega. All enzymes were used according to the recommended protocols.

(2) Chemicals: The following section lists the chemicals utilized in this study. The manufacturers were included in the square bracket. Acetic acid [Merck], Acrylamide [GE Healthcare], Agarose [USB], APS [GE Healthcare], α-Ala-L-His [Sigma],

β-Asp-L-His [Sigma], Bestatin [MP Biomedicals], Bacto™ Agar [DIFCO], L-carnosine [ICN Biomedicals, Inc.], Citric acid [Sigma], Coomassie® Brilliant blue R250 [Merck], Catechol [Alfa Aeser], Deoxyribonucleotide triphosphate (dNTP) 100mM Solutions [GE Healthcare], DNA 10kb Ladder [BioBasic Inc.], L-Dopa [Sigma], Dopamine [Sigma], Ethanol (95% and 99%) [Merck], GABA-His [Sigma], Glycine [Merck], Gly-Gly-His [Sigma], Gly-His-Gly [Sigma], Gly-His [Sigma], Glycerol [Merck], L-Histidine [Sigma], His-His [Bachem], His-Val [Bachem], His-Ile [Bachem], L-homocarnosine [Sigma], Hydrogen chloride [Merck], Ile-His [Bachem], Imidazole [USB], IPTG [GeneMark, Taiwan], Kanamycin sulfate [USB], LB Broth (Miller) [DIFCO], Leu-His [Bachem], Methanol [Merck], Oligonucletide Primers [BioBasic Inc.], Potassium chloride [Merck], Potassium diphosphate [Merck], Ser-His [Bachem], Sodium chloride [AMRESCO], Sodium hydroxide [Merck], SYBR® Green I [Roche], TEMED [GE Healthcare], Tris base [Merck], Tyr-His [Bachem], Val-His [Bachem], X-gal [GeneMerck, Taiwan], Yeast Extra [DIFCO].

(3) Kits: The following experimental kits were used in this study. BCA Protein Assay Reagent and Albumin Standard [PIERCE], GFX™ PCR DNA and Gel Band purification Kit [GE Healthcare], Plasmid Miniprep Purification Kit [GeneMark], QIAamp DNA Mini Kit [Qiagen], TOPO TA Cloning® Kit [Invitrogen], Plasmid Miniprep Purification Kit [GeneMark].

(4) Equipments: The following instruments were used in this thesis: ABI PRISM® 3100 Genetic Analyzer [Applied Biosystems], Amicon® Ultra [Millipore], Centrifuges 5415R [eppendorf], Electrophoresis Power Supply EPS 301 [GE Healthcare], Fluoroskan Ascent FL Microplate Reader [Thermo], GeneAmp® PCR System 9700 Thermal Cycler [Applied Biosystems], High-Performance Liquid Chromatography (HPLC) [Agilent], Kodak Electrophoresis Documentation an Analysis System 120 [Kodak], Mighty Small

II for 8×7 cm gels electrophoresis instruments [GE Heathcare], Millex®-GS 0.22 μm Filter Unit [Millipore], Millex®-GS 0.45 μm Filter Unit [Millipore], Multiskan Ascent Microplate Reader [Thermo], Steritop™ 0.22μm Filter Unit [Millipore], Ultrasonic Processor VCX 500/750 [Sonics], UV-visible spectrometer [Amersham Biosciences].

(5) Reagents

Ampicillin stock solution (100mg/mL):

Dissolve 1 g Ampicillin sulfate in 10 mL double distilled water (ddH_2O). Filter it through a 0.22 μm pore size filter and stock it at -20°C.

Destain buffer I:

Mix 400 mL methanol, 100 mL acetic acid and distilled water (dH_2O) to 1 L. Store at room temperature.

Destain buffer II:

Mix 50 mL methanol, 120 mL acetic acid and dH_2O to 1 L. Store at room temperature.

6 X DNA loading dye:

0.25% Bromophenol blue and 30% glycerol in ddH_2O. Store at -20 °C.

IPTG stock solution:

Dissolve 4.086 g IPTG in 10 mL ddH_2O. Filter through 0.22 μm pore size filter and store at -20 °C.

Kanamycin stock solution:

Dissolve 250 mg kanamycin sulfate in 10 mL ddH_2O. Filter through 0.22 μm pore size filter and store at -20 °C.

LB medium:

25 g LB Broth was dissolved in 1 L ddH_2O and sterilized.

LB plate:

25 g LB Broth and 20 g Bacto™ Agar was dissolved in 1 L ddH_2O and sterilized. The sterile solution was poured and dispersed in Petri dishes before coagulation.

OPA reagent (for enzymatic activity assay):

Dissolve 50 mg OPA in 5 mL methanol first and then mix with 20 mL borate buffer. The borate buffer was mixed by 0.2 M boric acid (dissolved in 0.2 M potassium chloride solution) and 0.2 M sodium hydroxide solution (50 : 50, v/v).

10 X SYBR Green solution:

10,000 X SYBR® Green I was diluted to 10 X with DMSO. Store it under darkness.

50 X TAE buffer:

Add 242 g Tris-base, 57.1 mL Acetic acid, and 0.5 M EDTA into 800 mL ddH_2O. Adjust the total volume into 1 L and pH value into pH 8.5. Store it at room temperature. Dilute the concentration to 1 X with ddH_2O. Adjust the pH value to 7.5~7.8 before utlization.

X-gal stock solution:

Dissolve 400 mg X-gal in 10 mL dimethylformamide (DMF) and store in the darkness at -20 °C

2.2 Experimental methods

2.2-1 Site-directed mutagenesis of *V. alginolyticus pepD*

Site-directed mutagenesis of the *V. alginolyticus pepD* gene was carried out using the Stratagene QuikChange site-directed mutagenesis kit (Agilent Technologies, Inc., Santa Clara, CA). Mutagenesis primers were designed for use with the pET-28a(+)-pepD plasmid (wild-type) template (Appendix 1). The PCR reaction was carried out via the nonstrand-displacing action of *pfuTurbo* DNA polymerase to extend and incorporate the

mutagenic primers, resulting in the nicked circular strands. The PCR products with wild-type and mutant plasmids were incubated with *Dpn I* for 4 hrs at 37 °C to selectively digest the methylated non-mutated parental wild-type plasmids. After *Dpn I* digestion, the mutant plasmids were transformed into *E. coli* XL-1 Blue competent cells, with selection for kanamycin resistance. Mutations were confirmed by restriction enzymes and DNA sequencing. The recombinant mutant plasmids were transformed into *E. coli* BL21(DE3) competent cells for expression of the mutated PepD proteins.

2.2-2 Construction of the truncated *V. alginolyticus pepD* catalytic domain gene

The truncated *V. alginolyticus* PepD catalytic domain gene ($pepD^{CAT}$) was composed of the *pepD* gene sequence of nucleotides 1-558 and 1203-1470. An 826-bp fragment, which included 558 bp of the 5'-end and 268 bp of the 3'-end of the *pepD* gene, was amplified by PCR using the following primer pairs: CYC-PepD-BamHI-1 (sense primer, 5'-CGGGATCCGTGTCTGAGTTCCATTCTG-3') and CYC-PepDcat-4 (antisense primer, 5'-TCCAGCCTGGTCCTGCACAACCCATGTACAC-3') and by CYC-PepDcat-3 (sense primer, 5'-TGGGTTGTGCAGGACCAGGCTGGAAACCAGATG-3') and CYC-PepD-XhoI-2 (antisense primer, 5'-CGCTCGAGTTACGCCTTTTCAGGAATG-3'). The PCR product was subcloned into pET-28a(+)-$pepD^{CAT}$, which was then transformed into *E. coli* BL21(DE3) pLysS competent cells for the production of the PepD catalytic domain protein ($PepD^{CAT}$).

2.2-3 Expression of the *V. alginolyticus pepD* gene, mutant *pepD* gene and truncated *pepD* gene in *E. coli*

The wild-type PepD, mutant PepD and PepD^{CAT} proteins were produced in the same manner. Colonies grown on an LB plate were inoculated into LB broth supplemented with 50 μg/mL of kanamycin and grown at 37 °C until A_{600} of 0.5-0.6 was reached. At this point, protein production was induced by the addition of isopropyl thio-β-D-galactoside to a final concentration of 0.5 mM, and the culture was incubated at 37 °C for an additional 4 hrs before harvest. The cells were collected by centrifugation and then resuspended in 15 mL of 20 mM Tris-HCl (pH 7.0) buffer containing 0.5 M NaCl. The mixture was sonicated, and the cell debris was removed by centrifugation at 11,000 ×g for 30 min at 4 °C.

2.2-4 Portein purification of wild-type PepD, mutant PepD and PepD^{CAT}

The wild-type PepD, mutant PepD and PepD^{CAT} proteins were purified in the same protocol. The supernatant containing recombinant protein was loaded onto a Ni-Sepharose^{TM} 6 Fast Flow column previously prepared by washing with 10 column volumes of buffer A (20 mM Tris-HCl, 0.5 M NaCl, pH 7.0) containing 20 mM imidazole. The protein-loaded column was first washed with 5 column volumes of buffer A + 20 mM imidazole, then with 5 column volumes of buffer A containing 70, 200, or 500 mM imidazole. Fractions of 1 mL each were collected, and the protein concentration in each fraction was determined using the PIERCE BCA Protein Assay Reagent with BSA as the standard. In addition, the eluted fractions were collected for SDS-PAGE analysis and enzymatic activity assay. By SDS-PAGE analysis, the high-purity eluted fractions were collected and dialyzed with 2 L of 50 mM Tris-HCl

(pH 7.0) buffer for 2 hrs, followed by 3 L buffer for 8 hrs. After enzymatic activity assay, the purified recombinant proteins were stored at -80 °C for up to 6 months without loss of activity.

2.2-5 Protein concentration determination

The protein concentrations of purified proteins were measured using BCA Protein Assay Reagent. To each well of the F96 MicroWell™ plate was added a 20 μL sample mixed with 200 μL BCA™ Working Reagents (BCA™ Reagent A : BCA™ Reagent B = 50 : 1). The reactions were incubated at 37 °C for 30 min in the dark. The absorbances of samples were measured at 562 nm on a Multiskan Ascent Microplate Reader. 2 mg/mL bovine serum albumin (BSA) stock and successive dilutions (1.5, 1.0, 0.75, 0.5, 0.25, 0.125, 0.025 mg/mL) served as standards, following the same procedure described above.

2.2-6 SDS-PAGE and Native-PAGE analysis

After protein purification, gel electrophoresis was used to confirm for protein expression level, purity, and molecular weight. The samples were separated by sodium dodecyl sulfate polyacrylamide gel electrophoresis (SDS-PAGE) on 12.5% gels. Each 10 μL sample was mixed with 2 μL 5X SDS-PAGE sample buffer and incubated at 95ºC for 5 min to denature proteins. Electrophoresis was performed with 1X SDS-PAGE running buffer at 90 Volts for 30 min, followed by 120 Volts for 1.5 hrs. The SDS-PAGE gel was stained with a stain buffer containing Coomassie Brilliant blue R-250 for 30 min and destained with destain buffer I (methanol/acetic acid/water = 4:1:5, v/v/v) for 20 min, followed by destain buffer II (methanol/acetic acid/water = 1.2:0.05:8.75)

overnight.

Native-PAGE was performed to examine the native form of PepD. The purified and dialyzed protein fractions were separated by Native-PAGE on 7.5% gels. The experimental steps were similar to SDS-PAGE analysis, except that the gel contained no SDS and there was no denaturing treatment. Each 10 μL sample was mixed with 2 μL 5X Native-PAGE sample buffer, and immediately followed by an iced 1X Native-PAGE running buffer at 90 Volts for 3 hrs in a 4ºC circulating water bath. The proteins were stained and destained in the same way as for SDS-PAGE analysis.

2.2-7 Enzymatic activity assay of PepD

PepD activity assay was according to a method described by Teufel *et al*[15]. on the basis of measurement of histidine derived with o-phthaldialdehyde (OPA) (Fig. 2.1). The reaction was initiated by addition of substrate and stopped by adding trichloroacetic acid (TCA) after 15 min incubation at 37 °C. Histidine was produced from the substrate hydrolyzing by the enzyme. Then, fluorescence of OPA-derived L-histidine was measured using Fluoroskan Ascent FL (λ_{Exc}: 355 nm and λ_{Em}: 460 nm). The reaction with L-histidine and L-carnosine only solution were treated in the same way to serve as the positive and negative control, respectively. All reactions were carried out in triplicate.

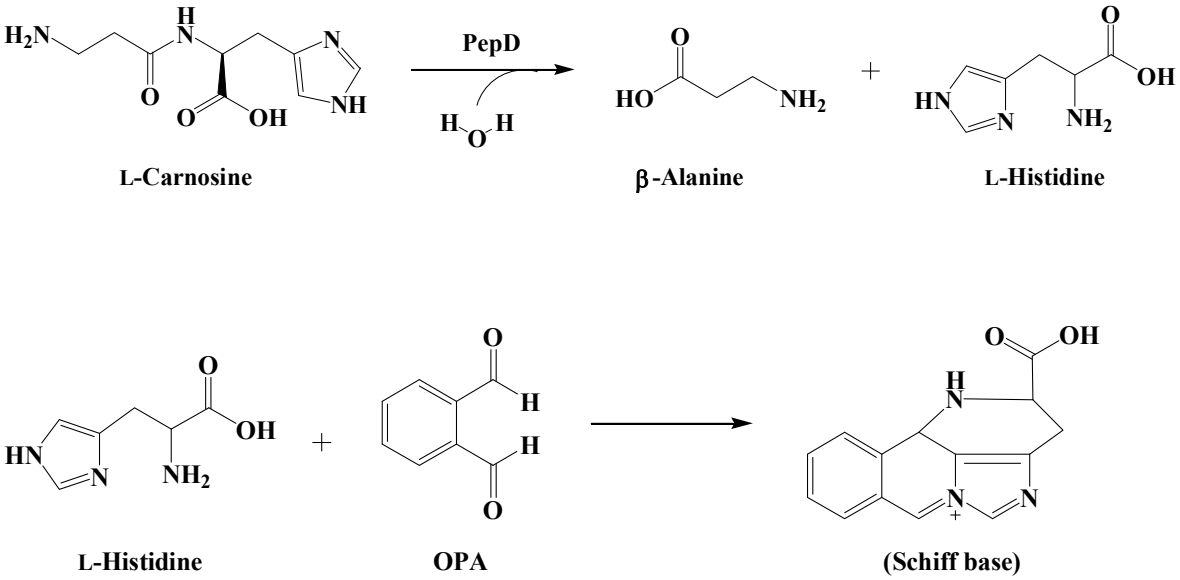

Figure 2.1. Formation of a Schiff base by L-histidine and o-phthalaldehyde.

2.2-8 Enzyme kinetics

For determination of V_{max}, K_m, and k_{cat} of *V. alginolyticus* PepD wild-type and mutant proteins, the method described by Csámpai *et al.* was slightly modified for use with High Performance Liquid Chromatography (HPLC) and fluorescence detection. A system consisting of an Agilent 1100 Series Quaternary pump, Autosampler, Fluorescence Detector and Inertsil ODS-3 (7 μm, 7.6 mm×250 mm) column was used. The eluent system consisted of two components: eluent A was 0.05 M sodium acetate at pH 7.2, while eluent B was prepared from 0.1 M sodium acetate–acetonitrile–methanol (46:44:10, v/v/v) (titrated with glacial acetic acid or 1 M sodium hydroxide to pH 7.2). The gradient program was as described in Table 2.1. The fluent flow-rate was 0.8 mL/min at 30 ºC.

Table 2.1: The fluent gradient program

Step	Time (min)	A (%)	B (%)
1	0	100	0
2	5	50	50
3	15	25	75
4	20	0	100

Different concentrations of L-carnosine (0.25, 0.5, 1, 1.5, 2, 5, and 10 mM) were added as to a nanomolar concentration of enzyme solution in 200 μL at pH 7.0 for 20 min at 37 °C. The liberated histidine was derivatized with 100 μL OPA reagent for 5 min at 37 °C, and the fluorescence was detected as described previously. Fluorescence of the histidine with derivatized OPA was measured by FLD (λ_{Exc}: 355 nm and λ_{Em}: 460 nm). Various concentrations of L-histidine solution derivatized with OPA reagent were detected, using the method described above, to serve as standards. The data collected were applied to the Lineweaver-Burk equation. The k_{cat}/K_m values reflect values assuming 100% activity of the enzyme preparation.

2.2-9 Circular dichroism (CD) spectroscopy

The secondary structure of the wild-type and the mutant PepD proteins were confirmed by monitoring CD spectra. The protein sample concentration was 0.2 mg/mL in 50 mM Tris-HCl, pH 7.0 buffer. The CD spectra were recorded every 1 nm between 200 to 300 nm wavelength used a quartz cuvette of 1 mm path-length in a Jasco J-715 spectropolarimeter, Only 50 mM Tris-HCl, pH 7.0 buffer was as the control. The results were scanned 4 times and averaged. Converted the data into mean residue ellipticity (MRE) by using the equation : $〔\theta〕_{MRE} = (MRW \times \theta_{obs}/c \times d)$. θ_{obs} is the observed ellipticity (in millidegrees) at the respective wavelength, MRW is the mean residue of

the enzyme (MRW = M/n, M = 53548.8 g/mole, n = 490 amino acid residues), d is the cuvette path-length in cm, and c is the protein concentration in mg/mL.

2.2-10 Analytical sedimentation velocity ultracentrifugation

Sedimentation velocity is an analytical ultracentrifugation (AUC) method that measures the molecular moved rate for providing both the molecular mass and the shape of molecules. This technique can distinguish the native state of the protein in either a monomer, dimmer, or even tetramer form. The data were evaluated according to the g*(s) method developed by Walter Stafford. Since the g*(s) analysis yields both the sedimentation coefficient s from the peak of the curve, the apparent molecular weight can also be determined. Depending on the application and optical system, the protein concentration ranging 0.1 mg/mL to 0.5 mg/mL was used and the sample volume was about 500 μL. Sample was equilibrated with 20 mM Tris-HCl pH 7.0 buffer and this equilibrated buffer was used as another reference control into the reference sector. The sedimentation velocity analysis was performed at National Tsing Hua University.

2.2-11 Crystallization and data collection of PepD crystals

Crystallization of PepD was performed at 291 K by the hanging-drop vapor-diffusion method against a reservoir solution containing PEG 400 (28%, v/v), 0.2 M $CaCl_2$ and 0.1M Na-HEPES buffer (pH 7.5), Crystals of a diamond shape appeared within six months and grew to maximum dimensions of 0.3 × 0.2 × 0.1 mm^3. The protein crystals were transferred to the cryo protectant solution containing glycerol (15%, v/v) prior to the X-ray diffraction experiment. Diffraction data were collected to 3.0 Å resolution on SPXF beamline BL13B1 at the National Synchrotron Radiation Research

Center (NSRRC) in Taiwan and beamline BL12B2 at SPring-8 in Japan. The data were processed using the *HKL2000* suite[79]. The redundancy independent merging *R* factor ($R_{r.i.m.}$) and the precision indicating merging *R* factor ($R_{p.i.m.}$) were calculated using the program *RMERGE*[80, 81]. The crystals belong to space group $P6_5$ with unit cell parameters a = 80.42 Å and c = 303.11 Å. The asymmetric unit contained two protein molecules, corresponding to a solvent content of 53.4%.

2.2-12 Structure determination and refinement

The structure was solved by molecular replacement with *MOLREP* (*CCP4*) using the structure of Xaa-His dipeptidase from *Haemophilus somnus* 129PT (PDB code 2QYV) as the search model. The orientation of the lid domain was first located and fixed, subsequently leading to the determination of the relative position of the single catalytic domain. For structural refinement, the model was built using *WinCOOT* and refined using *REFMAC5* (*CCP4*) to give the final R_{work} = 0.231 and R_{free} = 0.274[82], respectively. The Ramachandran results were determined using *MOLPROBITY*, and the percentage of residues in favored, allowed, and disallowed were 94.5, 98.6, and 1.4%, respectively[83]. The structure found to have good stereochemistry was fully defined from Glu3 to Glu488, with all main chain angles in the most favorable or generally allowed regions[84]. All figures were produced using PyMOL. The atomic coordinates and structure factor data have been deposited in the Protein Data Bank (www.rcsb.org): PDB ID codes 3MRU.

2.2-13 Substitution of zinc ions by copper ions to form CuCu-PepD

PepD protein first was dialyzed overnight with 50 mM Tris-HCl buffer at pH 7.5 containing 200 mM NaCl and 10 mM EDTA to remove divalent zin ions (apo-PepD). The apo-PepD was dialyzed twice with the same buffer but without EDTA and exchanged with 50 mM Tris-HCl buffer at pH7.5 before adding 2mM $CuCl_2$. After dialyzing overnight, the pooled CuCu-PepD protein then were dialyzed with a 50 mM Tris buffer (pH7.0) and stored at -20 °C.

2.2-14 Oxidative activity assay of CuCu-PepD

Oxidation of various catechol derivatives by CuCu-PepD were determined via the measurement of the products of *o*-quinone moiety (Fig. 2.2A). The oxidative products of dopamine, L-dopa, epinephrine and norepinephrine, which would be tautomerized to from the aminechrome derivertives (Fig. 2.2B) were detected at λ_{max}: 480 nm, 475 nm, 475 nm and 490 nm, respectively.

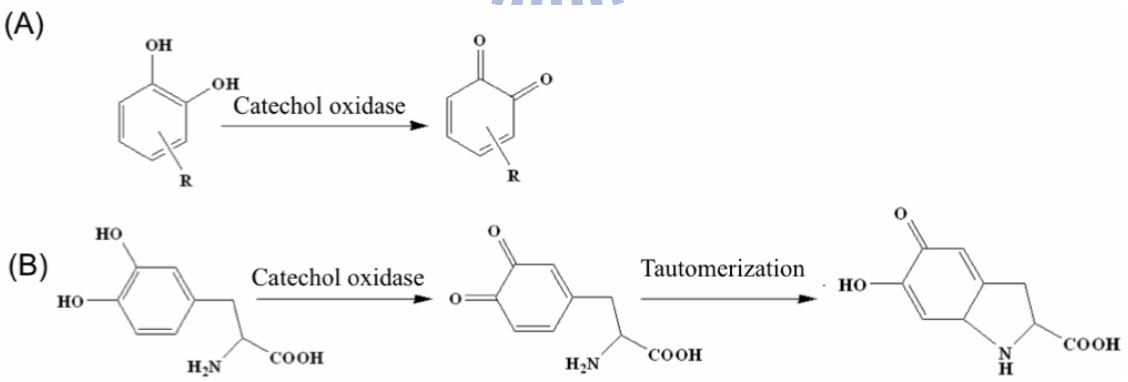

Figure 2.2. Enzyme function of catechol oxidase. (A) Oxidation of catechol derivatives by catechol oxidase to form *o*-quinone moieties. (B) Overall reaction catalyzed by catechol oxidase with the substrate L-dopa. L-dopa undergoes oxidation to dopaquinone. Tautomerization of the dopaquinone ring by intramolecular nuclerophilic attck results in the formation of dopachrome.

100 μL CuCu-PepD protein (1 mg/mL) and 900 μL 50 mM Tris buffer at pH 7.0 reacted with 2 mM substrates (catechol derivatives) at room temperature over 30 min. The reactions containing only buffer with the substrates as negative controls. The absorbances of products were measured at the individual absorption wavelengths on a UV-visible spectrometer. All reactions were carried out in triplicate.

2.2-15 Kinetic analysis of CuCu-PepD for oxidative activity

For determination of $V_{max,}$ K_m, and k_{cat} of the CuCu-PepD, the oxidation kinetics were performed by the method described by Chen *et al*.[85]. The activity were determined at room temperature by following the increasing absorbance (dopamine: 480 nm; L-dopa: 475 nm; epinephrine: 475 nm; norepinephrine: 490 nm) accompanying the oxidation of the substrate with the molar absorption coefficient (dopamine: 3300 $M^{-1}cm^{-1}$; L-dopa: 3700 $M^{-1}cm^{-1}$; epinephrine: 4020 $M^{-1}cm^{-1}$; norepinephrine: 3580 $M^{-1}cm^{-1}$). Therefore, substitution of absorbance value and molar absorption coefficient into the equation, $\Delta A = \varepsilon \times b \times \Delta c$, where A refers to absorbance change per minute (ΔA/min), b is the light path length through the cuvette (1 cm), ε is the molar absorption coefficient for the product, and c is the change of concentration of product. The assay system was 1 mL containing 50 mM Tris buffer at pH 7.0, 0.1-5 mM substrate, and 0.925 μM CuCu-PepD at room temperature for 20min. For each substrate prepare a Michaelis-Menten curve (μmolar product/min versus mmolar substrate) and a Lineweaver-Burk plot. Absorption and kinetic measurements were carried out using a UV-visible spectrometer.

2.2-16 Protein-ligand docking of CuCu-PepD for catechol derivatives

Docking is one of the useful tool to investigate the interaction between protein and ligand, protein and protein, and protein and DNA. Here, protein-ligand docking was carried out by the docking program – GOLD which was applied from National Center for High-Performance Computing (NCHC). We used the crystal structure of PepD (PDB code: 3MRU) as template, and the coordinates of ligands were download from PubChem. Firstly, the PepD template was hydrogenation. Secondly, the ligand was defined around the Zn2 within 10 Å. Then, "restrict atom selection to solvent-accessible surface" and "force all H bond donors/acceptors to be treated as solvent accessible" were selected. Scoring function was selected for "ChemScore", and parameter file was selected for "kinase.params". The program could be early termination, and used the internal ligand energy offset. After running the docking program, the protein-ligand binding states were ranked according to more stable energy. The interactions between proteins and ligands were shown by Pymol program.

CHAPTER 3

Results and Discussion

3.1 Expression, purification, and crystallization of *V. alginolyticus* PepD, and X-ray data collection of the PepD crystals

The *V. alginolyticus* PepD protein was overexpressed in *E. coli* BL21(DE3)pLysS and subsequently purified by Ni-NTA resin. SDS-PAGE analysis of the purified PepD showed a single band with a molecular mass of ~54 kDa (Fig. 3.1A). The purified PepD was crystallized using the hanging-drop technique. Diamond-shaped crystals of sufficient and appropriate size for effective crystallization appeared within two weeks under conditions of 100 mM Na-HEPES buffer at pH 7.5, 28% (v/v) PEG-400 and 200 mM $CaCl_2$. The crystals grew to maximum dimensions of 0.3 × 0.2 × 0.1 mm^3 (Fig. 3.1B).

The protein crystals exhibited sensitivity to changes in precipitant concentration that occurred upon transfer to the cryo protectant solution containing 15% (v/v) glycerol. Good-quality crystals were carefully screened and selected for data collection, since they frequently possessed fairly high mosaicities (>1°). The crystals produced diffraction data to 3.0 Å resolution on beamtime BL21B2 at SPring-8. Analysis of the diffraction pattern revealed that the crystals exhibited hexagonal symmetry; systematic absences indicated the space group to be $P6_1$ or $P6_5$. The unit-cell parameters were a = b = 80.42 Å, and c = 303.11 Å. When we assumed the presence of two molecules in the asymmetric unit and a molecular mass of 54 kDa, the calculated solvent content was 53.4% and the Matthews coefficient (V_M) was 2.63 $Å^3\ Da^{-1}$ [86], both of which are within the normal range for

protein crystals. The statistics of the collected data are summarized in Appendix 2.

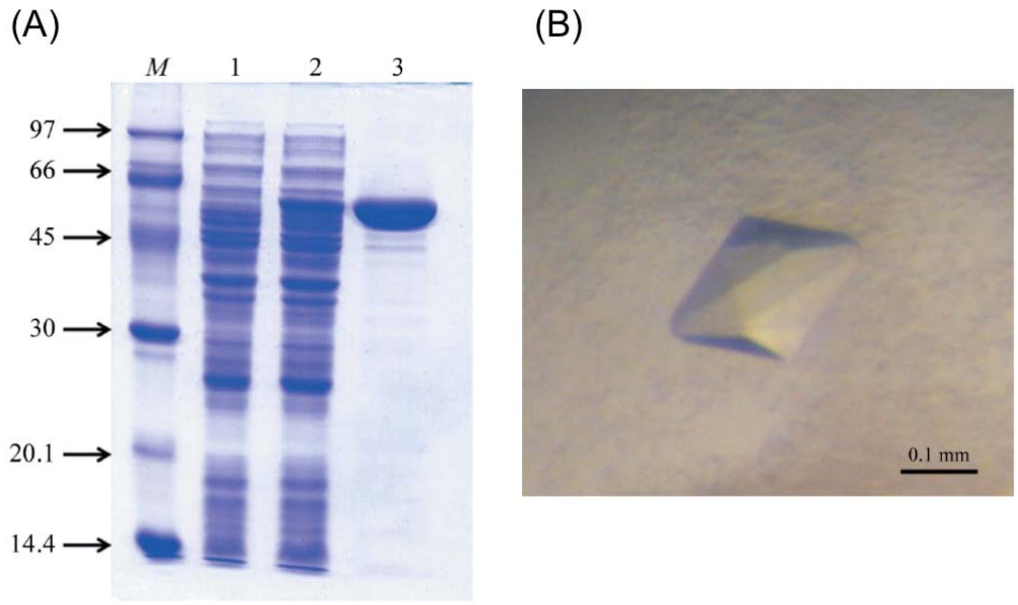

Figure 3.1. Crystallization of *V. alginolyticus* PepD by the hanging-drop method. (A) 12.5% SDS-PAGE of the purified *V. alginolyticus* PepD protein applied to crystallization conditions in the hanging-drop method. Lane M, marker proteins (kDa): phosphorylase b (97 kDa), bovine serum albumin (67 kDa), ovalbumin (45 kDa) and carbonic anhydrase (30 kDa). Lane 1, crude cell extracts of *E. coli* BL21(DE3)pLysS carrying the pET-28a(+) plasmid. Lane 2, crude cell extracts of *E. coli* BL21(DE3)pLysS carrying the pET-28a(+)-pepD plasmid. Lane 3, purified PepD from the Ni-NTA column. (B) A single crystal of *V. alginolyticus* PepD.

3.2 The crystal structure of *V. alginolyticus* PepD

3.2-1 Overall structure

The crystal structure of *V. alginolyticus* PepD was solved by the molecular replacement method using the structure of Xaa-His dipeptidase from *Haemophilus somnus* 129PT (PDB code 2QYV) as the search model (sequence identity: 50.9%). The 2QYV was solved and deposited with the PDB by the Joint Center of Structure Genomics (JCSG), but was not yet published. The structure of PepD was then refined to a resolution of 3.0 Å with an *R* factor of 23.1% and an R_{free} factor of 27.4% (Apprndix 2).

The overall structure of the PepD monomer was determined to be comprised of a total of 486 residues in two domains: a catalytic domain harboring two zinc ions for catalysis and a lid domain functioning in substrate recognition and protein dimerization (Fig. 3.2A). Analysis of the X-ray absorption measurement and electron density map confirmed the presence and locations of the di-Zn^{2+} ions held captive in the catalytic domain (Fig. 3.3). The high *B*-factors that were obtained were presumed to reflect the flexible open conformation of the catalytic and lid domains. Upon comparison with PepV and other related di-zinc-dependent M20/M28 family members, PepD was found to share similar structural folds, despite the low sequence similarities that exist among each. PepD and PepV showed root mean square deviations (rmsd) of 4.0 and 4.3 Å for Cα atoms of the catalytic and lid domains, respectively (Appendix 3).

In addition, two asymmetric unit of PepD having dimensions of ~90 × 90 × 95 Å was determined to be two PepD molecules packed together as a dimer (Fig. 3.2B). The apparent dimeric and monomeric characteristics of native and denatured PepD were further supported by evidence from analytical ultracentrifugation, which revealed

molecular masses of 100.7 and 51.1 kDa under physiological and denatured conditions, respectively (Appendix 4). The lid domain was found to utilize a hydrogen bonding network between helices from each monomer in order to form the dimer interface. PepD was determined to exist as a dimer, similar to the related di-zinc-dependent enzymes of the M20/M28 family, but different from PepV which uniquely exists as a monomer.

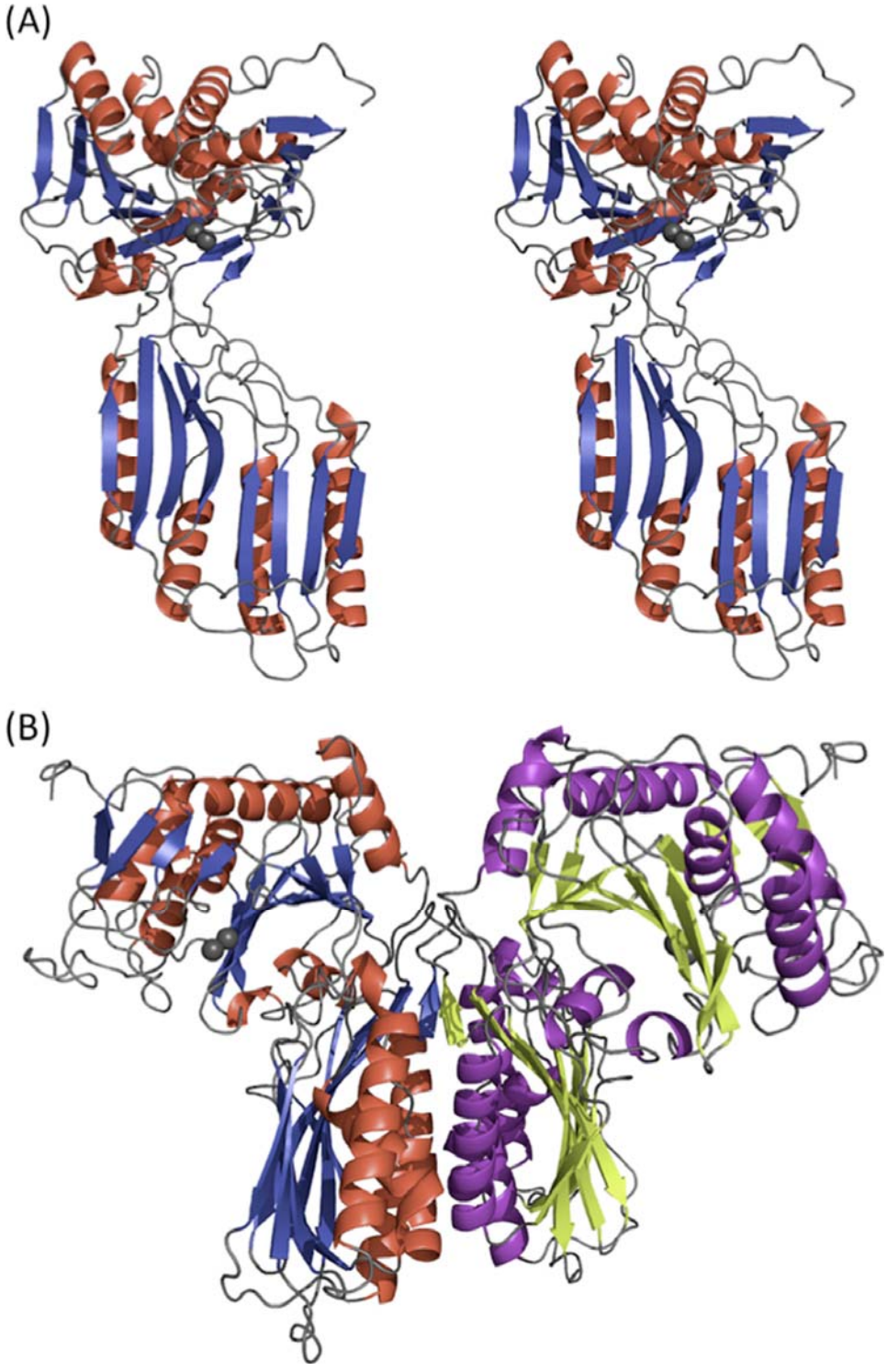

Figure 3.2. Overall structure of *V. alginolyticus* PepD. (A) Stereo view of a subunit of *V. alginolyticus* PepD. Secondary structure elements are shown in *red* (α-helices) and *blue* (β-strands). *Gray spheres* represent the zinc ions. (B) Ribbon diagram of the PepD dimer. The same color scheme in (A) was used for the left subunit, and the right subunit was distinguished by *purple* (helices) and *green* (strands).

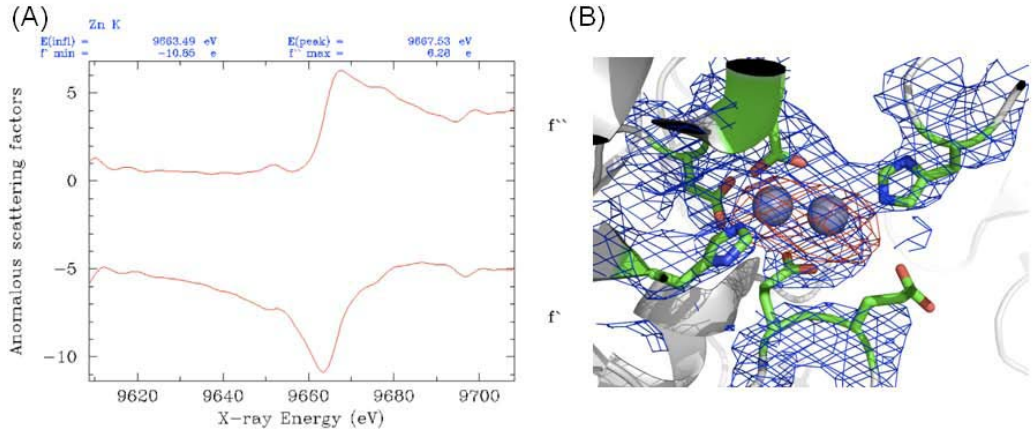

Figure 3.3. Determination of the PepD zinc ions. (A) The absorption spectra of anomalous scattering factors for zinc ions in PepD are presented as a function of X-ray energy. (B) The electron density map of PepD zinc ions binding site is presented as part of a composite-omit map contoured at 1.0 σ (*blue*), and anomalous difference Fourier map contoured at 4.0 σ (*red*).

3.2-2 The catalytic domain

Comparative analysis of the PepD catalytic domain indicated that it has a fold similar to those of PepV and the related di-zinc-dependent M20/M28 family of enzymes, including CPG_2, βAS, mouse CN2, PepT, *Ap*AP and *Sg*AP[26, 29, 32, 35, 87, 88]. The topology of PepD and PepV is illustrated in Fig. 3.4. The catalytic domain consists of residues 1–186 and 401–490 and has a mixed three-layer α/β/α-sandwich architecture composed

of two β-sheet groups and seven α-helices (Fig. 3.5). The large sheet group contains eight strands arranged in the order a-b-f-c-g-j-h-i, in which b is the only antiparallel strand. The small sheet group is composed of four shorter antiparallel strands arranged in the order of d-e-l-k and located on the surface of the catalytic domain. The zinc ions are located at the C-terminal end of the four central parallel strands.

The active site was found to be located within a deep cleft that formed between the lid and the catalytic domain (Fig. 3.2). In the dimer, the two active sites are ~57 Å apart, suggesting that each protomer can function independently. No distinct zinc-bound water molecule was found in our structure analysis; however, a higher electron density peak was observed with the closest zinc-water contact of 2.5 Å. The absence of the zinc-bound water molecule could be a reflection of the relatively limited resolution of the data. The N- and C-termini are both located at the top of the catalytic domain, opposite to the lid domain and the active site.

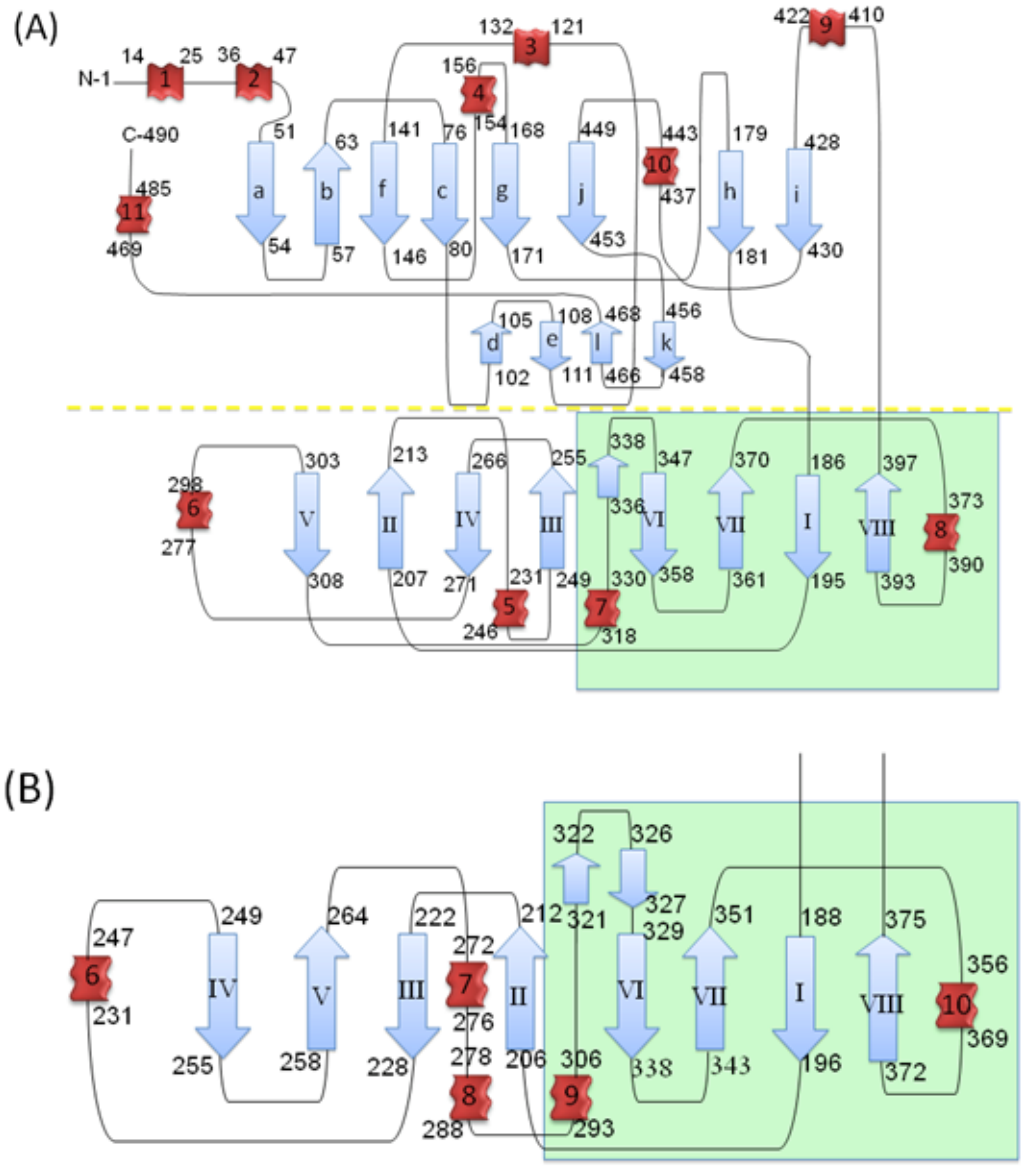

Figure 3.4. Topological diagrams of (A) *V. alginolyticus* PepD and (B) the lid domain of *L. delbrueckii* PepV. The secondary structural elements of α-helices and β-strands are represented by *ribbons* and *arrows*, respectively. The diagram (A) has been divided into two parts, separated accordingly by the *dotted line*; the region with *gray* in the lid domain represents the extra domain.

(A)

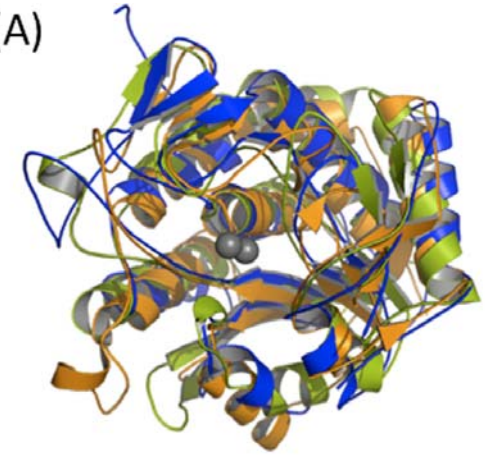

(B)

```
PepD   1  ----------------------------MSEFHSEISTLSPAPLWQFFDKICSIPHPSKHE---- 33
PepV   1  --------------------------MDLNFKELAEAKKDAILKDLEELIAIDSSEDLENATEEYP 40
CPG2   1  MRPSIHRTAIAAVLATAFVAGTALAQKRDNVLFQAATDEQPAVI-KTLEKLVNIETGTGDA---- 60

PepD  34  ------EALA---QYIVTWATEQGFDVRR--DPTGNVFIKKPATPGMENK--K-GVVLQAHIDMV 84
PepV  41  VGKGPVDAMT---KFL-SFAKRDGFDTENFANYAGRVNFGA------GDK--RLGII--GHMDVV 91
CPG2  61  ------EGIAAAGNFLEAELKNLGFTVTR--SKSAGLVVGDNIVGKIKGRGGK-NLLLMSHMDTV 116

PepD  85  PQKNEDTDHDFTQDPIQPYIDGEW-VTAKGTTLGADNGIGMASCLAVLASKEIK------HGP-- 140
PepV  92  PAGEGWTRD-----PFKMEIDEEGRIYGRGSA--DDKGPSLTAYYGMLLLKEAG------FKPKK 143
CPG2 117  YLKGI-----LAKAPFR--VEGD---KAYGPGIADDKG-GNAVILHTL--KLLKEYGVRDYGT-- 166

PepD 141  -IEVLLTIDEEAGMTGAFGLEAGWLK-G----DILLNTDSEQEGEVYMGCAG------ 186
PepV 144  KIDFVLGTNEE---TNWVGIDY-YLK-HEPTPDIVFSPDAEYPIINGEQE--PHYV-- 193
CPG2 167  -ITVLFNTDEEKGSFGSRDLIQEEAKLA----DYVLSFEPTSAGDEKLSLG-TAFNAG 218

PepD 401  PGWKPDADSEIMAIFRDMYEGIYGHKPNIMVIHAGLECGLFKEPYPNMDMVSFGPTIKF------ 459
PepV 386  ----PGSDPMVQTLLK-VYEKQTGKPGHEVVIGGGTYGRLFERG------VAFG-AQPENGPMVM 438
CPG2 331  ------EGGKKLVDKAVAYYKEAGGTLGVEERTGGGTDAAYAALSGKPVIESLGLPGFG------ 383

PepD 460  PHSPDEKVKIDTVQLFWDQMVALLEAIPEKA----- 490
PepV 439  -HAANEFMMLDDLIL---SIAIYAEAIYELTKDEEL 470
CPG2 384  YHSDKAEYVDISAIPRRLYMAARLIMDLGAGK---- 415
```

Figure 3.5. Comparisons of catalytic domains from PepD, PepV and CPG_2. (A) Superposition of catalytic domains from PepD (*blue*), PepV (*orange*), and CPG_2 (*yellow green*) after optimal fit. The zinc ions of PepD are depicted by two *gray spheres*. (B) Structure-based sequence alignment of the three catalytic domains. The sequence corresponding to the α-helices and β-strands are highlighted in *orange* and *blue*, respectively. The conserved metal ion binding residues are highlighted in *red*. Each of the three catalytic domains has the same di-zinc binding residues, with the exception of Glu^{200} in CPG_2.

Biochemical studies of *V. alginolyticus* PepD revealed its metal-dependent characteristics. Optimal activation of apo-PepD was observed with various divalent metal ions, including Mn^{2+}, Co^{2+}, Ni^{2+}, Cu^{2+}, and Cd^{2+}. Previous studies have shown that addition of Co^{2+} ions to apo-PepD can sufficiently augment the enzymatic activity by a factor of ~1.4 over that of the wild-type PepD containing Zn^{2+}. The fact that the simultaneous presence of the Zn^{2+} ions did not inhibit the Co^{2+}-loaded PepD activity indicates that the metal-binding cavity can not only accommodate forced ion loading but can retain functionality. On the other hand, when the Zn^{2+} ions were substituted for Mg^{2+} ions, the enzyme retained ~80% of its optimal activity.

We confirmed the presence and locations of zinc atoms by X-ray absorption and electron density map performed at beamline 13B1 (Fig. 3.3). The di-zinc center was located on the surface of the cleft between the catalytic and lid domains, suggesting it is solvent-accessible. Further analysis of the PepD crystal structure also revealed that several functional residues interact with one another to fix the two zinc ions (Zn1 and Zn2) in place, separated by a distance of 2.8 Å (Fig. 3.6). Zn1 was found to be coordinated by Nε2 from His^{461}, one of the carboxylate oxygens of Asp^{119}, and by a single putative water molecule bound via hydrogen bonding to the carboxylate group of Glu^{149}. Zn2 was found to be coordinated by Nε2 of His^{80}, the other carboxylate oxygen of Asp^{119}, and by two carboxylate oxygens of Asp^{173}. Asp^{119} appeared to be positioned as a bridging ligand between the two zinc ions. Notably, this residue is connected to an asparagine via a *cis* peptide bond, identical to the structure that has been observed in many of the other di-zinc-dependent enzymes of the M20/M28 family, including PepV and CPG_2 (Appendix 5). This particular peptide bond can break the α-helix at the N-terminal end in order to facilitate closer positioning of the Asp-Asn dipeptide and presumably modulate subsequent enzyme activity.

The orientation of the side chain carboxylate group of Glu^{150} was noted to differ between the active-site center of PepD and that of the related M20/M28 family metallopeptidases. In PepV, the two carboxylate oxygens of Glu^{154} point inward to Zn1 at a distances of 1.9 and 2.6 Å, respectively; in PepD, however, the two carboxylate oxygens of Glu^{150} point away from Zn1, increasing the distance between the carboxylate oxygen and Zn1 to 4.5 Å. Thus, the particular role played by Glu^{150} for metal ion binding in PepD remains ambiguous.

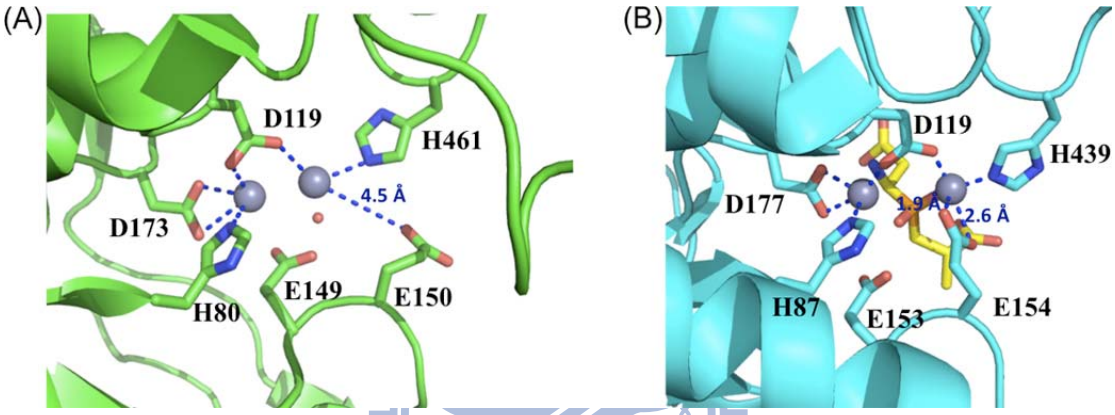

Figure 3.6. Comparison of the active sites in *V. alginolyticus* PepD and structural homologs. (A) Local view of the di-zinc center of PepD. The residues involved in coordination of Zn1 and Zn2 (*gray spheres*) are shown as *green sticks*. The putative water molecule is depicted by a *red dot*. Asp^{119} of PepD serves as a bridging ligand for metal coordination. (B) Local view of the di-zinc center of PepV. The residues involved in metal coordination are shown as *cyan sticks*, and the phosphinic inhibitor (AspΨ[PO_2CH_2]AlaOH) is represented by *yellow sticks*.

3.2-3 The lid domain

The lid domain of PepD consists of 214 residues (187–400) between strands *h* and *i* of the β-sheet in the catalytic domain (Fig. 3.4A). The lid domain folds into a central eight stranded antiparallel β-sheet, flanked on one side by four α-helices packed in

alternating orientations (Fig. 3.7). The antiparallel β-sheets are arranged in the order of V-II-IV-III and VI-VII-I-VIII, respectively (Fig. 3.4A). Interestingly, the structure of the lid domain of PepD resembles that of PepV, but shares only a portion of its structure with other related dimeric M20/M28 family enzymes, including CPG_2, βAS, CN1, CN2, and PepT. The CPG_2 dimer exhibits continuous β-sheets across the two monomers to form the dimer interface, whereas the lid domain of PepD formed the dimeric interface through hydrogen bonding between helices. Moreover, PepD formed a unique criss-cross configuration via the interface interaction of the respective lid domains. Helices 6, 7, and 8 (Fig. 3.4A) were found to participate in the monomer-monomer contacts. Specifically, the carboxylate oxygens of Glu^{294} and the hydroxyl group of Ser^{374}, as well as the C = O from the amide side chain of Asn^{329} and the hydroxyl group of Ser^{385}, are hydrogen-bonded to each other and form the dimeric interface (Fig. 3.8).

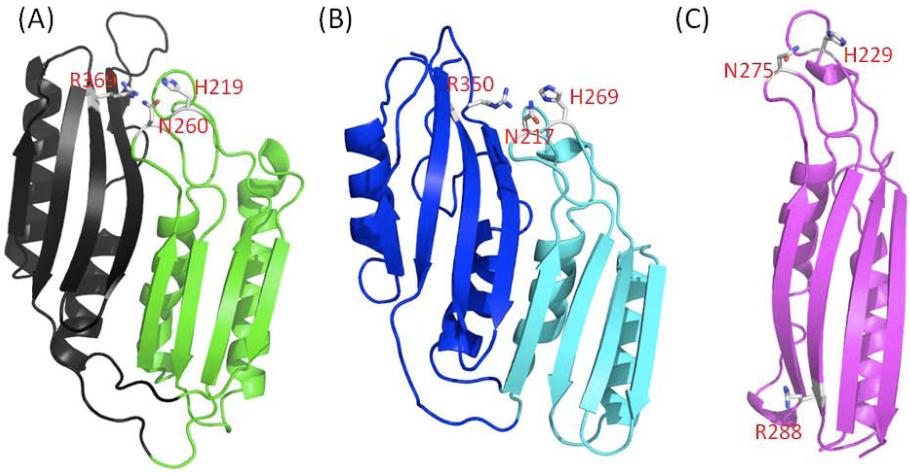

Figure 3.7. Comparison of the lid domain structures of PepD, PepV, and CPG_2. The three residues that are putatively involved in substrate C-terminal and/or transition state binding of PepD (A), PepV (B) and CP G_2 (C) are shown as *sticks* and labeled. The "extra" domain regions of PepD and PepV, which are absent in CPG_2, are shown in *black* and blue, respectively. Notably, the Arg^{288} of CPG_2 (C) is located on the opposite side of the monomer lid domain, which is spatially different from that of Arg^{369} of PepD (A) and Arg^{350} of PepV (B).

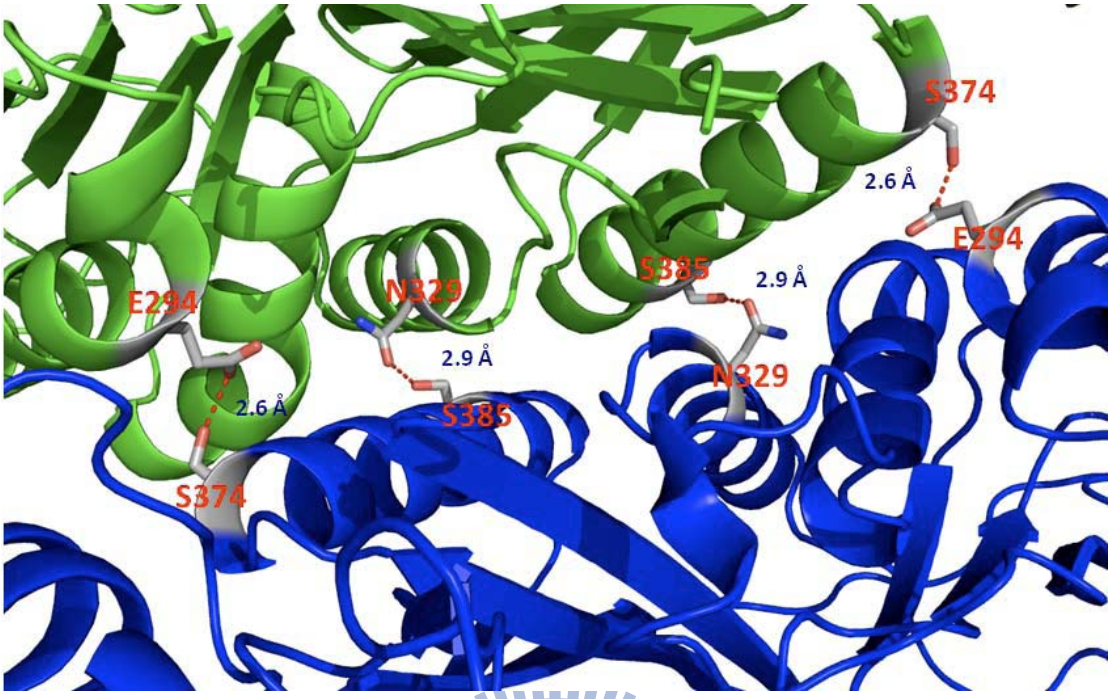

Figure 3.8. PepD dimeric interface. Residues involved in the dimeric interface, including Glu[294], Asn[329], Ser[374], and Ser[385] of PepD, are shown as *sticks* and annotated by labels.

3.2-4 Structure comparison of *V. alginolyticus* PepD and related di-zinc-dependent M20/M28 family enzymes

To further characterize the structural features of PepD, structures of related M20/M28 metallopeptidase family members were superimposed onto PepD. A close overall similarity was observed between PepD and the uncharacterized PDB code 2QYV protein that had been previously solved by the Joint Center for Structural Genomics (JCSG). However, the PepD shows an open conformation, and 2QYV shows a closed conformation (Appendix 6). Sequence alignment of these two proteins revealed a 50.9% sequence identity (Appendix 7). The root mean square deviation of structure similarity between PepD and 2QYV for Cα atoms was calculated to be 0.63 and 0.73 Å among the

catalytic and lid domains, respectively. Although both proteins share a structurally-conserved active site, two notable regions connecting the catalytic and lid domains (PepD residues 183–187 and 400–403 *vs* code 2QYV residues 179–183 and 397–400, respectively) showed minor differences between the proteins in loop conformations. In addition, the PepD protein also exhibited limited amino acid yet overall folding similarity to the M20/M28 metallopeptidases, except in the region of the dimer topology.

The catalytic domain of PepD superpositioned well with the single domain structures of the *S. griseus Sg*AP and *A. proteolytica Ap*AP, and to the two domain structures of the *Pseudomonas* sp. CPG_2, *S. typhimurium* PepT, *S. kluyveri βAS*, human Acy1, and mouse CN2, as well as to the counterpart of *L. delbrueckii* PepV. A major structural difference, however, was found to exist between PepD and the related di-zinc-dependent M20/M28 metallopeptidases in the lid domain; PepD consists of an eight-stranded β-sheet and four α-helices, similar to that of PepV, but the enzymes from the di-zinc-dependent M20/M28 family are composed of only one four-stranded antiparallel β-sheet flanked by two α-helices.

Furthermore, part of the lid domain of the PepD structure is completely superimposable to that of the two domain structures of *Pseudomonas* sp. CPG_2, *S. typhimurium* PepT, *S. kluyveri βAS*, human Acy1, and mouse CN2. These proteins are known to form a dimer interface through hydrophobic interactions between helices, as well as through hydrogen bonds between the two β-strands within the lid domain. Nevertheless, PepD exhibited a different dimeric architecture from that of the compared dimeric proteins in that the two lid domains of the dimeric proteins mediate enzyme dimerization through side-by-side packing of their four-stranded β-sheets to form a contiguous extended eight stranded sheets. In contrast, a crisscross configuration was

observed in PepD, wherein the lid domain formed the dimeric interface through hydrogen bonds between two sets of four α-helices (Fig. 3.8). Although the above-mentioned M20/M28 family metallopeptidases all consist of homodimer structures similar to CPG_2, no report has appeared in the literature to date that discusses the PepD-like criss-cross dimeric architecture.

The structure of PepD aligns well with the counterpart of PepV, which is a monomer and does not have a known function in subunit dimerization. The lid domain of PepV partially resembles the lid domain of CPG_2, but is about two times larger (Fig. 3.7). Moreover, the PepV lid domain extends itself away from the active site of the catalytic domain, folding back over the active site and facilitating the catalytic domain formation of a cavity that is uniquely involved in substrate specificity. Surprisingly, the lid domain of PepD, which is also about twice as large as that in CPG_2 and other related dimeric proteins, is able to form a dimer instead of a monomer. Lindner *et al.* reported that the eight-stranded β-sheets comprising the lid domain of PepV can be divided into two subdomains[10], both of which exhibit the same topology as the lid domain of CPG_2 and together can mimic the arrangement of the two lid domains within the CPG_2 and PepT dimers. However, dimerization of the subunits in PepD was found to be mediated through hydrogen bonding of the α-helices, and not by side-by-side packing of the β-sheets. Moreover, one additional region encompassing residues 186–203 and 311–400 within the lid domain of PepD was found to be similar to the lid domain of related dimeric proteins, and was renamed as the “extra" domain. Although the function of the extra domain has been hypothesized, the true physiological function of the extra domain of PepD remains unclear.

Currently, the crystal structures of the M20 family of proteins have been reported for two different (open and closed) conformations. When a protein is crystallized in its

free form, the catalytic and lid domains are expected to be in an orientation that exposes the active site to bulky water; whereas, when a protein is crystallized in complex with an inhibitor, the closed conformation is expected. In the PepV-inhibitor complex, a fixed "bridging" water molecule was found to be located between both zinc ions and close to the carboxylate group of the catalytic Glu^{153}; this residue corresponds to Glu^{149} of PepD and has been proposed as necessary for substrate hydrolysis (Fig. 3.6). Upon binding of the substrate, the water molecule will be positioned between the zinc ions and the carbonyl carbon of the scissile peptide bond. Then, an attacking hydroxyl ion nucleophile is able to be subsequently generated through activation of the water molecule by both the zinc ions and transfer of the resultant proton to the Glu^{153}. Proximal to the Glu^{153} of PepV is the conserved metal binding residue, Glu^{154}, which utilizes its carboxylate oxygen to bind to the zinc ion with a distance of less than 3.0 Å. The carboxylate oxygen of Glu^{154} of PepV is directed toward the Zn1. Nevertheless, our structural analysis of PepD in an open conformation revealed that the carboxylate oxygen of the corresponding Glu^{150} residue is directed away from the Zn1 at a distance of 4.5 Å.

It has been suggested that dipeptidases of M20 families can change their conformation from opened to closed during the process of enzymatic catalysis. The conformational change could be achieved by movement of the catalytic and lid domains (Fig. 3.9). Consistent with this notion is the presence of a large clearance between the two domains that would allow a peptide chain to move to the opened active site, as was observed for the PepD structure. We, therefore, speculated that upon substrate binding, the PepD protein may change its metal ions' coordination and/or its protein conformation; the carboxylate oxygen of Glu^{150} would be subsequently swung toward Zn1 and would push the Glu^{149}-bound water molecule toward Zn2, effectively bridging

the water between the two zinc ions. However, the precise molecular interactions between the enzyme active site and the substrate or inhibitor still await final X-ray structure determination.

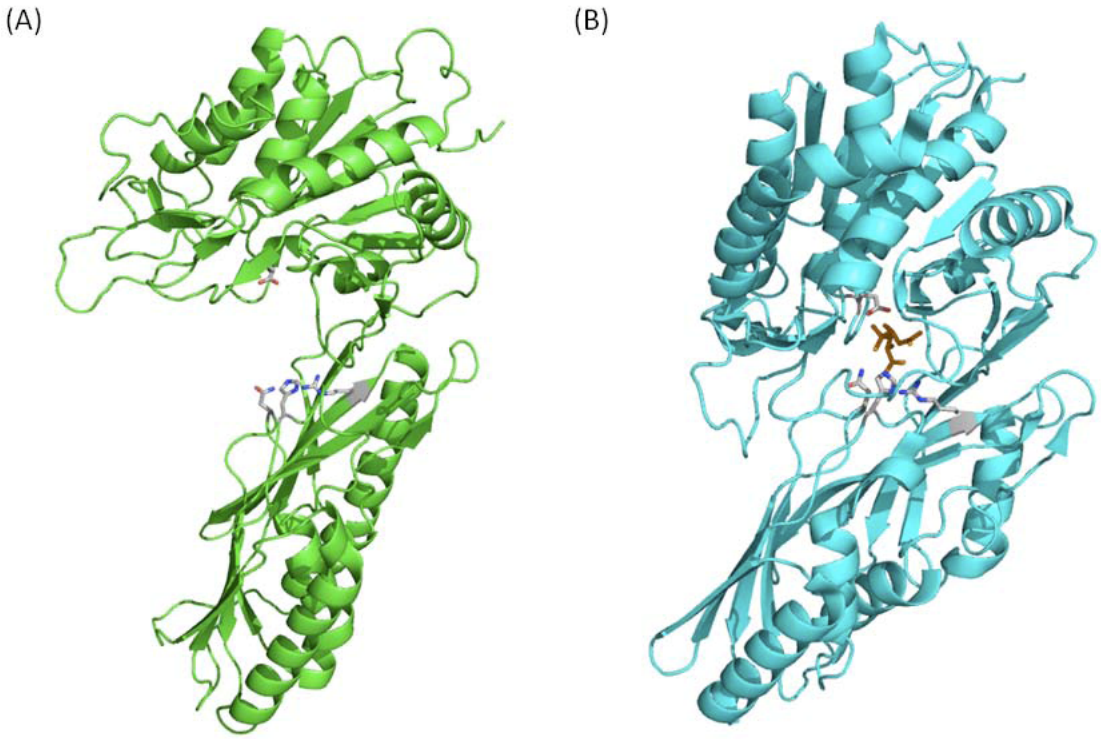

Figure 3.9. Open and closed conformations of PepD and PepV. (A) The overall structure of PepD in the open conformation is presented. (B) The overall structure of PepV in the closed conformation is presented. The substrate C-terminal binding and/or transition state binding residues, including Arg, His, and Asn, are shown as *sticks* from left to right in the lid domain; in the catalytic domains, Glu^{149} (PepD) and Glu^{153} (PepV) are shown, respectively. The phosphinic AspΨ[PO_2CH_2]AlaOH inhibitor in PepV is represented by *sticks*.

The di-zinc binding ligands, His^{80}, Asp^{119}, Glu^{150}, and His^{461}, were found to be conserved among all of the proteins compared in this study. In contrast, the ligand Asp^{173} was found to be replaced by a Glu residue in CPG_2 and hACy1. This finding is consistent with an earlier observation reported by Lindner *et al.*[10], in which all homologs

with proven aminopeptidase or dipeptidase specificity were found to contain an aspartic acid, whereas a glutamic acid residue has been identified in the same position in Acyl1/M20 family members that exhibit either aminoacylase or carboxypeptidase specificity. Moreover, four additional residues were found to be conserved among all of the compared proteins: 1) Asp^{82} is located at two residues downstream from the His^{80} and in the vicinity of the zinc center, and is assumed to clamp the imidazolium ring of His^{80}; 2) Glu^{149} is a putative general base for enzyme catalysis; and 3) His^{219} and Arg^{369} are putative substrate C-terminal and/or transition state binding residues. On the other hand, within the PepV, CPG_2, and related M20/M28 family metallopeptidases, a *cis* peptide bond exists between the bridging Asp and the proximal residue. In CPG_2, *Ap*AP, PepT, and PepV, this residue is an Asp, which is replaced by Asn in PepD (Asn^{120}) and *Sg*AP (Asn^{98}). The *cis*-peptide has been proposed to participate in forcing the bridging carboxylate to conform to the correct geometry required for metal binding.

3.3 Mutagenesis study and enzyme kinetics of *V. alginolyticus* PepD

3.3-1 Mutational analysis on metal-binding and catalytic residues of *V. alginolytic* PepD

Previously, His^{80}, Asp^{119}, Glu^{150}, Asp^{173}, and His^{461} were described as being putatively involved in metal binding in $PepD^{76}$. We individually mutated each of these residues using an alanine-scanning mutagenesis strategy, and characterized the expressed proteins with CD spectrometry (Fig. 3.10). Each of the mutated proteins was produced in similar quantities from the expression system and exhibited homologous CD spectra, indicating that the overall structure of the mutated enzymes was not affected by the manipulation of the amino acid sequence.

Nevertheless, we could detect no activity for any of the mutants. This suggested that each of these residues played an essential role in PepD enzymatic activity (Tables 3.1 and 3.2). In a parallel experimental procedure, Asp^{119} was substituted with Glu, Met, Leu, Ile, Arg, Phe, Ala, Ser, Thr, Cys, Pro or Asn, Glu^{150} was replaced with Arg or His, and Asp^{173} was mutated to a Glu residue. As expected, substitution of Asp^{119} with other proteinogenic amino acid residues completely abolished the enzymatic activity. On the other hand, substitution of Glu^{150} with Asp led to the retention of ~60% of the maximal hydrolytic activity of the wild-type enzyme, whereas substitution of Glu^{150} with Arg or His completely abolished enzymatic activity. Substitution of Asp^{173} with Glu also completely abolished the enzymatic activity.

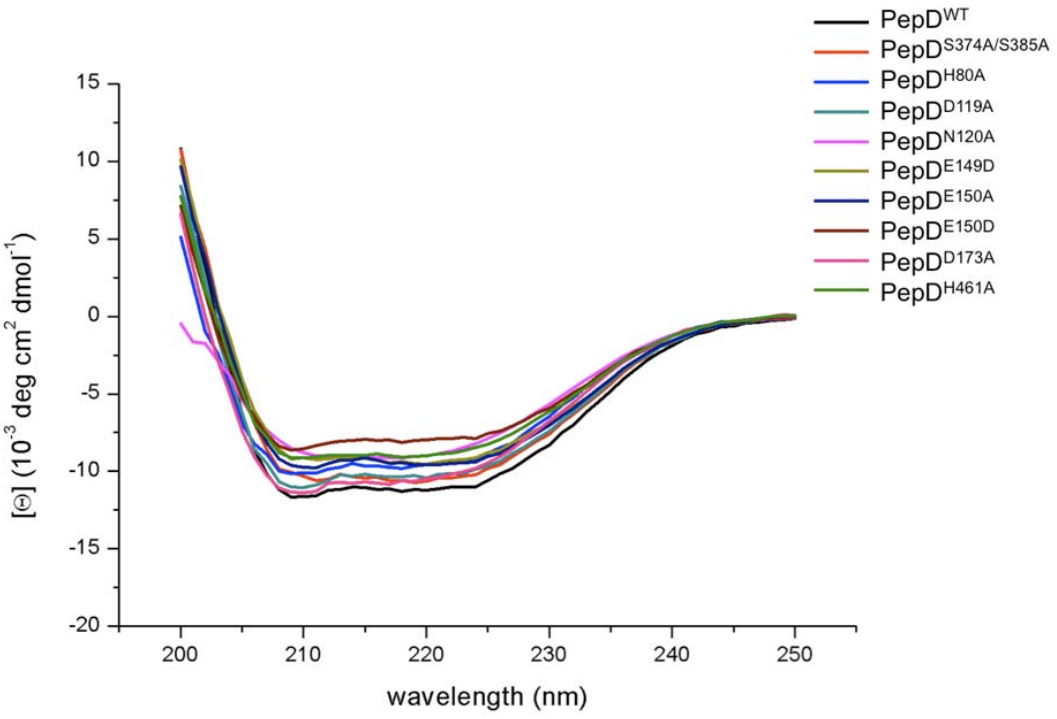

Figure 3.10. CD spectra of *V. alginolyticus* PepD wild-type and various mutants.

Next, we subjected the Asp^{82} and Glu^{149} residues to site-directed mutagenesis, to evaluate their putative roles in PepD catalysis. Asp^{82} was substituted for either Gly, Val, Phe, Tyr, His, or Glu, whereas the Glu^{149} was replaced with either Gly, Ala, Ile, Ser, His, Trp, or Asp. Again, no activity was detected for any of the Asp^{82} mutants. Substituting Glu^{149} with Gly, Ala, Ile, Ser, His, or Trp also resulted in the abolishment of enzymatic activity, with the exception of the Asp mutant being able to retain ~55% of the wild-type activity (Tables 3.1 and 3.2). It is interesting to note that replacement of Glu^{149} or Glu^{150} with aspartic acid led to partial retention of enzymatic activity, despite the residue being only one carbon shorter and having the same negative charge. We speculate that shortening the amino acid side chain in this particular position may allow for its acidic group to move away from an optimum position, consequently promoting activation of the catalytic water molecule, or perhaps the replacement of Glu with Asp at this position may partially affect the metal ligand-binding affinity and impair subsequent activation of the catalytic water for substrate-enzyme tetrahedral intermediate formation. Either or these processes may have ultimately resulted in partial loss of the enzymatic activity.

To investigate whether Asn^{120} of the *cis*-peptide is involved in catalysis or protein folding/stabilization, Asn^{120} was substituted with Ala and its enzymatic activity was examined. As expected, no activity was detected for the $PepD^{N120A}$ mutant. In addition, the CD spectra of the PepD wild-type and $PepD^{N120A}$ mutant proteins presented almost the same profile in the range of 198–250 nm (Fig. 3.10) implying that the $PepD^{N120A}$ mutant protein was not perturbed in either its stability or folding properties. These results indicate that Asn^{120} plays an essential role in the enzyme reaction.

Table 3.1: Enzyme kinetics of *V. alginolyticus* PepD wild-type and mutant proteins. Kinetic parameters are for the hydrolysis of L-carnosine at 37 °C and pH 7.0.

PepD	k_{cat}	K_m	k_{cat}/K_m
	min^{-1}	mM	$mM^{-1}s^{-1}$
WT	10.84 ± 0.22	0.244 ± 0.004	0.737 ± 0.007
H80A	ND[a]	ND	ND
H82X (X = G, V,F,Y,H,E)	ND	ND	ND
D119X (X = A,E,LR,F,P,M,I,F,S,C,N)	ND	ND	ND
N120A	ND	ND	ND
E149D	7.07 ± 0.07	0.408 ± 0.005	0.288 ± 0.001
E149X (X = A,G,I,S,H,W)	ND	ND	ND
E150D	7.3 ± 0.4	0.905 ± 0.195	0.139 ± 0.02
E150X (X = A,R,H)	ND	ND	ND
D173X (X = A,E)	ND	ND	ND
S374A/S385A	11.54 ± 0.34	0.221 ± 0.012	0.87 ± 0.02
H461A	ND	ND	ND

[a] ND, not detected

Table 3.2: Enzymatic studies of *V. alginolyticus* PepD wild-type and mutant proteins. Residual activity was determined for the hydrolysis of L-carnosine at 37 °C and pH 7.0.

PepD	Related activity
	%
WT	100 ± 0.5
H80A	ND[a]
H82X (X = G,V,F,Y,H,E)	ND
D119X (X = A,E,L,R,F,P,M,I,S,C,N)	ND
N120A	ND
E149D	53.1 ± 3.6
E149X (X = A,G,I,S,H,W)	ND
E150D	60.4 ± 1.3
E150X (X = A,R,H)	ND
D173X (X = A,E)	ND
H219A	119.1 ± 1.5
N260A	60.6 ± 0.3
R369A	ND
S374A,S385A	113 ± 0.8
H461A	ND

[a] ND, not detected

3.3-2 Mutational analysis on probable substrate C-terminal binding residues within the lid domain of *V. alginolyticus* PepD

Jozic *et al.* have previously identified three residues, Asn^{217}, His^{269}, and Arg^{350}, within the lid domain of PepV that are putatively involved in the substrate C-terminal and/or transition state binding through hydrogen bonding[26]. Due to the different topology of the β-sheet order, a simple primary sequence alignment was not able to identify the corresponding residues in the lid domain of PepD, except for Arg^{369}, which aligned with Arg^{350} of PepV. This residue also superimposed with Arg^{324}, Arg^{280}, and Arg^{276} in the small domains of the dimeric CPG_2, PepT, and hACy1, respectively. We then used structure-based sequence alignment to identify the other equivalent residues in PepD. A structure superimposition but inversed sequence order, in which the Asn^{217} and His^{269} residues of PepV superimposed with the Asn^{260} and His^{219} residues of PepD, was noticed. Asn^{260} is conserved among PepV, CPG_2, βAS, and PepT, but is substituted by Thr in human CN1 and mouse CN2 as well as by Tyr in PepT. Remarkably, the His^{219}, Asn^{260}, and Arg^{369} residues are located on the same side of the lid domain for both PepD dimers, but the corresponding residues are located on the opposite side of the lid domain of the same monomer for CPG_2 and related dimeric proteins (Fig. 3.7). Therefore, in CPG_2, the Arg^{288} from the lid domain of one monomer interacts with the His^{229} and Asn^{275} from the lid domain of the other monomer; in contrast, the Arg^{369} from the lid domain of the PepD monomer interacts with the Asn^{260} and His^{219} from the lid domain of the same monomer.

We also performed site-directed mutagenesis experiments to test the roles of these equivalent lid domain residues. The mutated PepD proteins were produced in a procedure similar to that of the wild-type PepD. All mutants exhibited similar purification characteristics and the same electrophoretic mobility as the wild-type

enzyme in SDS-PAGE. Although each of the mutations produced similar quantities of the protein, the Arg^{369} to Ala mutation resulted in complete loss of the enzymatic activity for hydrolyzing L-carnosine, whereas the Asn^{260} to Ala mutation decreased the catalytic activity to almost half. Interestingly, the His^{219} to Ala mutation did not affect the enzymatic activity significantly, yielding only a slight increase in activity of ~10% as compared with the wild-type PepD. In PepV, the Arg^{350} was located near the C terminus of the bound inhibitor (2.7 Å) but appeared to be too far away from the zinc ions (~8 Å), indicating a role in substrate binding but not in catalysis. The replacement of Arg with Ala might disrupt the hydrogen bond network between the Arg^{369} side chain and Asn^{260} Nδ with the carboxylate group of the substrate. In the case of PepV, Jozic *et al.* have argued that domain flexibility is required to allow substrate access. Moreover, the bad diffraction and high mosaicity observed in the inhibitor-free PepV crystal have been attributed to conformational variability between open and closed states. A significant opening of the protein conformation would clearly benefit access of the peptides to the active site cavity. It is conceivable that even the whole lid domain might move away from its site to allow for easier substrate access and product egress. Therefore, although the Arg^{369} guanidinium side chain and the Asn^{260} Nδ within the active site of PepD are both ~16 Å away from the zinc ion, a conformational change between the open and closed states might have contributed to the movement of both Arg^{369} and Asn^{260} upon substrate binding and subsequent transition state stabilization. Furthermore, binding of the His^{219} in PepD to the substrate likely persists during the conformational change between the open and closed states and contributes to transition-state stabilization through an electrostatic interaction between His^{219} and the free carboxyl group of the ligand, as shown in the PepV-inhibitor complex (Fig. 3.9).

3.3-3 Mutational analysis on dimeric interface of *V. alginolyticus* PepD

Based on the crystal structure, PepD and PepV revealed similar architecture, except that PepD is a dimer and PepV is a monomer. From the structural illustration of PepD, the dimeric interface appears to be formed by hydrogen bonds through Ser^{374} and Ser^{385} of one subunit to Glu^{294} and Asn^{329} of the other subunit, respectively (Fig. 3.8). We then performed site-directed mutagenesis experiments on these residues to investigate the putative dimeric interface interactions. According to the results obtained from analytical sedimentation velocity ultracentrifugation, the molecular mass of the $PepD^{S374A/S385A}$ double mutant was determined to be 54.4 ± 0.02 kDa, whereas the PepD wild-type was 96.8 ± 0.11 kDa. Size exclusion chromatography of $PepD^{WT}$ and the $PepD^{S374A/S385A}$ double mutant also revealed the corresponding sizes of ~103.7 and 50.6 kDa, respectively (Fig. 3.11). These results suggested that the $PepD^{S374A/S385A}$ mutant existed as a monomer in solution. Interestingly, the $PepD^{S374A/S385A}$ mutant exhibited ~130% activity of the wild-type, indicating independent function for the monomer (Table. 3.2). However, the exact reason for forming the dimeric structure remains unclear, but a physiochemical or regulatory function of PepD may be involved.

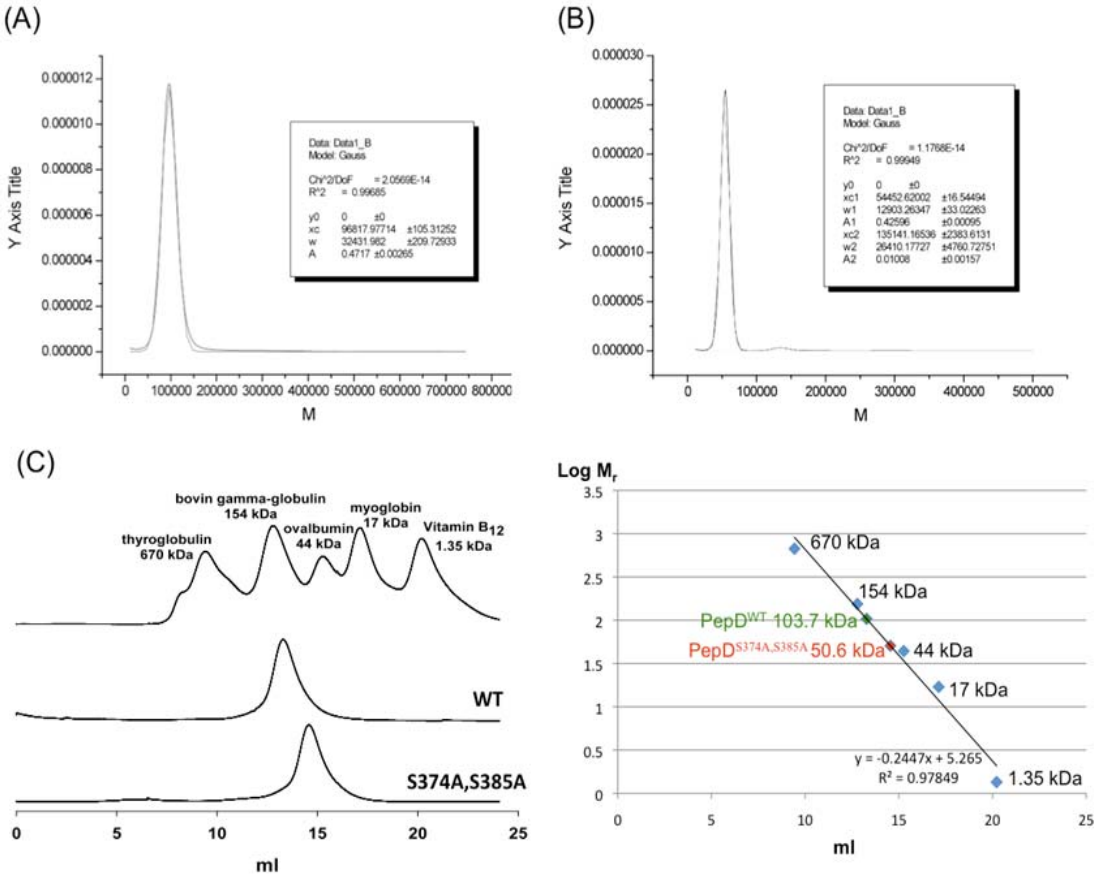

Figure 3.11. Molecular masses determination of PepD^{WT} and PepD$^{S374A/S385A}$ mutant. Analytical ultracentrifugation determination of (A) PepD^{WT} and (B) PepD$^{S374A/S385A}$ mutant, showing the calculated molecular weight from sedimentation coefficient (*s*) of approximately 96817.977 ± 105.3 g/mol and 54452.62 ± 16.5 g/mol, respectively. (C) Chromatographic separation and calibration curve for the standard proteins, PepD^{WT} and PepD$^{S374A/S385A}$ on Superdex 200 10/300 GL column (GE Healthcare^{TM}). In the calibration curve, the molecular mass of PepD^{WT} (*green dot*) and PepD$^{S174A/S385A}$ (*red dot*) were determined to be 103.7 and 50.6 kDa, respectively.

3.4 Substrate specificity alteration of the truncated PepD catalytic domain

We have previously observed that the catalytic domain of PepD contains metal binding sites and is responsible for substrate hydrolysis, whereas the lid domain plays a role in substrate recognition. To further substantiate the functional role of the catalytic domain, we constructed a truncated enzyme of the PepD catalytic domain alone ($PepD^{CAT}$) and investigated the preference for substrate specificity. The catalytic domain regions, comprised of residues 1–186 and 401– 490, were PCR amplified, ligated, and subcloned into the pET-28a(+) vector to construct the $PepD^{CAT}$ recombinant plasmid. The truncated protein was produced similar to the wild-type PepD and exhibited the expected size of ~31 kDa. The substrate specificity of $PepD^{CAT}$ was determined at pH 7.4 and 37 °C with 14 peptides, including 10 Xaa-His dipeptides, two His-Xaa dipeptides, and two His-containing tripeptides (Table 3.3). Compared with the enzymatic activity of wild-type PepD, the activity of $PepD^{CAT}$ was significantly reduced or not measurable, except for L-carnosine or L-homocarnosine. The $PepD^{CAT}$ exhibited ~20% of the wild-type activity toward the L-carnosine substrate. Unexpectedly, the $PepD^{CAT}$ protein exhibited altered substrate specificity to L-homocarnosineas compared with that of the full-length PepD protein, and with ~6% of the activity (Appendix 8). The results suggested that the substrate selectivity of the $PepD^{CAT}$ protein hold the potential for application in GABAergic therapies or as a neuroprotector, because L-homocarnosine is a precursor for GABA and acts as a GABA reservoir.

Table 3.3: Substrate specificity of PepD^{WT} and PepD^{CAT} for 10 Xaa-His dipeptides, 2 His-Xaa dipeptides, and 2 His-containing tripepides. Values are expressed as relative activity setting the degradation of PepD^{WT} for carnosine to 100%.

	PepD^{WT}	PepD^{CAT}
	%	%
L-Carnosine	100	24.5
α-Ala-His	155.7	4.7
Gly-His	118.1	4.2
Val-His	117.2	5.5
Leu-His	157.5	3.7
Ile-His	146.1	5.8
Tyr-His	125	5.3
Ser-His	126.8	5.5
His-Arg	112.3	4.7
His-Asp	131.7	5.9
β-Asp-His	3.9	3.8
L-Homocarnosine	1.6	6.8
Gly-His-Gly	4.8	4.8
Gly-Gly-His	3.7	4.2

3.5 Proposed catalytic mechanism

The structural similarity between PepD and related M20/M28 family metallopeptidases led to the hypothesis that these enzymes share a common catalytic mechanism. Based on superimposition of putative metal and substrate-binding residues among these enzymes, a general mechanism may be described that: (a) before substrate binding, a bridging water molecule is positioned between two Zn^{2+} ions and spatially close to the carboxylate group of the catalytic Glu^{149}; (b) the PepD undergoes a conformational change upon substrate binding and hydrolysis; (c) during catalysis, the catalytic Glu^{149} acts as a general base by promoting the nucleophilic attack of the metal-bound water on the substrate carbonyl carbon and transfers the proton to the Glu^{149}; (d) the carbonyl oxygen then binds in an "oxyanion binding hole" formed by Zn1 and the imidazole group of His^{219} in PepD, resulting in polarization of the carbonyl group and facilitating the nucleophilic attack of the scissile bond by the zinc-oriented

hydroxyl group; (e) this leads to a tetrahedral intermediate, which subsequently decays to the product after one additional proton transfer from the catalytic Glu^{149} carboxylate to the amide nitrogen in His^{219}. In addition to the catalytic Glu^{149}, mutational analyses indicated that putative substrate binding residues Asp^{82}, Glu^{149}, and Arg^{369} play essential roles in the hydrolysis reaction (Fig. 3.12).

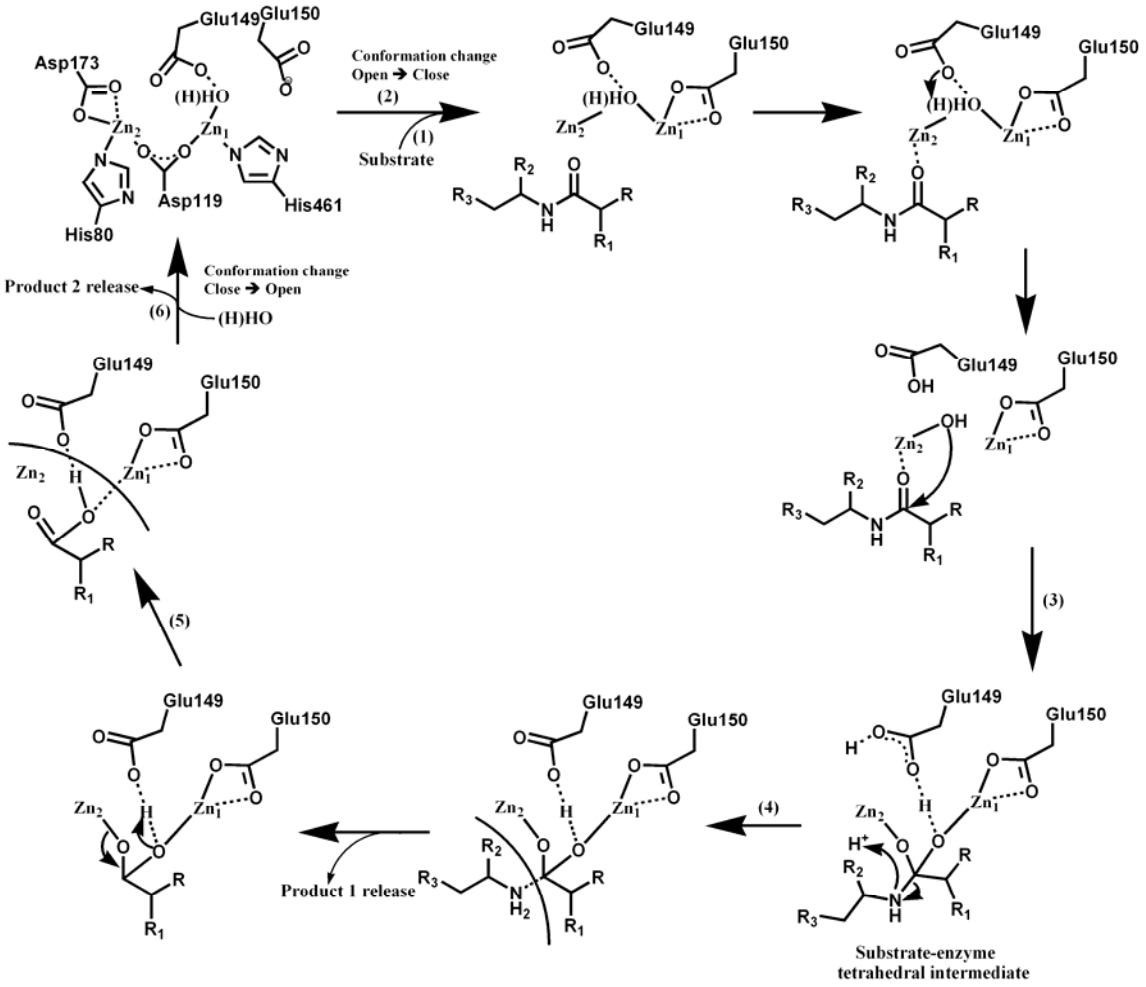

Figure 3.12. Proposed reaction mechanism of *V. alginolyticus* PepD. (1) Binding of the substrate to the substrate C-terminal anchoring residues; (2) protein conformational change from the open to closed form upon substrate binding, displacing the zinc-bound water by the substrate and activating the bridging water molecule by Glu^{149}; (3) nucleophilic attack of the carbonyl carbon of the substrate by the activated water molecule and formation of the tetrahedral intermediate; (4) cleavage of the

carbon-nitrogen bond and formation of product; (5) opening of the active site and release of the product; (6) addition of a new bridging water molecule.

3.6 Catechol derivatives oxidative activity of copper-substituted PepD (CuCu-PepD)

In our previous study, the hydrolysis activity of PepD was found to be inhibited by dopamine or L-dopa. Interestingly, the peptide-bond hydrolysis activity of PepD can be converted to catechol oxidative activity by substitution of zinc ions with copper ions in active site (CuCu-PepD). However, even though CuCu-PepD can oxidize catechol derivatives, which are catecholamine hormones produced from tyrosine metabolism (dopamine, L-dopa, epinephrine and norepinephrine) (Fig. 3.13), it is unable to oxidize catechol or 3,5-di-*tert*-butylcatechol (DTC), which has distinguished by their non-polar side chains (Fig. 3.14). This result indicated that CuCu-PepD specifically reacts with only substrates having a polar tail. No other enzyme to date, to our knowledge, has been reported to have such a property of specialized substrate selectivity.

Furthermore, enzyme kinetics analysis revealed similar catalytic efficiency (k_{cat}/K_m) of CuCu-PepD for several catecholamine hormones. CuCu-PepD oxidation of epinephrine was more efficient than that of other related substrates (Table 3.4). This observation likely reflects the good binding that exists between enzyme and epinephrine (K_m = 0.073 mM). Comparison of the enzyme kinetics between CuCu-PepD and copper-substituted *Sg*AP (CuCu-*Sg*AP), as reported by Ming *et al.*[72], indicated that CuCu-PepD exhibited better substrate binding affinity for dopamine (K_m = 0.6 mM) and DTC (K_m = 0.44 mM) than did CuCu-*Sg*AP. However, the low k_{cat} of CuCu-PepD for several catechol derivatives leads to decreased oxidative efficiency (Table 3.4).

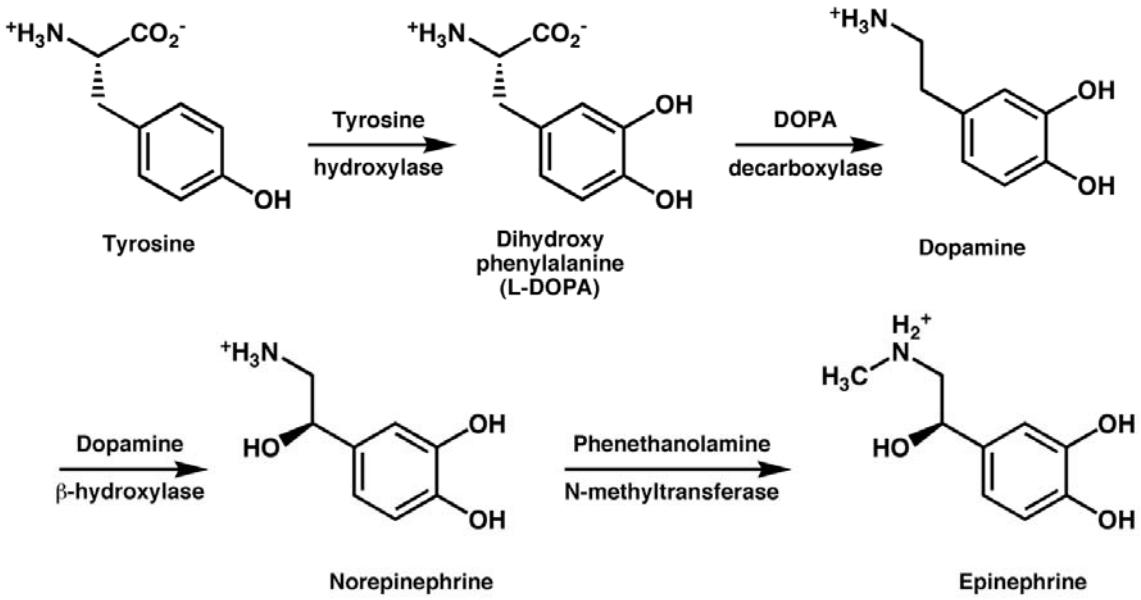

Figure 3.13. Catecholamine hormones produced from tyrosine metabolism.

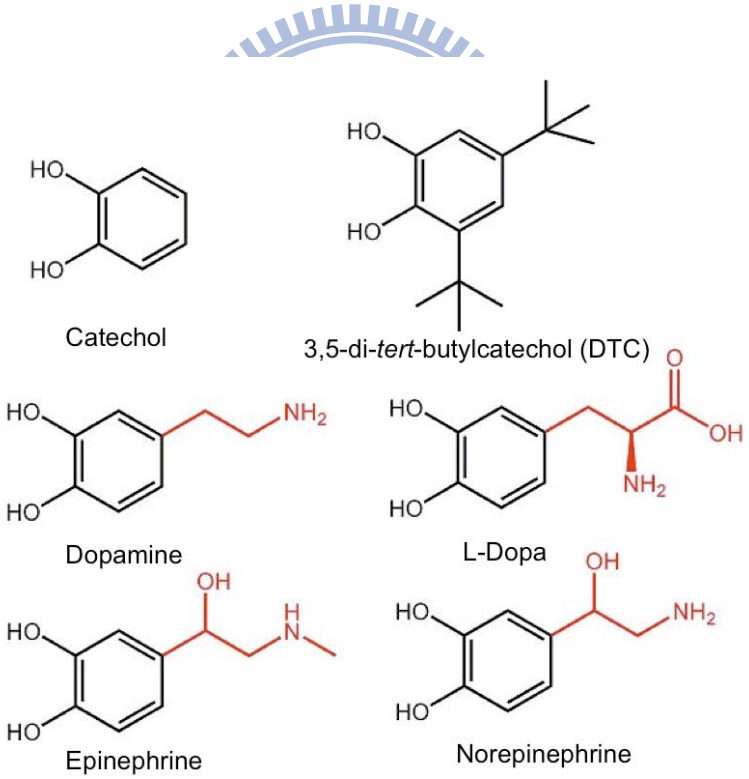

Figure 3.14. Structures of catechol and its derivatives. The polar tail of catechol derivatives are indicated by *red* color.

Table 3.4: Comparison of enzyme kinetics of PepD, CuCu-PepD, and CuCu-*Sg*AP* for different substrates. *Referred from Ming *et al*.[72] (*gray* background).

	k_{cat} (s^{-1})	K_m (mM)	k_{cat}/K_m ($M^{-1}s^{-1}$)
PepD with carnosine	10.84 ± 0.22	0.244 ± 0.004	0.737 ± 0.007
CuCu-PepD with Dopamine	1.98 ± 0.048	0.43 ± 0.053	0.0776 ± 0.008
CuCu-PepD with L-Dopa	1.56 ± 0.006	0.41 ± 0.053	0.0656 ± 0.0054
CuCu-PepD with Epinephrine	2.16 ± 0.018	0.073 ± 0.004	0.487 ± 0.0204
CuCu-PepD with Norepinephrine	1.38 ± 0.006	0.499 ± 0.034	0.0457 ± 0.003
CuCu-*Sg*AP with Dopamine	5.82	0.6	0.162
CuCu-*Sg*AP with DTC	87	0.44	3.295

•DTC : 3,5-di-tert-butylcatechol

3.7 Protein-ligand docking between CuCu-PepD and catecholamine hormones (L-dopa, dopamine, epinephrine, and norepinephrine)

In the previous report by Ming *et al*., the active site of CuCu-*Sg*AP provides the hydrophobic pocket for specific recognition in binding of DTC via its di-tert-butyl groups. However, CuCu-PepD was unable to oxidize catechol or DTC, but it could oxidize the catechol derivatives with polar tail. In order to understand the binding network for each catecholamine hormones with CuCu-PepD, a protein-ligand docking strategy was applied to investigate the molecular interaction that occurred between enzyme and substrate. Based on the results obtained, dopamine, L-dopa, epinephrine, and norepinephrine could be bound by CuCu-PepD in the enzyme's metal ions binding center. The docking model of the CuCu-PepD-dopamine complex indicated that *ortho*-hydroxyl group of dopamine could be bound by Asp^{119}, Glu^{149}, Asp^{173} and His^{461}, and the amine group could be bound by the Glu^{175} side chain via hydrogen bonding (Fig. 3.15A). In addition, the binding network of L-dopa with CuCu-PepD was found to be similar to that for dopamine (Fig. 3.15B). Since the amine group of L-dopa is distant

from Glu[175], the combination between the hydroxyl group of Tyr[181] and the carboxylate group of L-dopa is more likely (Fig. 3.15B). When the binding networks between epinephrine and norepinephrine were compared, they were found to be similar in that hydroxyl groups of both substrates were bound by Glu[175] at a distance of 2.7 Å (Fig. 3.15 C and D). However, the end-methyl group of epinephrine was able to further interaction via the hydrophobic pocket produced by Ile[432] and Ala[434]. Therefore, the protein-ligand docking results indicated that the better catalytic efficiency of CuCu-PepD for epinephrine was a result of epinephrine fitting better into the PepD active site.

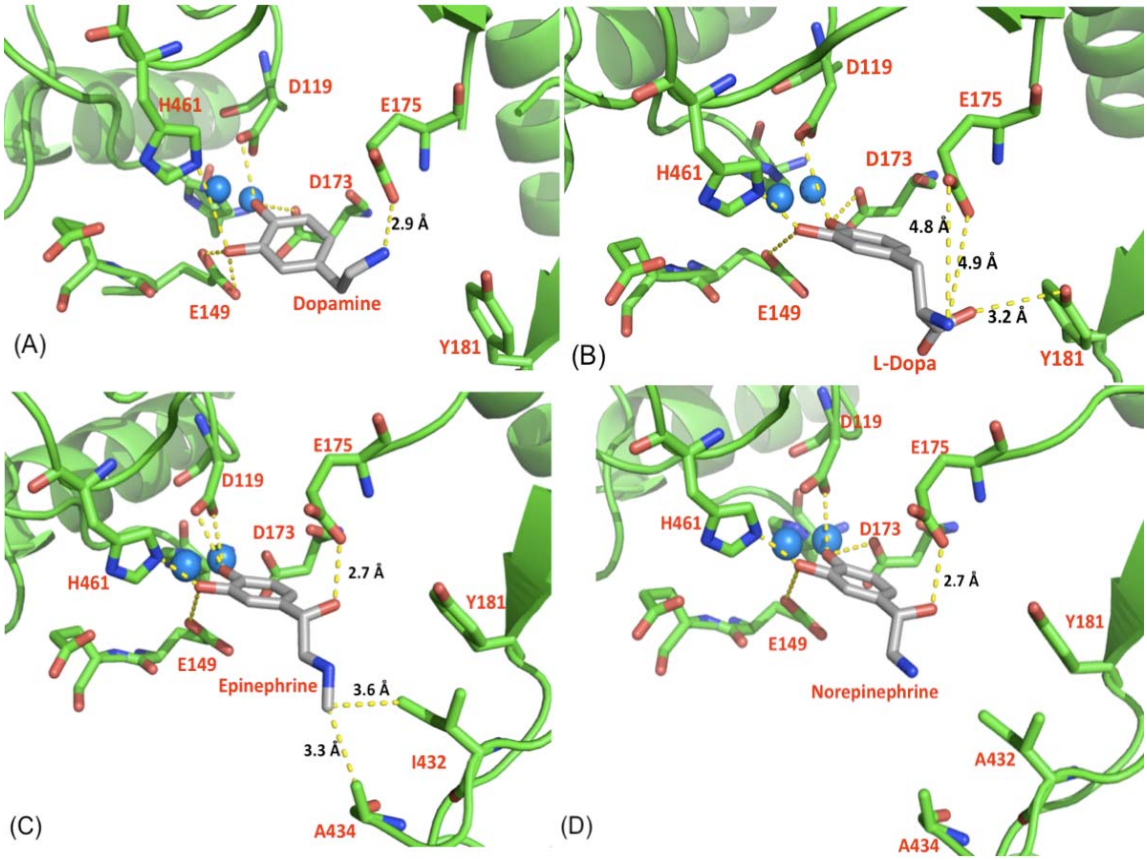

Figure 3.15. Protein-ligand docking of CuCu-PepD with (A) dopamine, (B) L-dopa, (C) epinephrine, and (D) norepinephrine. A local view of the di-metal ions center of PepD is presented for each. Residues are shown as sticks and labeled accordingly. The copper ions of CuCu-PepD are depicted by two *light blue* spheres.

CHAPTER 4

Conclusions and Future Perspectives

In conclusion, despite the lack of detectable sequence homology, the PepD enzyme has clear structural homology to other di-zinc-dependent M20 and M28 family enzymes. The crystal structure of *V. alginolyticus* PepD reveals it to be a dimer with two domains in each subunit. The catalytic domain of PepD contains two zinc ions and is structurally homologous to other proteolytic enzymes with dinuclear zinc catalytic sites. The lid domain, on the other hand, is structurally homologous to that of PepV, but having a distinct topology of β-sheet order. Interestingly, part of the lid domain of the PepD structure is also homologous to the lid domain of the dimeric proteins. Nevertheless, PepV exists as a monomer, while the PepD and related di-zinc-dependent M20/M28 family of enzymes are determined to be dimers. Structural comparisons between PepD and related di-zinc-dependent metallopeptidases suggest that formation of the catalytically competent active site in the PepD family of enzymes may be associated with transition from an open to a closed enzyme conformation. In parallel, the site-directed mutation of the putative substrate C-terminal binding residues, N260A and R369A, resulted in complete loss or partial decrease of the enzymatic activity. Furthermore, enzymatic assay of the truncated PepD catalytic domain, $PepD^{CAT}$, further demonstrated the functional role of the lid domain in substrate binding and selectivity. The structural data on PepD reported here may inspire strategies for the improvement of the PepD family of enzymes toward applications in biotechnology and allow the design of targeted disease peptidases or prodrugs with altered specificity.

On the other hand, it is important to consider the observation that substitution of zinc ions with copper ions in the PepD active site generated an enzyme, CuCu-PepD, preferred catechol derivatives containing polar tails. Based on the model of protein-ligand docking, the *ortho*-hydroxyl groups of each substrate are bound by Asp^{119}, Glu^{149}, Asp^{173} and His^{461} through hydrogen bonding as well as through polar tail interactions with Glu^{175} and Tyr^{181}. The model of CuCu-PepD-epinephrine fitted better into the active site by additional hydrophobic interactions between the PepD Ile^{432} and Ala^{434} and the terminal methyl group of epinephrine. Enzyme kinetics studies indicated that oxidation of epinephrine produced notable catalytic efficiency, explaining its low K_m value. In all, PepD is a unique enzyme, whose function can be effectively altered by simple metal ions substitution. This study not only unveiled a correlation of enzyme function between peptide hydrolysis and catechol oxidation, but also may provide a new direction by which divergent enzyme evolution occurs.

There are several possible directions that could be considered for future studies based upon the findings presented here. To better understand the PepD structure-function relationship and biological function, and to determine potential applications in enzymatic therapy, the following investigations are suggested:

I. Structure analysis of PepD-inhibitor complex by X-ray crystallography

In our previous report, the crucial residues in PepD for metal ions binding and substrate C-terminal and/or transition state binding were identified. We used PepD native structure and mutational analysis; however, the substrate binding network and substrates can induce conformational changes in the enzyme that were not addressed by our study. Therefore, co-crystallization of PepD with inhibitor (bestatin or dopamine) would provide further insights into the substrate binding sites and catalytic mechanism.

Furthermore, the enzyme conformational change from the open to closed form might also be determined by complex structure.

II. Proteomic study of *V. alginolyticus pepD*-deficient knockout strain

Proteomic study includes not only the identification and quantification of a particular protein panel under certain physiologic conditions, but also the determination of their localization, modifications, interactions, activities, and ultimately their function. A previous report by Brombacher *et al*., in which *pepD* gene was overexpressed in *E. coli*, indicated that PepD was vital to reducing biofilm formation[23]. In a similar manner, a *V. alginolyticus pepD*-deficient strain might be used to investigate morphology and biofilm formation by comparing with wild-type. Two-dimensional protein electrophoresis and mass spectrometry would help to provide more detailed proteomic information about the biological effect on protein signaling pathways by PepD.

III. Potential application in antibody directed enzyme prodrug therapy (ADEPT)

In ADEPT, the range of potential enzymes is limited by several constraints. For example, the enzyme's function is to efficiently convert an inactive prodrug into the active drug; thus, its optimal pH must be near the pH of the tumor extracellular fluid.

V. alginolyticus PepD considered a promising candidate for use in ADEPT because it works at pH 6.8-7.4, which is similar to the environment of human body. In addition, it can hydrolyze a dipeptide into two amino acids, which is affectively the same mechanism of prodrug hydrolyzation. The analysis of *V. alginolyticus* PepD performed to date (including functional residues characterization, protein structure, mutagenesis analysis and enzyme kinetics analysis) would aid in the design of a PepD mutant with improved digestion efficiency for a particular prodrug with a dipeptide

skeleton. Therefore, it is feasible that enzymatic engineering of PepD can generate desired mutant proteins to hydrolyze a prodrug, such as benzoic acid mustard prodrug (Fig. 1.9). This type of PepD study will require the development of an animal model to determine the efficacy and safety of a PepD-based ADEPT strategy, prior to its use in humans.

IV. Molecular evolution of metal-substituted dipeptidase for protein plasticity

A unique enzyme catalytic promiscuity has recently been observed for the dinuclear aminopeptidase from *Streptomyces griseus*. *Sg*AP exhibits a high efficiency of catalytic promiscuity toward phosphonate and phosphodiester hydrolysis under different physiological conditions[67, 68]. Moreover, the peptide hydrolysis activity of *Sg*AP[70, 71] could be converted to catechol oxidative activity by manipulation of its metal derivatives[72].

In PepD, we have observed catechol oxidative activity induced by copper ions substitution in the active site. Using the crystal structure of PepD and attaining a better understanding of the critical role of individual amino-acid residues involved in metal ions binding and substrate recognition, it may be possible to create an artificial enzyme with phosphoester hydrolysis activity. This might be achieved by a combination of site-directed mutagenesis and metal substitution of PepD protein. Development of an artificial PepD exhibiting phosphoesterase function might generate new potentials in chemical warfare, such as degradation of the nerve agent Soman toxin[89-91].

References

1. Wilcox, D. E., Binuclear Metallohydrolases. *Chem Rev* **1996,** *96* (7), 2435-2458.

2. Dismukes, G. C., Manganese Enzymes with Binuclear Active Sites. *Chem Rev* **1996,** *96* (7), 2909-2926.

3. Lipscomb, W. N.; Strater, N., Recent Advances in Zinc Enzymology. *Chem Rev* **1996,** *96* (7), 2375-2434.

4. Munih, P.; Moulin, A.; Stamper, C. C.; Bennett, B.; Ringe, D.; Petsko, G. A.; Holz, R. C., X-ray crystallographic characterization of the Co(II)-substituted Tris-bound form of the aminopeptidase from Aeromonas proteolytica. *J Inorg Biochem* **2007,** *101* (8), 1099-107.

5. Rawlings, N. D.; Barrett, A. J., Evolutionary families of metallopeptidases. *Methods Enzymol* **1995,** *248*, 183-228.

6. Rawlings, N. D.; Morton, F. R.; Barrett, A. J., MEROPS: the peptidase database. *Nucleic Acids Res* **2006,** *34* (Database issue), D270-2.

7. Kwon, K.; Hasseman, J.; Latham, S.; Grose, C.; Do, Y.; Fleischmann, R. D.; Pieper, R.; Peterson, S. N., Recombinant expression and functional analysis of proteases from Streptococcus pneumoniae, Bacillus anthracis, and Yersinia pestis. *BMC Biochem* **2011,** *12* (1), 17.

8. Chen, S. L.; Marino, T.; Fang, W. H.; Russo, N.; Himo, F., Peptide hydrolysis by the binuclear zinc enzyme aminopeptidase from Aeromonas proteolytica: a density functional theory study. *J Phys Chem B* **2008,** *112* (8), 2494-500.

9. Rawlings, N. D.; Barrett, A. J., Evolutionary families of peptidases. *Biochem J* **1993,** *290 (Pt 1)*, 205-18.

10. Lindner, H. A.; Alary, A.; Boju, L. I.; Sulea, T.; Menard, R., Roles of dimerization

domain residues in binding and catalysis by aminoacylase-1. *Biochemistry* **2005,** *44* (48), 15645-51.

11. Henrich, B.; Monnerjahn, U.; Plapp, R., Peptidase D gene (pepD) of Escherichia coli K-12: nucleotide sequence, transcript mapping, and comparison with other peptidase genes. *J Bacteriol* **1990,** *172* (8), 4641-51.

12. Savijoki, K.; Palva, A., Purification and molecular characterization of a tripeptidase (PepT) from Lactobacillus helveticus. *Appl Environ Microbiol* **2000,** *66* (2), 794-800.

13. Hellendoorn, M. A.; Franke-Fayard, B. M.; Mierau, I.; Venema, G.; Kok, J., Cloning and analysis of the pepV dipeptidase gene of Lactococcus lactis MG1363. *J Bacteriol* **1997,** *179* (11), 3410-5.

14. Hershcovitz, Y. F.; Gilboa, R.; Reiland, V.; Shoham, G.; Shoham, Y., Catalytic mechanism of SGAP, a double-zinc aminopeptidase from Streptomyces griseus. *FEBS J* **2007,** *274* (15), 3864-76.

15. Teufel, M.; Saudek, V.; Ledig, J. P.; Bernhardt, A.; Boularand, S.; Carreau, A.; Cairns, N. J.; Carter, C.; Cowley, D. J.; Duverger, D.; Ganzhorn, A. J.; Guenet, C.; Heintzelmann, B.; Laucher, V.; Sauvage, C.; Smirnova, T., Sequence identification and characterization of human carnosinase and a closely related non-specific dipeptidase. *J Biol Chem* **2003,** *278* (8), 6521-31.

16. Sherwood, R. F.; Melton, R. G.; Alwan, S. M.; Hughes, P., Purification and properties of carboxypeptidase G2 from Pseudomonas sp. strain RS-16. Use of a novel triazine dye affinity method. *Eur J Biochem* **1985,** *148* (3), 447-53.

17. Gojkovic, Z.; Sandrini, M. P.; Piskur, J., Eukaryotic beta-alanine synthases are functionally related but have a high degree of structural diversity. *Genetics* **2001,** *158* (3), 999-1011.

18. Born, T. L.; Zheng, R.; Blanchard, J. S., Hydrolysis of

N-succinyl-L,L-diaminopimelic acid by the Haemophilus influenzae dapE-encoded desuccinylase: metal activation, solvent isotope effects, and kinetic mechanism. *Biochemistry* **1998,** *37* (29), 10478-87.

19. Meinnel, T.; Schmitt, E.; Mechulam, Y.; Blanquet, S., Structural and biochemical characterization of the Escherichia coli argE gene product. *J Bacteriol* **1992,** *174* (7), 2323-31.

20. van der Drift, C.; Ketelaars, H. C., Carnosinase: its presence in Pseudomonas aeruginosa. *Antonie Van Leeuwenhoek* **1974,** *40* (3), 377-84.

21. Schroeder, U.; Henrich, B.; Fink, J.; Plapp, R., Peptidase D of Escherichia coli K-12, a metallopeptidase of low substrate specificity. *FEMS Microbiol Lett* **1994,** *123* (1-2), 153-9.

22. Klein, J.; Henrich, B.; Plapp, R., Cloning and expression of the pepD gene of Escherichia coli. *J Gen Microbiol* **1986,** *132* (8), 2337-43.

23. Brombacher, E.; Dorel, C.; Zehnder, A. J.; Landini, P., The curli biosynthesis regulator CsgD co-ordinates the expression of both positive and negative determinants for biofilm formation in Escherichia coli. *Microbiology* **2003,** *149* (Pt 10), 2847-57.

24. Miller, C. G.; Schwartz, G., Peptidase-deficient mutants of Escherichia coli. *J Bacteriol* **1978,** *135* (2), 603-11.

25. Kirsh, M.; Dembinski, D. R.; Hartman, P. E.; Miller, C. G., Salmonella typhimurium peptidase active on carnosine. *J Bacteriol* **1978,** *134* (2), 361-74.

26. Jozic, D.; Bourenkow, G.; Bartunik, H.; Scholze, H.; Dive, V.; Henrich, B.; Huber, R.; Bode, W.; Maskos, K., Crystal structure of the dinuclear zinc aminopeptidase PepV from Lactobacillus delbrueckii unravels its preference for dipeptides. *Structure* **2002,** *10* (8), 1097-106.

27. Albrecht, A. M.; Boldizsar, E.; Hutchison, D. J., Carboxypeptidase displaying

differential velocity in hydrolysis of methotrexate, 5-methyltetrahydrofolic acid, and leucovorin. *J Bacteriol* **1978,** *134* (2), 506-13.

28. Tucker, A. D.; Roswell, S.; Melton, R. G.; Paupitt, R. A., A new crystal form of carboxypeptidase G2 from Pseudomonas sp. strain RS-16 which is more amenable to structure determination. *Acta Crystallogr D Biol Crystallogr* **1996,** *52* (Pt 4), 890-2.

29. Rowsell, S.; Pauptit, R. A.; Tucker, A. D.; Melton, R. G.; Blow, D. M.; Brick, P., Crystal structure of carboxypeptidase G2, a bacterial enzyme with applications in cancer therapy. *Structure* **1997,** *5* (3), 337-47.

30. Vongerichten, K. F.; Klein, J. R.; Matern, H.; Plapp, R., Cloning and nucleotide sequence analysis of pepV, a carnosinase gene from Lactobacillus delbrueckii subsp. lactis DSM 7290, and partial characterization of the enzyme. *Microbiology* **1994,** *140 (Pt 10)*, 2591-600.

31. Biagini, A.; Puigserver, A., Sequence analysis of the aminoacylase-1 family. A new proposed signature for metalloexopeptidases. *Comp Biochem Physiol B Biochem Mol Biol* **2001,** *128* (3), 469-81.

32. Hakansson, K.; Miller, C. G., Structure of peptidase T from Salmonella typhimurium. *Eur J Biochem* **2002,** *269* (2), 443-50.

33. Lundgren, S.; Gojkovic, Z.; Piskur, J.; Dobritzsch, D., Yeast beta-alanine synthase shares a structural scaffold and origin with dizinc-dependent exopeptidases. *J Biol Chem* **2003,** *278* (51), 51851-62.

34. Agarwal, R.; Burley, S. K.; Swaminathan, S., Structural analysis of a ternary complex of allantoate amidohydrolase from Escherichia coli reveals its mechanics. *J Mol Biol* **2007,** *368* (2), 450-63.

35. Unno, H.; Yamashita, T.; Ujita, S.; Okumura, N.; Otani, H.; Okumura, A.; Nagai, K.; Kusunoki, M., Structural basis for substrate recognition and hydrolysis by mouse

carnosinase CN2. *J Biol Chem* **2008,** *283* (40), 27289-99.

36. Perry, T. L.; Hansen, S.; Love, D. L., Serum-carnosinase deficiency in carnosinaemia. *Lancet* **1968,** *1* (7554), 1229-30.

37. Perry, T. L.; Hansen, S.; Tischler, B.; Bunting, R.; Berry, K., Carnosinemia. A new metabolic disorder associated with neurologic disease and mental defect. *N Engl J Med* **1967,** *277* (23), 1219-27.

38. Terplan, K. L.; Cares, H. L., Histopathology of the nervous system in carnosinase enzyme deficiency with mental retardation. *Neurology* **1972,** *22* (6), 644-55.

39. Murphey, W. H.; Lindmark, D. G.; Patchen, L. I.; Housler, M. E.; Harrod, E. K.; Mosovich, L., Serum carnosinase deficiency concomitant with mental retardation. *Pediatr Res* **1973,** *7* (7), 601-6.

40. Lunde, H.; Sjaastad, O.; Gjessing, L., Homocarnosinosis: hypercarnosinuria. *J Neurochem* **1982,** *38* (1), 242-5.

41. Karita, M.; Etterbeek, M. L.; Forsyth, M. H.; Tummuru, M. K.; Blaser, M. J., Characterization of Helicobacter pylori dapE and construction of a conditionally lethal dapE mutant. *Infect Immun* **1997,** *65* (10), 4158-64.

42. Minton, N. P.; Atkinson, T.; Bruton, C. J.; Sherwood, R. F., The complete nucleotide sequence of the Pseudomonas gene coding for carboxypeptidase G2. *Gene* **1984,** *31* (1-3), 31-8.

43. Khan, T. H.; Eno-Amooquaye, E. A.; Searle, F.; Browne, P. J.; Osborn, H. M.; Burke, P. J., Novel inhibitors of carboxypeptidase G2 (CPG2): potential use in antibody-directed enzyme prodrug therapy. *J Med Chem* **1999,** *42* (6), 951-6.

44. Krause, A. S.; Weihrauch, M. R.; Bode, U.; Fleischhack, G.; Elter, T.; Heuer, T.; Engert, A.; Diehl, V.; Josting, A., Carboxypeptidase-G2 rescue in cancer patients with delayed methotrexate elimination after high-dose methotrexate therapy. *Leuk Lymphoma*

2002, *43* (11), 2139-43.

45. Bagshawe, K. D., Antibody directed enzymes revive anti-cancer prodrugs concept. *Br J Cancer* **1987,** *56* (5), 531-2.

46. Bagshawe, K. D., Antibody-directed enzyme/prodrug therapy (ADEPT). *Biochem Soc Trans* **1990,** *18* (5), 750-2.

47. Bagshawe, K. D.; Sharma, S. K.; Springer, C. J.; Rogers, G. T., Antibody directed enzyme prodrug therapy (ADEPT). A review of some theoretical, experimental and clinical aspects. *Ann Oncol* **1994,** *5* (10), 879-91.

48. Adams, G. P.; Weiner, L. M., Monoclonal antibody therapy of cancer. *Nat Biotechnol* **2005,** *23* (9), 1147-57.

49. Springer, C. J.; Bagshawe, K. D.; Sharma, S. K.; Searle, F.; Boden, J. A.; Antoniw, P.; Burke, P. J.; Rogers, G. T.; Sherwood, R. F.; Melton, R. G., Ablation of human choriocarcinoma xenografts in nude mice by antibody-directed enzyme prodrug therapy (ADEPT) with three novel compounds. *Eur J Cancer* **1991,** *27* (11), 1361-6.

50. Antoniw, P.; Springer, C. J.; Bagshawe, K. D.; Searle, F.; Melton, R. G.; Rogers, G. T.; Burke, P. J.; Sherwood, R. F., Disposition of the prodrug 4-(bis (2-chloroethyl) amino) benzoyl-L-glutamic acid and its active parent drug in mice. *Br J Cancer* **1990,** *62* (6), 909-14.

51. Eccles, S. A.; Court, W. J.; Box, G. A.; Dean, C. J.; Melton, R. G.; Springer, C. J., Regression of established breast carcinoma xenografts with antibody-directed enzyme prodrug therapy against c-erbB2 p185. *Cancer Res* **1994,** *54* (19), 5171-7.

52. Francis, R. J.; Sharma, S. K.; Springer, C.; Green, A. J.; Hope-Stone, L. D.; Sena, L.; Martin, J.; Adamson, K. L.; Robbins, A.; Gumbrell, L.; O'Malley, D.; Tsiompanou, E.; Shahbakhti, H.; Webley, S.; Hochhauser, D.; Hilson, A. J.; Blakey, D.; Begent, R. H., A phase I trial of antibody directed enzyme prodrug therapy (ADEPT) in patients with

advanced colorectal carcinoma or other CEA producing tumours. *Br J Cancer* **2002,** *87* (6), 600-7.

53. Gasparetti, C.; Faccio, G.; Arvas, M.; Buchert, J.; Saloheimo, M.; Kruus, K., Discovery of a new tyrosinase-like enzyme family lacking a C-terminally processed domain: production and characterization of an Aspergillus oryzae catechol oxidase. *Appl Microbiol Biotechnol* **2009,** *86* (1), 213-26.

54. Chen, Q. X.; Liu, X. D.; Huang, H., Inactivation kinetics of mushroom tyrosinase in the dimethyl sulfoxide solution. *Biochemistry (Mosc)* **2003,** *68* (6), 644-9.

55. Lerch, K., Neurospora tyrosinase: structural, spectroscopic and catalytic properties. *Mol Cell Biochem* **1983,** *52* (2), 125-38.

56. Cary, J. W.; Lax, A. R.; Flurkey, W. H., Cloning and characterization of cDNAs coding for Vicia faba polyphenol oxidase. *Plant Mol Biol* **1992,** *20* (2), 245-53.

57. Deverall, B. J., Phenolase and pectic enzyme activity in the chocolate spot disease of beans. *Nature* **1961,** *189* (28), 311.

58. Tief, K.; Hahne, M.; Schmidt, A.; Beermann, F., Tyrosinase, the key enzyme in melanin synthesis, is expressed in murine brain. *Eur J Biochem* **1996,** *241* (1), 12-6.

59. Tief, K.; Schmidt, A.; Aguzzi, A.; Beermann, F., Tyrosinase is a new marker for cell populations in the mouse neural tube. *Dev Dyn* **1996,** *205* (4), 445-56.

60. Klabunde, T.; Eicken, C.; Sacchettini, J. C.; Krebs, B., Crystal structure of a plant catechol oxidase containing a dicopper center. *Nat Struct Biol* **1998,** *5* (12), 1084-90.

61. Pauling, L., Chemical achievement and hope for the future. *Am Sci* **1948,** *36* (1), 51-8.

62. O'Brien, P. J.; Herschlag, D., Catalytic promiscuity and the evolution of new enzymatic activities. *Chem Biol* **1999,** *6* (4), R91-R105.

63. Copley, S. D., Enzymes with extra talents: moonlighting functions and catalytic

promiscuity. *Curr Opin Chem Biol* **2003,** *7* (2), 265-72.

64. Bornscheuer, U. T.; Kazlauskas, R. J., Catalytic promiscuity in biocatalysis: using old enzymes to form new bonds and follow new pathways. *Angew Chem Int Ed Engl* **2004,** *43* (45), 6032-40.

65. Kazlauskas, R. J., Enhancing catalytic promiscuity for biocatalysis. *Curr Opin Chem Biol* **2005,** *9* (2), 195-201.

66. Senior, S. Z.; Mans, L. L.; VanGuilder, H. D.; Kelly, K. A.; Hendrich, M. P.; Elgren, T. E., Catecholase activity associated with copper-S100B. *Biochemistry* **2003,** *42* (15), 4392-7.

67. Park, H. I.; Ming, L. J., A 10(10) Rate Enhancement of Phosphodiester Hydrolysis by a Dinuclear Aminopeptidase-Transition-State Analogues as Substrates? *Angew Chem Int Ed Engl* **1999,** *38* (19), 2914-2916.

68. Ercan, A.; Tay, W. M.; Grossman, S. H.; Ming, L. J., Mechanistic role of each metal ion in Streptomyces dinuclear aminopeptidase: PEPTIDE hydrolysis and 7x10(10)-fold rate enhancement of phosphodiester hydrolysis. *J Inorg Biochem* **2009,** *104* (1), 19-29.

69. Ercan, A.; Park, H. I.; Ming, L. J., Remarkable enhancement of the hydrolyses of phosphoesters by dinuclear centers: Streptomyces aminopeptidase as a 'natural model system'. *Chemical Communications* **2000,** (24), 2501-2502.

70. Spungin, A.; Blumberg, S., Streptomyces griseus aminopeptidase is a calcium-activated zinc metalloprotein. Purification and properties of the enzyme. *Eur J Biochem* **1989,** *183* (2), 471-7.

71. Lin, L. Y.; Park, H. I.; Ming, L. J., Metal Binding and Active Site Structure of Di-Zinc Streptomyces griseus Aminopeptidase. *J Biol Inorg Chem* **1997,** *2*, 744-49.

72. da Silva, G. F.; Ming, L. J., Catechol oxidase activity of di-Cu2+-substituted aminopeptidase from Streptomyces griseus. *J Am Chem Soc* **2005,** *127* (47), 16380-1.

73. da Silva, G. F. Z.; Ming, L. J., Catechol oxidase activity of Di-Cu2+-substituted aminopeptidase from Streptomyces griseus. *J Am Chem Soc* **2005,** *127* (47), 16380-1.

74. Rompel, A.; Fischer, H.; Meiwes, D.; Buldt-Karentzopoulos, K.; Magrini, A.; Eicken, C.; Gerdemann, C.; Krebs, B., Substrate specificity of catechol oxidase from Lycopus europaeus and characterization of the bioproducts of enzymic caffeic acid oxidation. *FEBS Lett* **1999,** *445* (1), 103-10.

75. Torelli, S.; Belle, C.; Hamman, S.; Pierre, J. L.; Saint-Aman, E., Substrate binding in catechol oxidase activity: biomimetic approach. *Inorg Chem* **2002,** *41* (15), 3983-9.

76. Wang, T. Y.; Chen, Y. C.; Kao, L. W.; Chang, C. Y.; Wang, Y. K.; Liu, Y. H.; Feng, J. M.; Wu, T. K., Expression and characterization of the biofilm-related and carnosine-hydrolyzing aminoacylhistidine dipeptidase from Vibrio alginolyticus. *FEBS J* **2008,** *275* (20), 5007-20.

77. Chang, C. Y.; Hsieh, Y. C.; Wang, T. Y.; Chen, C. J.; Wu, T. K., Purification, crystallization and preliminary X-ray analysis of an aminoacylhistidine dipeptidase (PepD) from Vibrio alginolyticus. *Acta Crystallogr Sect F Struct Biol Cryst Commun* **2009,** *65* (Pt 3), 216-8.

78. Chang, C. Y.; Hsieh, Y. C.; Wang, T. Y.; Chen, Y. C.; Wang, Y. K.; Chiang, T. W.; Chen, Y. J.; Chang, C. H.; Chen, C. J.; Wu, T. K., Crystal structure and mutational analysis of aminoacylhistidine dipeptidase from Vibrio alginolyticus reveal a new architecture of M20 metallopeptidases. *J Biol Chem* **2010,** *285* (50), 39500-10.

79. Otwinowsk, Z.; Minor, W., Processing of X-ray diffraction data collected in oscillation mode. *Methods Enzymol* **1997,** *276*, 307-26.

80. Weiss, M. S., Global indicators of X-ray data quality. *J Appl Cryst* **2001,** *34*, 130-5.

81. Evans, P., Scaling and assessment of data quality. *Acta Crystallogr D Biol Crystallogr* **2006,** *62* (Pt 1), 72-82.

82. Emsley, P.; Cowtan, K., Coot: model-building tools for molecular graphics. *Acta Crystallogr D Biol Crystallogr* **2004,** *60* (Pt 12 Pt 1), 2126-32.

83. Lovell, S. C.; Davis, I. W.; Arendall, W. B., 3rd; de Bakker, P. I.; Word, J. M.; Prisant, M. G.; Richardson, J. S.; Richardson, D. C., Structure validation by Calpha geometry: phi,psi and Cbeta deviation. *Proteins* **2003,** *50* (3), 437-50.

84. Laskowski, R. A.; MacArthur, M. W.; Moss, D. S.; Thornton, J. M., PROCHECK - a program to check the stereochemical quality of protein structures. *J Appl Cryst* **1993,** *26*, 283-91.

85. Espin, J. C.; Morales, M.; Varon, R.; Tudela, J.; Garcia-Canovas, F., A continuous spectrophotometric method for determining the monophenolase and diphenolase activities of apple polyphenol oxidase. *Anal Biochem* **1995,** *231* (1), 237-46.

86. Matthews, B. W., Solvent content of protein crystals. *J Mol Biol* **1968,** *33* (2), 491-7.

87. Chevrier, B.; Schalk, C.; D'Orchymont, H.; Rondeau, J. M.; Moras, D.; Tarnus, C., Crystal structure of Aeromonas proteolytica aminopeptidase: a prototypical member of the co-catalytic zinc enzyme family. *Structure* **1994,** *2* (4), 283-91.

88. Greenblatt, H. M.; Almog, O.; Maras, B.; Spungin-Bialik, A.; Barra, D.; Blumberg, S.; Shoham, G., Streptomyces griseus aminopeptidase: X-ray crystallographic structure at 1.75 A resolution. *J Mol Biol* **1997,** *265* (5), 620-36.

89. Hill, C. M.; Li, W. S.; Thoden, J. B.; Holden, H. M.; Raushel, F. M., Enhanced degradation of chemical warfare agents through molecular engineering of the phosphotriesterase active site. *J Am Chem Soc* **2003,** *125* (30), 8990-1.

90. Jao, S. C.; Huang, L. F.; Tao, Y. S.; Li, W. S., Hydrolysis of organophosphate triesters by Escherichia coli aminopeptidase P. *J Mol Cata B:Enzymatic* **2004,** *27* (1), 7-12.

91. Huang, L. F.; Su, B. S.; Jao, S. C.; Liu, K. T.; Li, W. S., Aminopeptidase P mediated detoxification of organophosphonate analogues of sarin: Mechanistic and sterecichemical study at the phosphorus atom of the substrate. *Chembiochem* **2006,** *7* (3), 506-514.

Appendix 1

Primers used in this thesis

Mutagenesis		
H80A-1	5’-GTGCTTCAAGCAGCGATCGACATGGTGCCAC-3’	(*Pvu*I)
H80A-2	5’-GTGGCACCATGTCGATCGCTGCTTGAAGCAC-3’	(*Pvu*I)
H82A-1	5’-GCACACATCGCCATGGTGCCACAAAAGAACG-3’	(*Nco*I)
H82A-2	5’-CGTTCTTTTGTGGCACCATGGCGATGTGTGC-3’	(*Nco*I)
D82X-1	5’-GCACACATCNNNATGGTACCACAAAAGAACG-3’	(*Kpn*I)
D82X-2	5’-CGTTCTTTTGTGGTACCATNNNGATGTGTGC-3’	(*Kpn*I)
D119A-1	5’-CGCTCGGGGCAGCTAACGGCATCGGCATGGC-3’	(*Ava*I)
D119A-2	5’-GCCATGCCGATGCCGTTAGCTGCCCCGAGCG-3’	(*Ava*I)
E149A-1	5’-CTGACGATCGATGCAGAAGCAGGCATGACAGG-3’	(*Pvu*I)
E149A-2	5’-CCTGTCATGCCTGCTTCTGCATCGATCGTCAG-3’	(*Pvu*I)
E149X-1	5’-CTGACAATTGATNNNGAAGCAGGCATGACAGG-3’	(*Mfe*I)
E149X-2	5’-CCTGTCATGCCTGCTTCNNNATCAATTGTCAG-3’	(*Mfe*I)
E150A-1	5’-ACTATTGATGAAGCCGCGGGCATGACAGGTGC-3’	(*Sac*II)
E150A-2	5’-GCACCTGTCATGCCCGCGGCTTCATCAATAGT-3’	(*Sac*II)
E150X-1	5’-GTTTTACTGACGATCGATGAANNNGCAGGCATGACAGG-3’	(*Pvu*I)
E150X-2	5’-CCTGTCATGCCTGCNNNTTCATCGATCGTCAGTAAAAC-3’	(*Pvu*I)
D173A-1	5’-CCTTCTAAATACAGCTAGCGAACAAGAAGGCG-3’	(*Nhe*I)
D173A-2	5’-CGCCTTCTTGTTCGCTAGCTGTATTTAGAAGG-3’	(*Nhe*I)
H461A-1	5’-CCAACCATCAAGTTCCCTGCTAGCCCAGATGAG-3’	(*Nhe*I)
H461A-2	5’-CTCATCTGGGCTAGCAGGGAACTTGATGGTTGG-3’	(*Nhe*I)
H219A-1	5’-GGTCTAAAAGGCGGTGCCTCGGGCTGTGACATCC-3’	(*Ava*I)
H219A-2	5’-GGATGTCACAGCCCGAGGCACCGCCTTTTAGACC-3’	(*Ava*I)
N260A-1	5’-GGTAGTTTGCGTGCCGCGATTCCGCGGGAAGCTTTTG-3’	(*Sca*II)
N260A-2	5’-CAAAAGCTTCCCGCGGAATCGCGGCACGCAAACTACC-3’	(*Sca*II)
R369A-1	5’-GCCTAATTGCATCGCTGATCGACTCAGG-3’	(*Pvu*I)
R369A-2	5’-CCTGAGTCGATCAGCGATGCAATTAGGC-3’	(*Pvu*I)
S374AS385A-1	5’-GARCGATGCAGGTCGTAGCCAAGTTGAAGGTATGCTTCAA GCTGTCGCTG-3’	(*Cla*I)
S374AS385A-2	5’-CAGCGACAGCTTGAAGCATACCTTCAACTTGGCTACGACCT GCATCGATC-3’	(*Cla*I)
G435A-1	5’-GGTTATCCACGCAGCTCTAGAATGTGGTCTG-3’	(*Xba*I)
G435A-2	5’-CAGACCACATTCTAGAGCTGCGTGGATAACC-3’	(*Xba*I)

Appendix 2

Appendix 2. Data collection and refinement statistics for the PepD structure

Data collection	
Space group	$P6_5$
Cell dimensions	
a, *b*, *c* (Å)	80.4, 80.4, 303.1
α, β, γ (°)	90, 90, 120
Wavelength (Å)	1.00
Resolution[a] (Å)	30-3.0 (3.14-3.00)
$\langle I/\sigma_I \rangle$[a]	17.6 (4.8)
Completeness[a] (%)	99.8 (99.9)
Redundancy[a]	4.2 (4.4)
R_{sym}[a,b]	4.6 (32.0)
$R_{r.i.m.}$[a,c]	8.8 (45.0)
$R_{p.i.m.}$[a,c]	2.7 (13.1)
Refinement	
Resolution (Å)	30-3.0
No. of reflections	43,703
R_{work}[d]/R_{free}[e] (%)	23.1/27.4
No. of atoms	7,528
Protein	7,524
Ion	4 (Zn)
B-factors (Å^2)	86.27
Protein	86.28
Ion	90.25
Root mean square deviations	
Bond lengths (Å)	0.013
Bond angles (°)	1.9

[a] Values in parentheses correspond to the highest-resolution shell.

[b] $R_{sym} = \Sigma_h \Sigma_i [|I_i(h) - \langle I(h) \rangle|/\Sigma_h \Sigma_i I_i(h)]$, where I_i is the *i*th measurement and $\langle I(h) \rangle$ is the weighted mean of all measurements of $I(h)$.

[c] $R_{r.i.m.} = \Sigma_h [N/(N-1)]^{1/2} \Sigma_i |I_{hi} - \langle I_h \rangle|/\Sigma_h \Sigma_i I_{h,i}$. $R_{p.i.m.} = \Sigma_h [1/(N-1)]^{1/2} \Sigma_i |I_{hi} - \langle I_h \rangle|/\Sigma_h \Sigma_i I_{h,i}$. $R_{r.i.m.}$ and $R_{p.i.m.}$ are as defined by Weiss

[d] $R_{work} = \Sigma_h |F_o - F_c|/\Sigma_h F_o$, where F_o and F_c are the observed and calculated structure factor amplitudes of reflection *h*.

[e] R_{free} is as R_{work}, but calculated with 10% of randomly chosen reflection omitted from the refinement.

Appendix 3

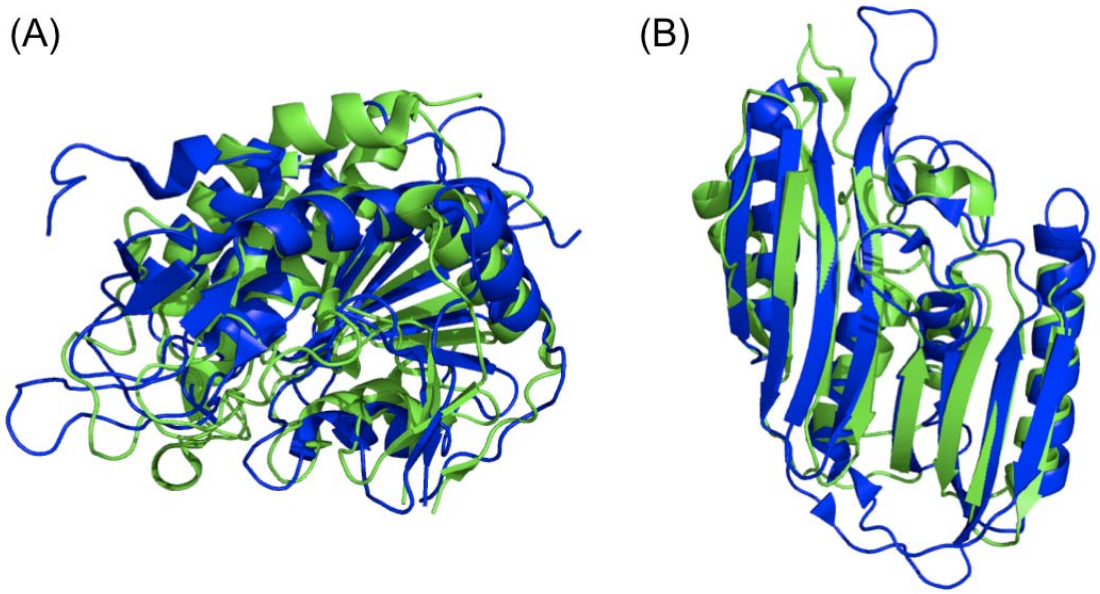

Appendix 3. Structure alignment of PepV and PepD with catalytic domain and lid domain. PepD is shown by *blue,* and PepV is shown by *green*. PepD and PepV showed root mean square deviations (rmsd) of 4.0 and 4.3 Å for Cα atoms of the catalytic and lid domains, respectively

Appendix 4

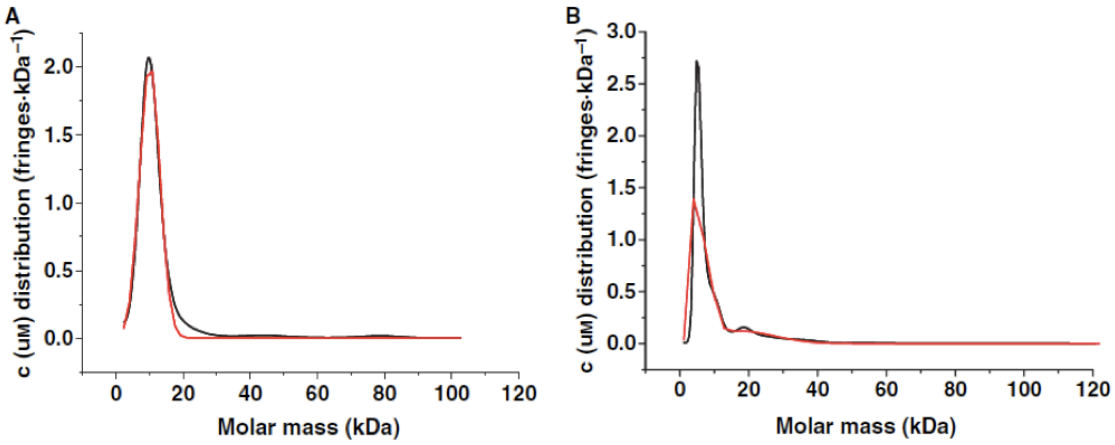

Appendix 4. Analytical ultracentrifugation of PepD protein. (A) The calculated molecular mass of native PepD from sedimentation coefficient (*s*) is approximately 100 664.94 ± 295 g.mol^{-1}. (B) The calculate molecular mass of urea denatured PepD protein from sedimentation coefficient (*s*) is approximately 51 091.49 ± 113 g.mol^{-1}.

Appendix 5

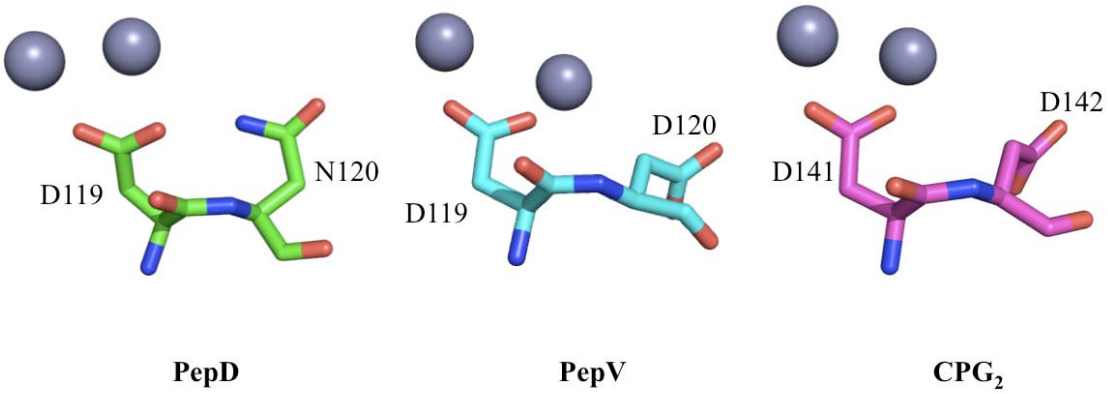

Appendix 5. *Cis* peptide bond of PepD, PepV and CPG_2. Zinc ions are shown by *gray spheres*. The *cis* peptide bond of PepD is composed by Asp-Asn peptide different from Asp-Asp peptides in PepV and CPG_2.

Appendix 6

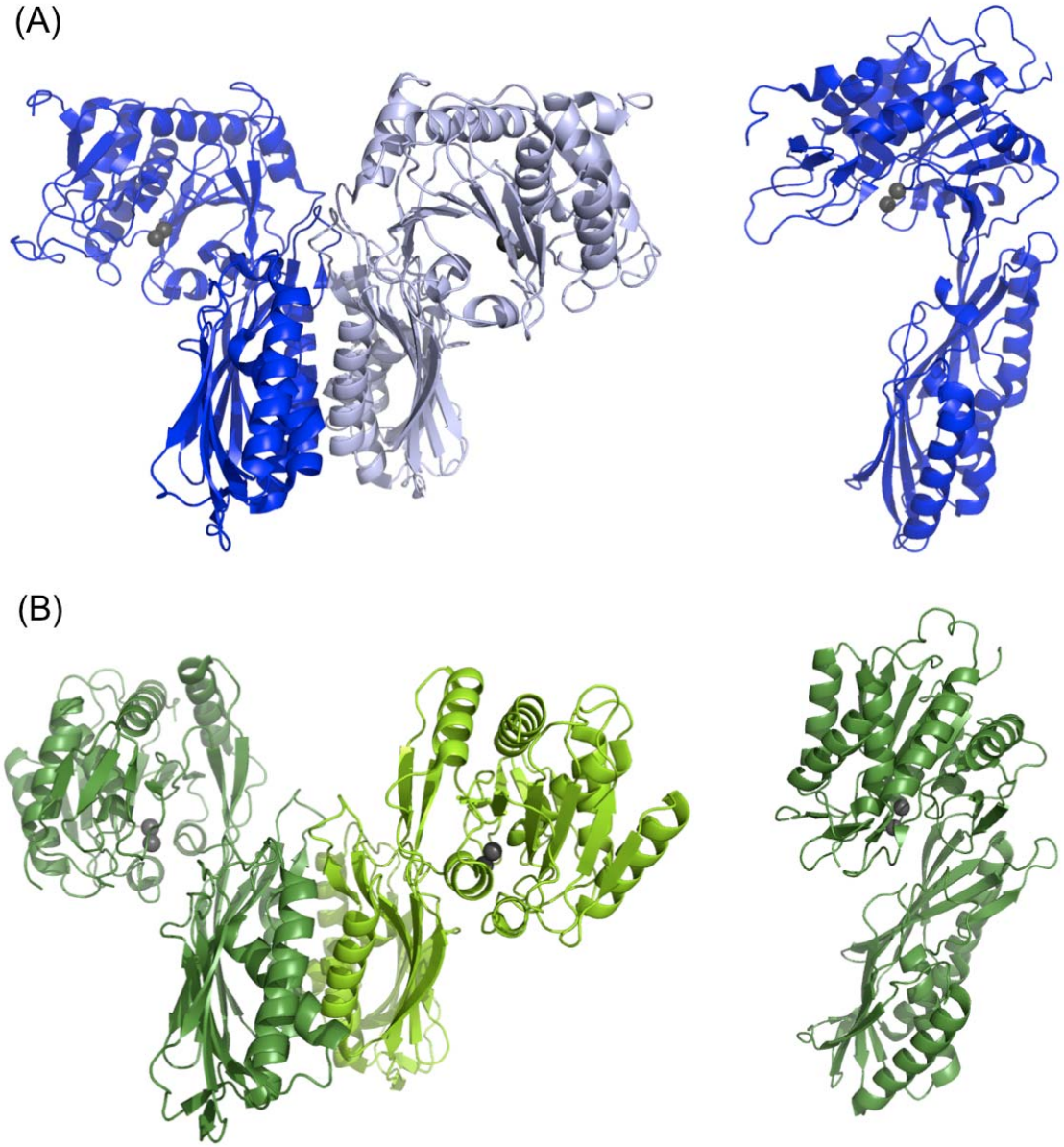

Appendix 6. Overall structure of (A) PepD and (B) 2QYV. The structure are shown by ribbon diagrams, and the right figures are one of subunits from PepD and 2QYV, respectively. The structure of PepD shows a close overall similarity to the uncharacterized PDB code 2QYV protein solved by the Joint Center for Structural Genomics (JCSG), but PepD shows an open comformation and 2QYV shows a closed comformation.

Appendix 7

```
PepD            MSEFHSEISTLSPAPLWQFFDKICSIPHPSKHEEALAQYIVTWATEQGFDVRRDPTGNVF 60
2QYV            ---GXSDLQSLQPKLLWQWFDQICAIPHPSYKEEQLAQFIINWAKTKGFFAERDEVGNVL 57
                     *::.:*.*  ***:**:**:***** :** ***:*:.**. :** ..** .***:

PepD            IKKPATPGMENKKGVVLQAHIDMVPQKNEDTDHDFTQDPIQPYIDGEWVTAKGTTLGADN 120
2QYV            IRKPATVGXENRKPVVLQAHLDXVPQANEGTNHNFDQDPILPYIDGDWVKAKGTTLGADN 117
                *:**** * **:* ******:* *** **.*:*:* **** *****:**.**********

PepD            GIGMASCLAVLASKEIKHGPIEVLLTIDEEAGMTGAFGLEAGWLKGDILLNTDSEQEGEV 180
2QYV            GIGXASALAVLESNDIAHPELEVLLTXTEERGXEGAIGLRPNWLRSEILINTDTEENGEI 177
                *** **.**** *::* *  :*****  ** *  **:**...**:.:**:***:*::**:

PepD            YMGCAGGIDGAMTFDITRDAIPAGFITRQLTLKGLKGGHSGCDIHTGRGNANKLIGRFLA 240
2QYV            YIGCAGGENADLELPIEYQVNNFEHCY-QVVLKGLRGGHSGVDIHTGRANAIKVLLRFLA 236
                *:***** :. : : *  :.    .   *:.****:***** ******.** *:: ****

PepD            GHAQ---ELDLRLVEFRGGSLRNAIPREAFVTVALPAENQDKLAELFNYYTELLKTELGK 297
2QYV            ELQQNQPHFDFTLANIRGGSIRNAIPRESVATLVFNG-DITVLQSAVQKFADVIKAELAL 295
                   *   .:*: *.::****:*******:..*:.: . :   * . .: :::::*:**.

PepD            IETDIVTFNEEVATDAQVFAIADQQRFIAALNACPNGVMRMSDEVEGVVETSLNVGVITT 357
2QYV            TEPNLIFTLEKVEKPQQVFSSQCTKNIIHCLNVLPNGVVRNSDVIENVVETSLSIGVLKT 355
                 *.:::   *:* .  ***:    :.:* .**. ****:* ** :*.******.:**:.*

PepD            EENKVTVLCLIRSLIDSGRSQVEGMLQSVAELAGAQIEFSGAYPGWKPDADSEIMAIFRD 417
2QYV            EDNFVRSTXLVRSLIESGKSYVASLLKSLASLAQGNINLSGDYPGWEPQSHSDILDLTKT 415
                *:* *    *:****:**:* * .:*:*:*.** .:*::** ****:*:::*:*: : :

PepD            MYEGIYGHKPNIMVIHAGLECGLFKEPYPNMDMVSFGPTIKFPHSPDEKVKIDTVQLFWD 477
2QYV            IYAQVLGTDPEIKVIHAGLECGLLKKIYPTIDXVSIGPTIRNAHSPDEKVHIPAVETYWK 475
                :*  : * .*:* **********:*: **.:* **:****: .*******:* :*: :*.

PepD            QMVALLEAIPEKA 490
2QYV            VLTGILAHIPSR- 487
                 :..:*  **.:
```

Appendix 7. Sequence alignment of PepD and 2QYV. PepD is comsisted by 490 amino acids, and 2QYV is comsisted by 487 amino acids. The sequence alignment of PepD and 2QYV showed 50.9% sequence identity.

Appendix 8

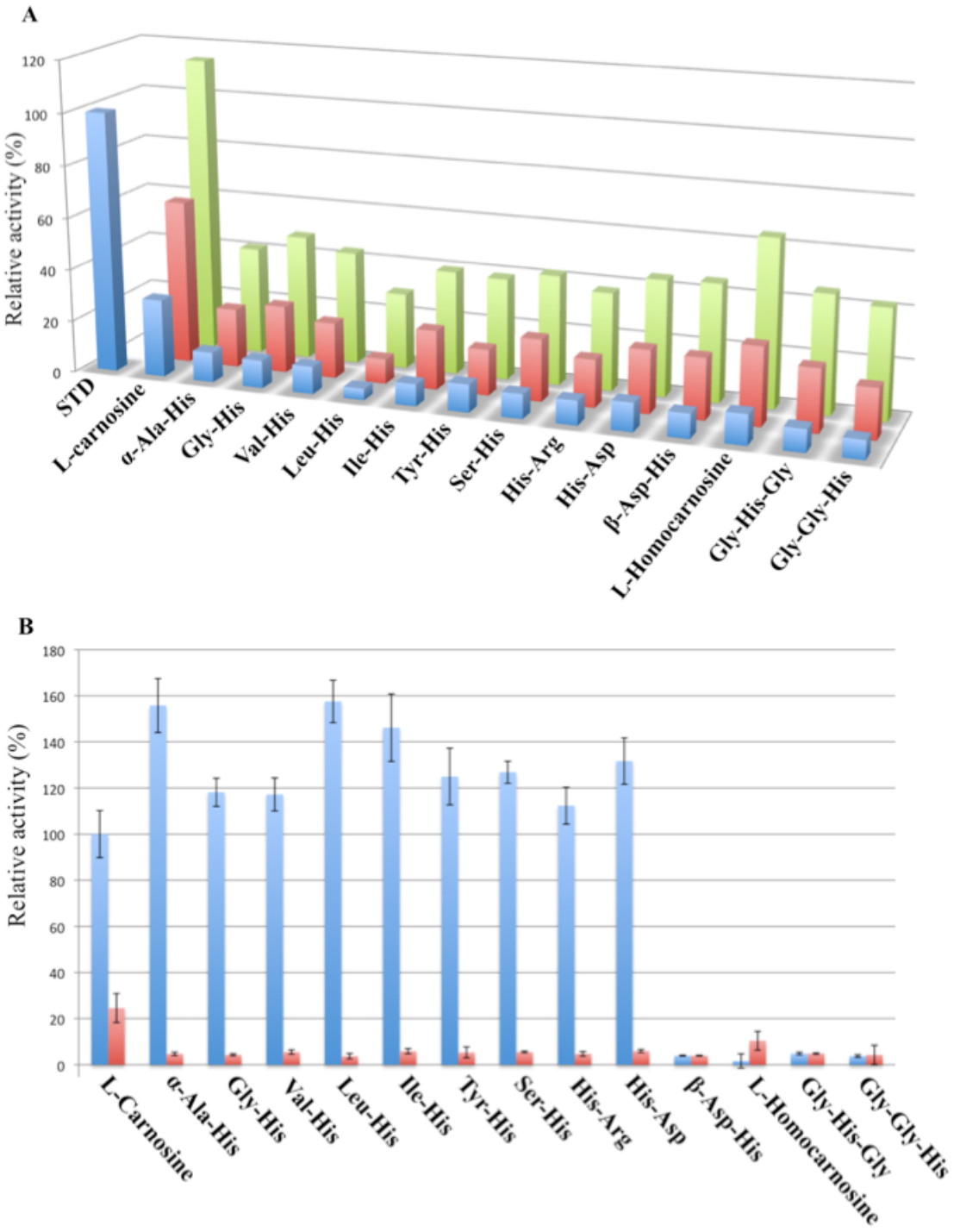

Appendix 8. Substrate specificity of PepD^{CAT} for various Xaa-His, His-Xaa dipeptides and two histidine-containing tripeptides. (A) Various concentrated purified recombinant PepD^{CAT} proteins (2μM in *blue*, 5μM in *red*, 10μM in *green*) were

incubated with one of 14 different substrates for 25 min at 37°C. The activity of wild type PepD (2μM), taking L-carnosine as a substrate, was defined as 100% (STD). (B) The comparison of the enzymatic activities with 14 different substrates between PepD full length proteins (*blue*) and $PepD^{CAT}$ truncated proteins (*red*). Values are expressed as relative activity compared to the wild type PepD, taking L-carnosine as the substrate, which was set to 100%. All the enzymatic activities were measured using the standard activity assay as previously.

Appendix 9

Appemdix 9.1 Expression and purification of human carnosinase 1 (hCN1) by baculovirus expression system

Humcan carnosinase 1 (Sigma) gene was amprified and cloned into a transfer vector (pBacPAK8-MTEGFP) to construct the recombinant pBacPAK8-CN1 plasmid that contains flanking sequences which are homologous to the Baculovirus genome. BaculoGold™ DNA (baculovirus DNA) and the recombinant transfer vector (pBacPAK8-CN1) were co-transfected into *Sf9* insect cell. Recombination takes place within the insect cells between the homologous regions in the transfer vector and the BaculoGold™ DNA to produce the recombinant virus (baculo-CN1 virus). The recombinant protein (CN1) was produced via recombinant virus which infected additional insect cells thereby resulting in additional recombinant virus. Then, the amplified recombinant virus (baculo-CN1 virus) were used to infect 20 mL *Hi5* ($2x10^6$ cells/ml) insect cell at 27°C for 4 days to express CN1 enzyme. After 4 days, green fluorescence was observed in all insect cells. The collected cells were then resuspended in 20 mM Tris buffer containing 0.5 M NaCl at pH 7.6 (Buffer A) and lysed by sonicator with 30% energy (pulse on 2 sec, pulse off 3 sec for 10 min). After removal of cellular debries by centrifugation at 9,500 rpm for 50 min at 4°C, the supernatant will be applied to a Ni Sepharose™ 6 Fast Flow column, pre-equilibrated with Buffer A and washed with Buffer A containing 60 mM imidazole. Finally, the CN1 protein was eluted with Buffer A containing 500 mM imidazole. The human CN1 gene is 1530 nucleotides in length, consists of 510 amino acids encoding a protein with predicted molecular mass of 56 kDa. The recombinant human CN1 protein has been confirmed by MALDI-TOF.

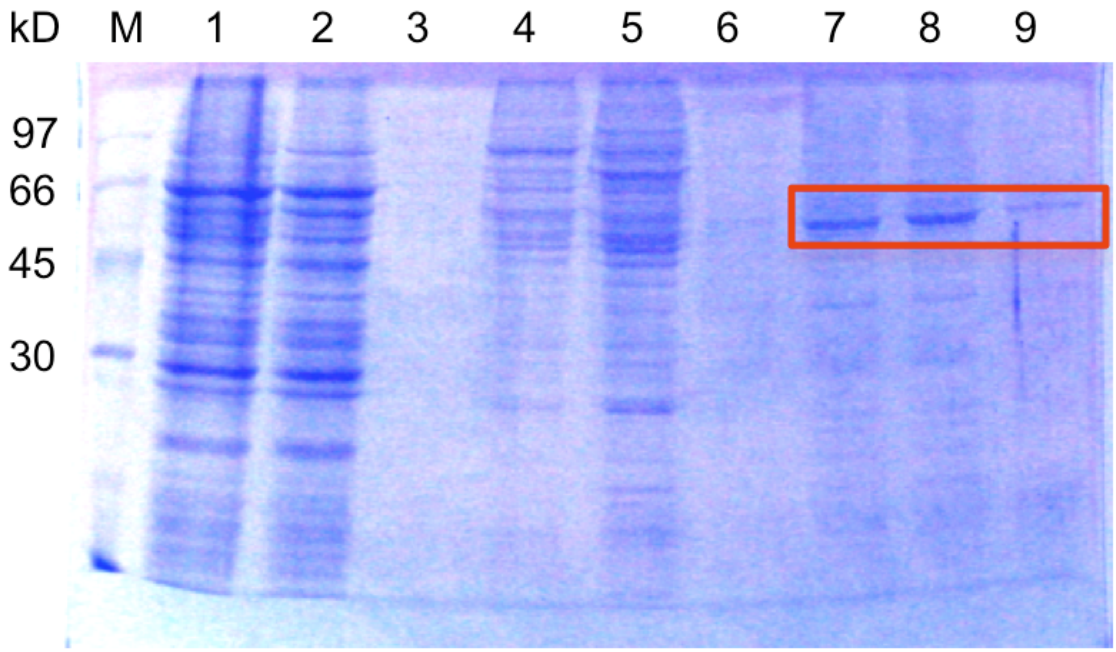

12.5% SDS-PAGE of the purified human CN1 protein. Lane M: Marker proteins; Lane 1: crude cell extracts of *Hi5* infected by baculo-CN1 virus; Lane 2: flowthrough after Ni-NTA column; Lane 3-5: Washed by Buffer A containing 60 mM imidazole; Lane 6-9: Washed by Buffer A containing 500 mM imidazole. The *red* frame shows the recombinant CN1 protein.

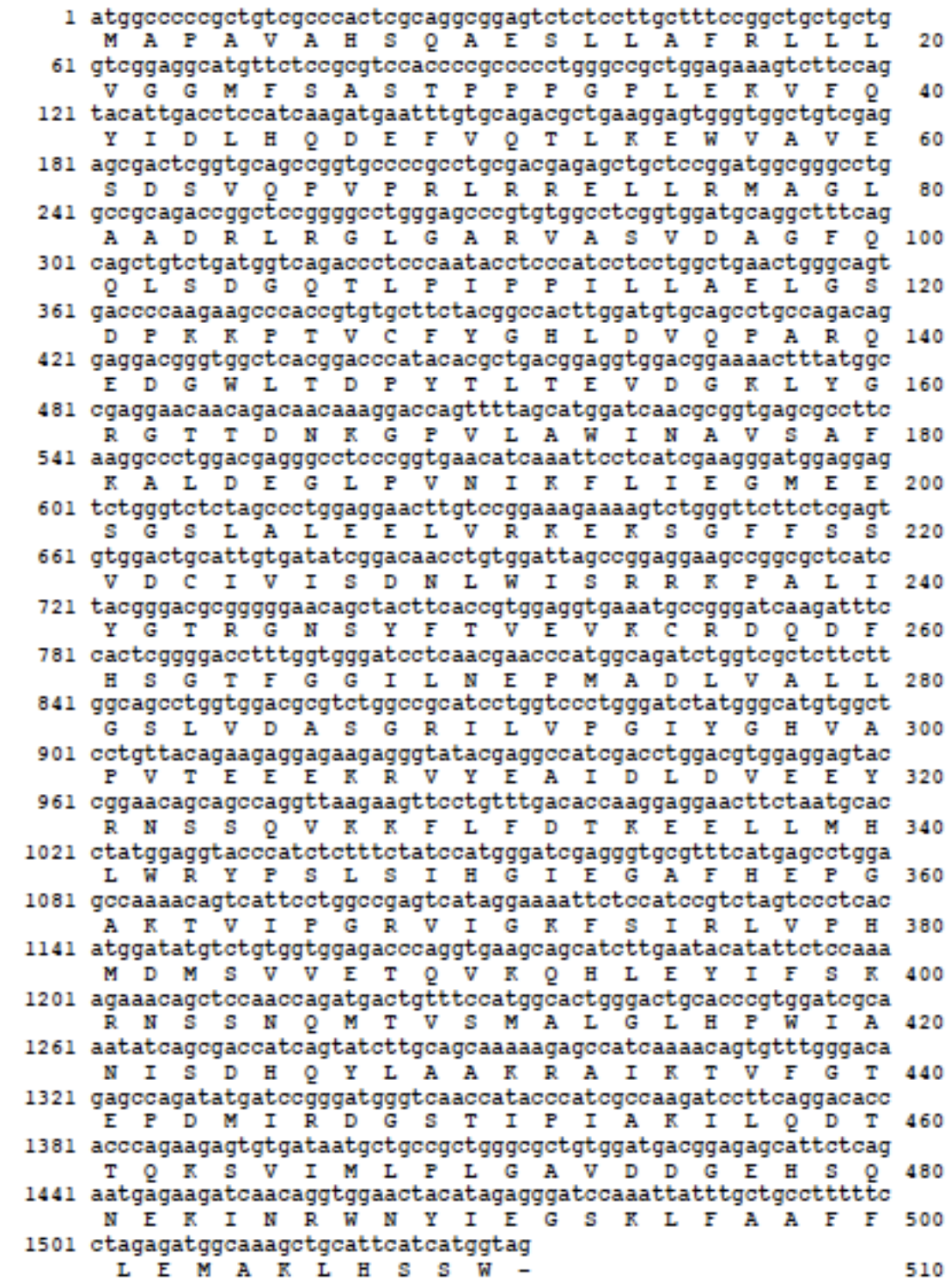

Nucleotide sequences and translated amino acid sequences of human CN1.

Appendix 9.2 Enzymatic activity assay of human CN1

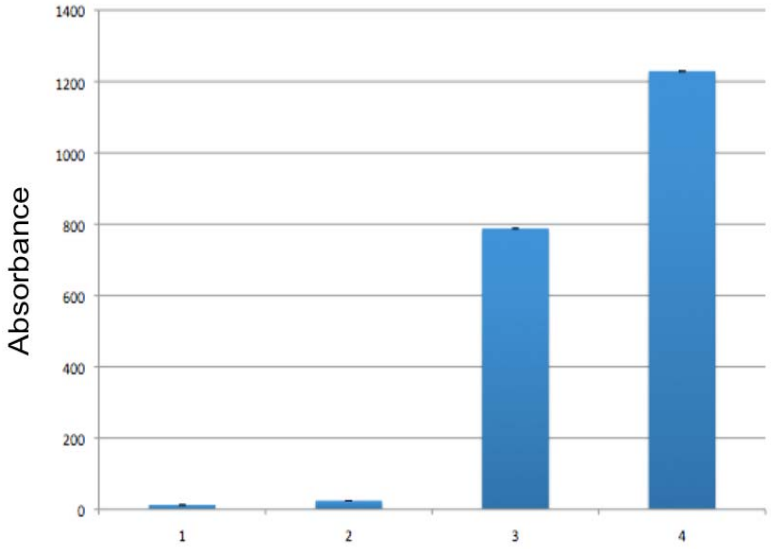

Human CN1 activity assay. Human CN1 activity assay was the same with the method to measure the activity of PepD.

Column 1: Nagtive control, only human CN1 protein (10 μg) in reaction.

Column 2: Nagtive control, only carnosine (1 mM) in reaction.

Column 3: Human CN1 protein (10 μg) + carnosine (1 mM)

Column 4: Positive control, only Histidine (1 mM) in reaction.